Impact of texturing on sliding wear behaviour of UHMWPE

Fatima Eddoumy

N° d'ordre : PHD-08-068 Année 2012

Ecole Doctorale Mathématiques, Sciences de l'Information et de l'Ingénieur

Université de Strasbourg – Centre de Recherche Public Henri Tudor – Katholieke Universiteit Leuven

THÈSE

Présentée pour obtenir le grade de

Docteur de l'Université de Strasbourg

Discipline: Science des Matériaux

Impact of texturing on sliding wear behaviour of UHMWPE

Présentée et soutenue publiquement par

Fatima EDDOUMY

le 29 février 2012 à Strasbourg

Jury composé de :

Pierre PONTHIAUX	Professeur	Rapporteur (Ecole Centrale Paris)
Roland SEGUELA	Directeur de Recherche	Rapporteur (INSA de Lyon)
René MULLER	Professeur	Directeur de thèse (Université de Strasbourg)
Jean-Pierre CELIS	Professeur	Co-directeur de thèse (Katholieke Universiteit Leuven)
Christian GAUTHIER	Professeur	Examinateur (Université de Strasbourg)
David RUCH	Docteur (HDR)	Examinateur (CRP Henri Tudor)
Frédéric ADDIEGO	Docteur	Examinateur (CRP Henri Tudor)

- Centre de Recherche Public Henri Tudor, Advanced Materials and Structures (AMS), Esch-sur-Alzette, Luxembourg
- Université de Strasbourg, Institut de Mécanique des Fluides et des Solides (IMFS), Strasbourg, France
- Katholieke Universiteit Leuven - Metaalkunde en Toegepaste Materiaalkunde (MTM), Leuven, Belgium

Acknowledgments

No thesis could ever be successfully completed without the advice, support, and encouragement of a wide variety of people.

The person who I would like to thank first is Dr. David Ruch. He gave me the opportunity to start this PhD in the Centre de Recherche Public Henri Tudor, with the financial support of the Fond National de la Recherche Luxembourg (FNR).

I am grateful to Prof. Jean-Pierre Célis for his sage advice and wisdom during all of our meetings and for having him as a leadership role model. His suggestions, advices and supervision contributed to the advancement of my work. Working alongside him helped me to become a better researcher by experiencing his zeal and creativity for finding solutions to problems. My sincere gratitude goes to Prof. René Muller, my thesis supervisor, who supported my research work. His scientific background and ideas made a valuable learning experience for me. I am thankful to Dr. Olivier Buchheit and Dr. Frédéric Addiego for all guidance and management of my work which helped me to complete this project.

I would like to address my gratitude to Prof. Pierre Ponthiaux, Prof. Roland Séguéla and Prof. Christian Gauthier, who accepted to be members of the jury for my PhD. defence.

I would like to thank all the team of Centre de Recherche Public Henri Tudor, and in particular the researchers and my lab-mates. I would also like to thank the university and staff of the Katholieke Universiteit Leuven for providing me access to their cutting-edge equipments. Using such facilities has been a great learning experience. I would like also to thank the University of Nancy and specially Prof. Abdesselam Dahoun for the mechanical testing.

I would like to thank all my friends, I met during my stay in Esch-sur-Alzette and Leuven who directly or indirectly contributed, and particularly Dr. Abdelghani Laachachi, Dr. Fatima Hassouna, Houcine Dhieb, Wassim Zein Eddine and Dr. Ivan Buijnsters. I have learnt a great deal working alongside them during this period.

I would like to specially thank from the depth of my heart my parents and my family for their support, understanding, encouragement and confidence. They were always supportive and helpful to provide me the zeal to complete this project.

- Centre de Recherche Public Henri Tudor, Advanced Materials and Structures (AMS), Esch-sur-Alzette, Luxembourg
- Université de Strasbourg, Institut de Mécanique des Fluides et des Solides, (IMFS), Strasbourg, France
- Katholieke Universiteit Leuven - Metaalkunde en Toegepaste Materiaalkunde (MTM), Leuven, Belgium

A ma mère, Zahra

A mon père, Thami

A ma soeur, Jamila

A mes frères, Fouad et Marouane

Table of Contents

Chapter I

Introduction

I.1 Background

For applications that require the use components in relative motion, the quantification of wear volume and the identification of the underlying mechanisms are essential to predict the lifetime of the components, and hence, to improve their design. In the case of total hip arthroplasty, wear particles are released during movement between the metal or ceramic femoral head and ultra-high molecular weight polyethylene (UHMWPE) cup. The generated debris cause osteolysis phenomena, and in extreme cases, produce a loosening of the prosthesis that can lead to its failure [1, 2]. In these extremes cases, a medical revision is required, which is an additional burden for the patient and represents an additional cost for healthcare organizations. Therefore, it is of high interest to found ways to increase the durability of such prosthesis. It has been shown that wear mechanisms depend on the design of the prosthesis, the mechanical and chemical properties of the UHMWPE, the mechanical properties of the counterbody, and age / activities of the patient [3, 4]. The present research work is focused on the properties of UHMWPE. Numerous in-vitro and in-vivo studies investigated the effect of chemical structure of UHMWPE on its wear resistance under cyclic loading conditions. The results of these previous works show that irradiation-induced cross-linking considerably improves wear resistance. For example, it was shown that cross-linked UHMWPE treated by gamma irradiation exhibited a reduction by about 40-50% of the wear volume compared to conventional UHMWPE [5]. However, due to the new cross-linked molecular network, cross-linking causes a drastic decrease of tensile strength and toughness, which is not desirable [6, 7].

I.2 Problem statement

A new processing of UHMWPE is developed in this work. This method consists of stretching the material in the solid state to induce a permanent orientation of the macromolecular chains. This process is usually called texturing process and can be seen i) as an alternative to cross-linking, or ii) as a cross-linking pre-treatment. Under certain conditions, texturing may significantly increase the wear resistance of UHMWPE without altering the chemical properties [8, 9]. Texturing is also

known to increase tensile strength and toughness [10-12] prior to the irradiation cross-linking procedure. Notwithstanding that the texturing process should not decrease the wear resistance of UHMWPE prior to cross-linking. Whatever, the selected strategy, it is of fundamental interest to study the impact of the initial chain orientation state on the wear behaviour of UHMWPE. To date, only a limited number of works deals with this topic [8, 12, 13], and it is unclear whether texturing has a positive or negative effect on the sliding wear resistance of UHMWPE.

I.3 Research objectives and methodology

The main aim of this study is to investigate the influence of an initial chain orientation state of UHMWPE on the sliding wear behaviour, and to determine the underlying mechanisms. Texturing procedures were conducted by uni-axial tensile deformation procedures at 30 °C. We first analyzed the impact of the tensile deformation level on the structural, topographical and viscoelastic properties of the material. The attention is particularly focused on the evolution of the microstructure, index of crystallinity, long spacing, lamellae thickness, relaxation processes, and roughness with axial strain. Then, reciprocating sliding wear experiments were performed (ball-on-plate contact configuration, use of a corundum balls as counterbody). To this end, we developed a specific testing procedure based on the applied load, the initial UHMWPE surface state, and an energetic approach to assess with precision the sliding / wear behaviour of the material. The impact of different tensile deformation levels was studied on the friction behaviour of UHMWPE to verify whether the texture state has an impact or not on the sliding behaviour. Last, we assessed the topographical, morphological and chemical (oxidation) aspects of non-textured and the textured UHMWPE before and after sliding testing to identify the wear mechanisms active on these materials. As characterization tools, we used Fourier transform infrared spectroscopy (FTIR), scanning electron microscopy (SEM), small- and wide-angle X-ray scattering (SAXS/WAXS), differential scanning calorimetry (DSC), dynamic mechanical analysis (DMA), and white light interferometry (WLI).

I.4 Manuscript description

This thesis manuscript consists of four parts:

- Chapter 2 is a literature review on the general properties of polyethylene, degradation mechanisms of UHMWPE, and challenge to improve the durability of UHMWPE.
- Chapter 3 provides information about the material preparation and the characterization tools used in this research work to characterize chemical, microstructural, topographical, bulk and surface mechanical properties of the tested materials.
- Chapter 4 is dedicated to the identification of texturing mechanisms, the setting-up of the sliding testing, the study of sliding behaviour of non-textured and textured UHMWPE, including the identification of sliding / wear mechanisms.
- Chapter 5 contains the main conclusions and the prospects of this work.

I.5 References

[1] P. Schaaff, The role of fretting damage in total hip arthroplasty with modular design hip joints -evaluation of retrieval studies and experimental simulation methods, J Appl Biomater Biomech, 2(3) (2004).

[2] A. Wang, C. Stark, J.H. Dumbleton, Role of cyclic plastic deformation in the wear of UHMWPE acetabular cups, Journal of Biomedical Materials Research, 29 (1995) 619-626.

[3] S. Affatato, W. Leardini, M. Zavalloni, Hip Joint Simulators: State of the Art, in: Bioceramics and Alternative Bearings in Joint Arthroplasty, 2006, pp. 171-180.

[4] S.P. Ho, R.W. Carpick, T. Boland, M. LaBerge, Nanotribology of CoCr-UHMWPE TJR prosthesis using atomic force microscopy, Wear, 253 (2002) 1145-1155.

[5] J.M. Martell, J.J. Verner, S.J. Incavo, Clinical performance of a highly cross-linked polyethylene at two years in total hip arthroplasty: a randomized prospective trial, The Journal of Arthroplasty, 18 (2003) 55-59.

[6] O.K. Muratoglu, D.O. O'Connor, C.R. Bragdon, J. Delaney, M. Jasty, W.H. Harris, E. Merrill, P. Venugopalan, Gradient crosslinking of UHMWPE using irradiation in molten state for total joint arthroplasty, Biomaterials, 23 (2002) 717-724.

[7] M.C. Sobieraj, S.M. Kurtz, A. Wang, M.M. Manley, C.M. Rimnac, Notched stress-strain behavior of a conventional and a sequentially annealed highly crosslinked UHMWPE, Biomaterials, 29 (2008) 4575-4583.

[8] D.S. Li, H. Garmestani, S. Ahzi, M. Khaleel, D. Ruch, Microstructure Design to Improve Wear Resistance in Bioimplant UHMWPE Materials, Journal of Engineering Materials and Technology, 131 (2009) 041211.

[9] D. Li, H. Garmestani, A. Chu, H. Ahzi, G. Alapati, M. Khatonabadi, O. Es-Said, M. Siniawski, L. Matrisciano, S. Ahzi, Wear resistance and microstructure in annealed ultra high molecular weight polyethylenes, Polymer Science Series A, 50 (2008) 533-537.

[10] F. Addiego, O. Buchheit, D. Ruch, S. Ahzi, A. Dahoun, Does Texturing of UHMWPE Increase Strength and Toughness?: A Pilot Study, Clinical Orthopaedics and Related Research®, 469 (2011) 2318-2326.

[11] A. Galeski, Strength and toughness of crystalline polymer systems, Progress in Polymer Science, 28 (2003) 1643-1699.

[12] S.M. Kurtz, D. Mazzucco, C.M. Rimnac, D. Schroeder, Anisotropy and oxidative resistance of highly crosslinked UHMWPE after deformation processing by solid-state ram extrusion, Biomaterials, 27 (2006) 24-34.

[13] H. Marrs, D.C. Barton, C. Doyle, R.A. Jones, E.L.V. Lewis, I.M. Ward, J. Fisher, The effect of molecular orientation and acetylene-enhanced crosslinking on the wear of UHMWPE in total artificial joints, Journal of Materials Science: Materials in Medicine, 12 (2001) 621-628.

Chapter II

Literature review

The objectives of this chapter is to provide an overview about the general properties of polyethylene and to highlight the scientific challenges of ultra-high molecular weight polyethylene (UHMWPE) used as biomaterial. Attention is first focused on the multiscale structure, the mechanical properties, the deformation mechanisms, and the application of polyethylene as a component of medical prosthesis. Then, relevant information about the chemical and mechanical durability of UHMWPE is reported. Last, we describe how the durability of UHMWPE can be improved by cross-linking, addition of anti-oxidant, modification of the crystallinity and texturing. Finally the scientific challenges arising from these strategies are listed

II.1 General features of polyethylene

II.1.1 Chemical and physical properties

Polyethylene is a material obtained by polymerization of ethylene C_2H_4 (Figure II-1) leading to macromolecules composed of the repeating monomer unit $-(CH_2-CH_2)_n-$. The molecular architecture of this material can be controlled through the polymerization process in terms of chain length, distribution of chain length and branching type and length.

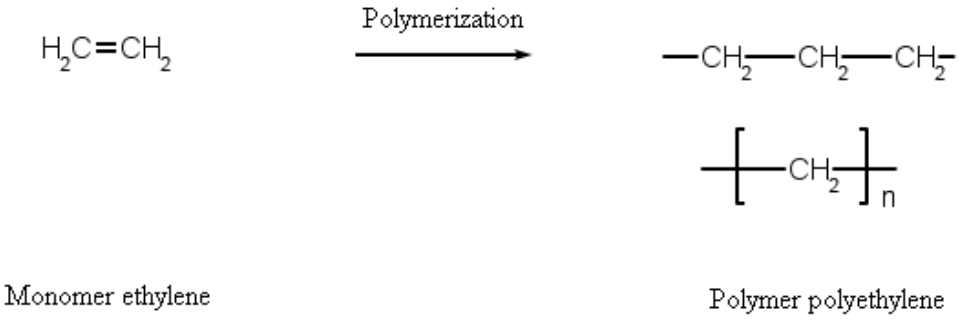

Figure II-1: Polymerization of polyethylene

Polyethylene grades are generally classified into three categories: low density polyethylene (LDPE) with long branches, linear low density polyethylene (LLDPE) with short branches and high density polyethylene (HDPE) composed of linear chains. Ultra-high molecular weight polyethylene (UHMWPE) is a particular case of HDPE characterized by very long chains. HDPE has a molecular weight that is typically comprised between 50,000 and 250,000 g/mol, while that of UHMWPE is of about 3 to 6 million g/mol. UHMWPE is synthesized by a catalytic polymerization process named Ziegler-Natta catalysis with the use of a titanium chloride catalyst [1].

This polymerization process is carried out in a solvent which allows the reaction for mass and heat transfer; UHMWPE is in powder state after synthesis. One of the main producers of this product is the company Ticona that kindly provided the UHMWPE grade used for this study in the form of a powder (GUR1050). The designation GUR means Granular Ruhrchemie. The first digit (1) corresponds to the loose bulk density of the resin, that, is the weight measurement of a fixed volume of loose, unconsolidated powder density, the second number corresponds to the presence (1) or absence of calcium (0), the third digit (5) corresponds to the molecular weight (million g/mol) and last digit is an internal code of Ticona [2].

As semi-crystalline polymer, UHMWPE contains crystalline lamellae that have a planar shape and are formed by chain folding (Figure II-2). The typical thickness of UHMWPE crystalline lamellae is of about 15-25 nm, while for HDPE it is comprised between 5 and 15 nm. Lamellae are interconnected by a few chains, called tie molecules that pass from one lamella through a small amorphous region, to another lamella (Figure II-2).

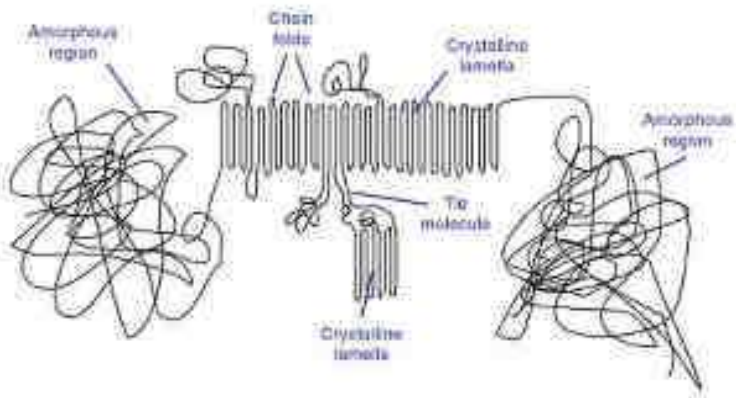

Figure II-2: Morphological features of UHMWPE [2]

Table II-1 shows the main characteristics of three polyethylene types in terms of density, molecular weight, and weight fraction of crystalline phase [1].

Table II-1: Typical physical properties of LDPE, HDPE and UHMWPE [1]

	Density (g / m^3)	Molecular weight (g / mol)	crystallinity (%)
LDPE	0.910 – 0.940	10,000	40
HDPE	0.952 – 0.965	50,000 – 250,000	60-75
UHMWPE	0.930 – 0.945	3,000 000 – 6,000000	50-60

Whatever the chain architecture, polyethylene is composed by an amorphous phase and a crystalline phase with variables proportions. In the amorphous phase, the amorphous chains have a random arrangement and are entangled. Among the three polyethylenes reported in the Table II-1, UHMWPE is characterized by the highest density of entanglements. Regarding the crystalline phase, molecular chains have a zigzag conformation induced by the crystallization process (Figure II-3).

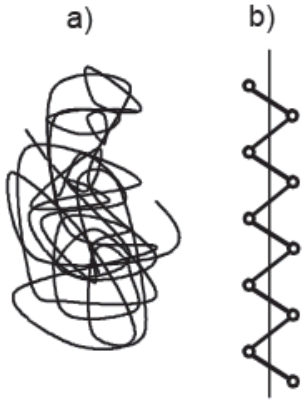

Figure II-3: Schematic conformation of macromolecular chains of polyethylene; a) random conformation, b) Zigzag conformation [3]

At the nanoscale (1 nm), the most stable crystalline lattice of polyethylene is the orthorhombic system characterized by the following parameters (measured by Bunn in 1939): a = 0.740 nm, b = 0.493 nm and c = 0.253 nm (Figure II-4).

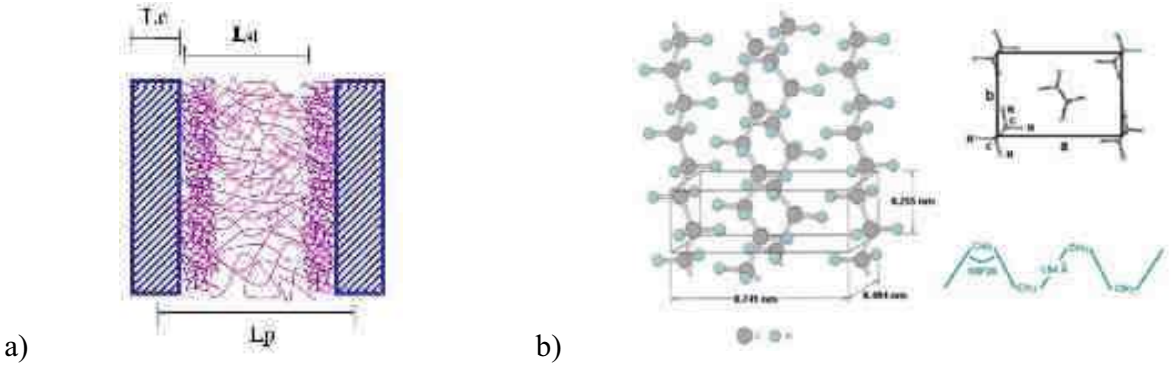

Figure II-4: General aspects of crystalline lamellae of polyethylene, a) two successive crystalline lamellae, and b) chain configuration in a lamella [3]

The thickness of crystalline lamellae (L_c) is the length of the chain segment between two successive folds. L_c is typically a few tens of monomer units (about 15 -25 nm for UHMWPE). Between two crystalline lamellae there is an amorphous phase with a thickness (L_a) which is comparable to that of crystallites. A typical characteristic of this specific morphology is the long spacing L_p that is given by:

$$L_p = L_c + L_a \qquad \text{II-1}$$

Note that the radial arrangement of stacks of crystalline lamellae and amorphous layers is called spherulites which have a diameter ranging between 5 and 100 µm. In the case of UHMWPE, the high viscosity of this material and the important density of entanglements do not enable the formation of spherulites. In this case, the supercrystalline structure is an aggregate of intertwined crystalline lamellae (Figure II-5).

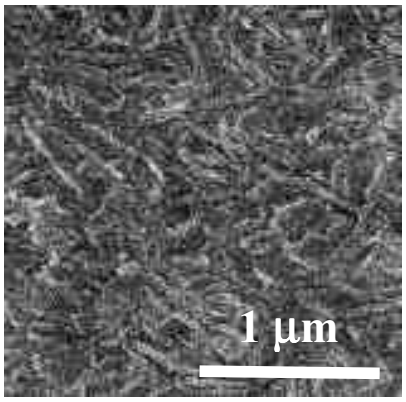

Figure II-5: Typical supercrystalline structure of UHMWPE [4]

II.1.2 Mechanical properties

We qualitatively describe here the mechanical properties of polyethylene through the description of tensile behaviour which provides information about the viscoelastic, and viscoplastic properties of this polymer, while Table II-2 reports some general characteristics of the tensile behaviour.

During a tensile test (Figure II-6), the behaviour of polyethylene is characterized by two stages: i) the viscoelastic stage up to the true strain of about 0.1, and then the viscoplastic stage up to the breakup of the material. The initial slope of the stress-strain curve provides the value of the elastic modulus of the material that is comprised between 0.1 and 1.5 GPa. Elastic modulus generally decreases with increasing temperature or decreasing strain rate. Moreover, elastic modulus increases with the degree of crystallinity and the entanglements density of the amorphous phase. The transition between the two deformation stages is characterized by a knee-like shape where the stress gradually stabilizes. The stress at the transition between these two stages is called the yield stress and is generally comprised between 10 MPa and 30 MPa depending on crystalline lamellae thickness, temperature and strain rate. In the final part of viscoplastic stage, a marked increase of stress with strain is noted: it is called strain-hardening process. This latter is much more marked for UHMWPE than for the other polyethylene categories due to the high density of entanglement and tie molecules in UHMWPE that causes a high resistance to deformation during stretching [5].

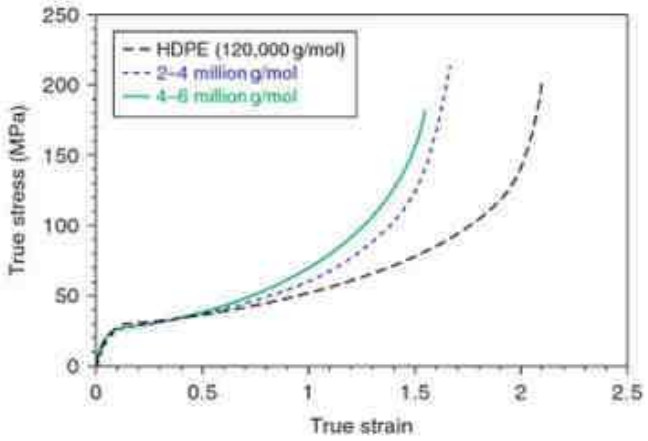

Figure II-6: True-stress strain behaviour in uniaxial tension (room temperature, dε/dt = 30 mm/min) for two grades of UHMWPE, in comparison to HDPE [5].

Table II-2 summarizes the physical and mechanical properties generally reported for HDPE and UHMWPE.

Table II-2: Physical and mechanical properties of HDPE and UHMWPE [2]

Property	**HDPE**	**UHMWPE**
Molecular Weight (10^6 g/mole)	0.05-0.25	2-6
Melting Temperature (°C)	130-137	125-138
Poisson's Ratio	0.40	0.46
Specific Gravity	0.952-0.965	0.932-0.945
Tensile Modulus of Elasticity* (GPa)	0.4-4.0	0.8-1.6
Tensile Yield Strength* (MPa)	26-33	21-28
Tensile Ultimate Strength* (MPa)	22-31	39-48
Tensile Ultimate Elongation* (%)	10-1200	350-525
Impact Strength, Izod* (J/m of notch; 3.175 mm thick specimen)	21-214	>1070 (No Break)
Degree of Crystallinity (%)	60-80	39-75

*Testing conducted at 23°C.

As shown in Table II-2, UHMWPE has a higher ultimate strength and impact strength than HDPE.

UHMWPE has a higher energetic toughness (ability to absorb energy) owing to its very high molecular weight, crystallinity, and chain entanglement density.

Moreover, UHMWPE is significantly more abrasion resistant and wear resistant than HDPE. These properties make UHMWPE suitable for bearing surface application requiring a polymeric material as artificial joints for prosthesis. For example, some hip simulator procedures show that the volumetric wear rate of UHMWPE is 4.3 times lower than that of HDPE (Figure II-7).

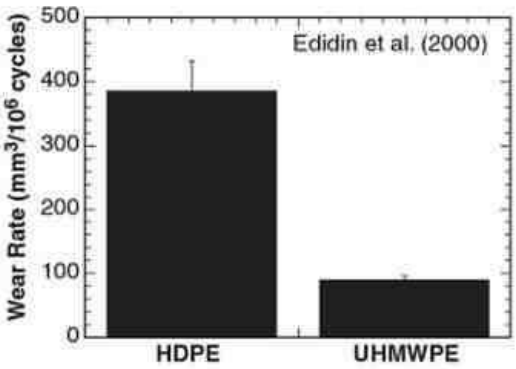

Figure II-7: Wear rate of HDPE and UHMWPE in multidirectional hip simulator [2, 6]

II.1.3 Deformation mechanisms

We describe here the deformation mechanisms occurring during the tensile deformation of polyethylene, which are at the origin of the texturing. Indeed, the stretching procedure of polyethylene implies first reversible mechanisms and then non-reversible mechanisms that lead to permanent deformation, and hence a texture. Generally, tension induces a gradual chain orientation process in amorphous layers and rotation, shear and fragmentation of crystalline lamellae [7, 8]. The elementary deformation mechanisms are reported below [3].

When stress is applied to the material, deformation occurs first in the amorphous phase that deforms by (Figure II-8):

- interlamellar shear,
- interlamellar separation, or
- interlamellar compression

The occurrence of these mechanisms depends on the orientation of the lamellae towards the stress. In particular, lamellae oriented perpendicular to tensile direction are subjected to interlamellar separation, lamellae oriented along tensile direction are subjected to interlamellae compression, while the lamellae oriented at 45° toward the tensile direction are subjected to interlamellar shear mechanism. For all the other configurations, the amorphous phase is subjected to a combination of these three elementary deformation mechanisms.

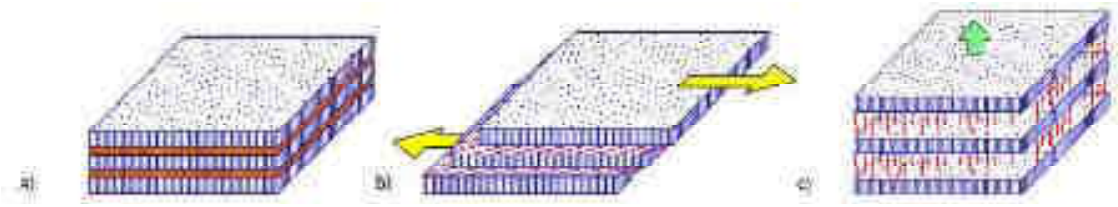

Figure II-8: Mechanisms of deformation of the amorphous phase in semi-crystalline polymers; a) undeformed state, b) interlamellar slip and c) interlamellar separation [3].

From a certain strain level, the stresses are transmitted from the amorphous chains to the crystalline ones via the tie molecules. This transition corresponds to the yield point. Then, the deformation appears within the crystalline phases and is characterized by intralamellar slip mechanisms parallel (chain slip) or perpendicular (transverse slip) to chain axis (Figure II-9). Note that chain slip requires less energy than transverse slip. The combination of all these elementary deformation mechanisms leads to a gradual orientation of the chain along the tensile direction and in the same time to a fragmentation of crystalline lamellae into small blocks (Figure II-10). The resulting microstructure is called micro-fibrillar morphology.

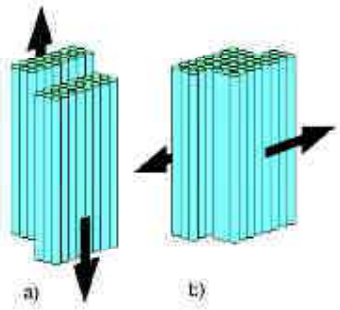

Figure II-9: The process of intralamellar sliding a) parallel b) perpendicular to the chains of crystalline lamellae [3].

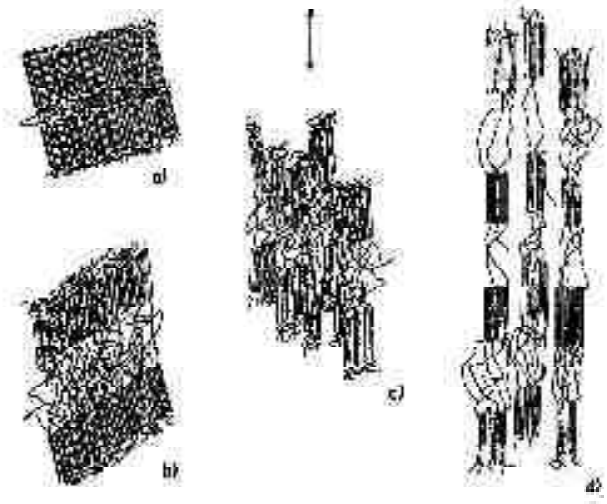

Figure II-10: Schematic representation of the mechanisms of fragmentation of crystalline lamellae; a) undeformed state, b) interlamellar separation and shear, c) intralamellar slip mechanisms and fragmentation of the lamellae, d) resulting microfibrillar morphology [9].

As regards UHMWPE, the intralamellar slip mechanisms are partially activated. Indeed, the high lamellae thickness, associated with an important number of entanglements in the amorphous phase, leads to a restriction of lamellae fragmentation. In particular, a bending mechanism of lamellae is active instead of a fragmentation which generates the formation of chevron-like lamellae (Figure II-11) [8].

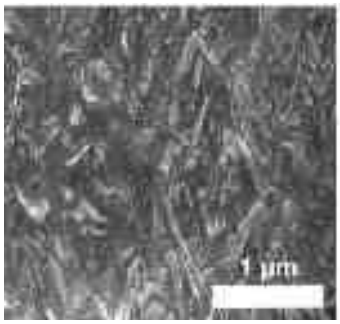

Figure II-11: Example of chevron type-patterns lamellae in UHMWPE strained up to a true axial strain of 1.3 [4]

II.1.4 Biomaterial application

Each year more than 800,000 total hip arthroplasty (THA) are performed worldwide [10]. THA enables the replacement of the two articular surfaces of a hip joint. The prosthesis consists of a rod implanted in the femur in contact with a prosthetic cup implanted in the hip. The materials used for the design of this hip replacement must address the following specifications:

- to be biocompatible, the ability to adapt to the biological media [11]. As this environment is generally very corrosive, a good corrosion resistance is also required;
- to have a high mechanical durability due to high cyclic stress during the movement [12];
- to have a high wear resistance and low friction to prevent the release of particles (wear debris) that may negatively affect the mechanical and the biological properties in the body (inflammatory reactions that lead to the release of osteolytic substances or loosening of the implant was observed by the isolation of macrophages containing wear debris). Currently, the debris appears as the main factor that dictates the lifetime of the prosthesis [13].

Depending on the element of the prosthesis, different materials are used (Figure II-12):

- the majority of the implanted cup are made of UHMWPE, some cups are on ceramic;
- materials used in the stem are made of titanium alloy (Ti6Al4V) or cobalt-chromium alloy (Co-Cr-Mo) or stainless steel (316L);
- prosthetic head can be made in Co-Cr-Mo and 316L or ceramic.

Figure II-12: Components of a total hip replacement [13]

The use of UHMWPE in total joint replacement prosthesis was introduced in the 1960s. Initially, polyetrafluoroethylene (PTFE) was used as a bearing material because of its low friction coefficient against metallic counterface but it exhibited high wear rate and hence important inflammatory reactions of the human body. Therefore, PTFE was replaced by UHMWPE, a material that has a lower wear rate than PTFE. It is foreseen that the demand of THA will increase within the next years, for both young and old patients. However, despite its good wear resistance, the durability of UHMWPE is not high enough and gives rise to an important number of prosthesis revisions [14, 15]. One of the scientific challenges is to reduce the revision rate of the prosthesis and hence to avoid additional burden for the patients and further cost for the health system.

II.2 Degradation mechanisms of UHMWPE

II.2.1 Degradation mechanisms by oxidation

During compression-moulding, it is quite difficult to avoid oxidation of the polymer, even when compression-molding is performed in the presence of an inert gas such as nitrogen [16]. In particular, hydroperoxides functions (ROOH) are present in the UHMWPE. These functions are thermally unstable since they can transform into hydroperoxides macroradicals ($ROO^{\cdot}$). The latter can react with oxygen which leads to a series of reactions, which involves an oxidation process.

The extent of this oxidative process depends on the number of radicals and the amount of oxygen in the polymer. Due to this oxidation, there is a significant decrease in molecular weight which results in lower mechanical properties and possible delamination mechanisms. In the case of THA, a sterilization procedure by gamma rays irradiation is performed on the polyethylene component to kill bacteria that could affect the patient. One drawback of this procedure is that free-macroradicals are formed and hence, react with oxygen given rise to a marked degradation [17, 18]. For both compression-molding and sterilization procedures, the polymer is exposed to oxygen and therefore to degradation. This degradation process is schematically shown in Figure II-13 by the cycle of Bolland.

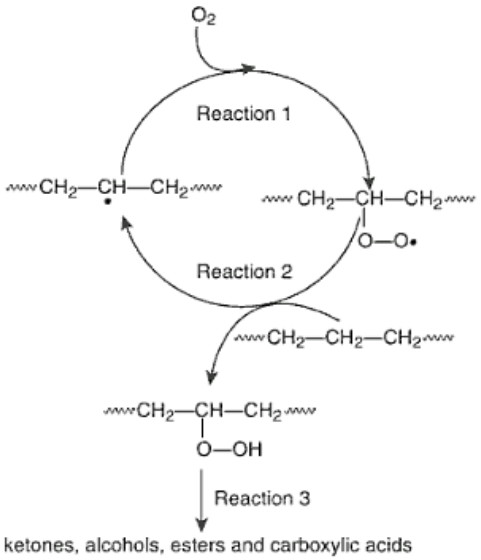

Figure II-13: Bolland's cycle [16]

In these reactions, the initial radical reacts with oxygen to form a peroxyl radical (reaction 1). After this step, the peroxyl radical may react with a neighbouring polymer chain to form a hydroperoxide (Reaction 2). Such a hydroperoxide is thermally unstable and decomposes photochemically into an alkoxide radical $PO^{\cdot}$ and a hydroxyl radical OH. Alkoxide radicals generated can evolve into ketones (-C = O), aldehydes (-CH = O), and alcohols (-C-OH) (Reaction 3). The aldehyde can oxidize very rapidly into acid (-COOH). The chemical functions present can be identified by FTIR.

II.2.2 Degradation mechanisms by wear

Abrasive wear, adhesive wear and fatigue wear have been identified as the three driving mechanisms which induce surface damage and deterioration of UHMWPE used as a bearing surface [19-21].

Abrasive wear produces surface topographies characterized by long grooves as the result of plastic deformation and rupture at the micron and sub-micron scales (microcutting). One can differentiate abrasive wear by two bodies or by three bodies. The two body abrasive wear occurs when a hard rough surface slides against a softer surface. The wear rate depends then on surface roughness of hard material and its relative hardness compared to that of the counterface material. In total joint replacements this form of wear is decreased by polishing the metallic counterface surface (for example Co-Cr in the case of THA). As regards three body abrasive wear, it occurs when hard particles are abraded onto two sliding surfaces. Generally hard abrading particles will be embedded in the softer material. In clinical cases, abrasive wear occurs when bone cement particles or metallic particles are present between the two sliding surfaces of a hip implant [22, 23].

Regarding adhesive wear, it is generally due to unwanted displacement and attachment of wear particles from one surface to another. This mechanism can be characterized by the release of wear particles and material transfer, as well as cohesive forces which hold the two surfaces together. This kind of wear is indicative of high frictional forces and is generally more prevalent between similar materials (i.e., metal against metal) [24].

Last, fatigue wear (or delaminating wear) mainly depends on the load and the number of cycles. The general sequence of events is as follows: the two sliding surfaces come into contact, asperity against asperity. The asperities of the softer material are deformed and some of them are fractured through repetitive loading resulting eventually in the formation of a smooth surface. Consequently there is no longer an asperity/asperity contact but an asperity/plane contact. Then, accumulation of

plastic shear deformation from repetitive loads takes place on the softer material due to the elongation of the hard asperities. Afterwards, crack nucleation takes place below the surface. Finally, these cracks propagate along the joining surface, coalesce, and propagate to the surface. This mechanism generates long and thin wear debris [24].

The study of wear in total joint replacement has taken two major routes, *in vivo* and *in vitro* [25]. For *in vivo* studies [26-29], attention is focused on the characterization of the wear features that caused the failure of prosthesis by studying the two sliding surfaces. In the case of THA, clinicians generally investigate the wear tracks of UHMWPE bearing component and the characteristics of the wear debris accumulated in the periprosthetic tissue. Regarding *in vitro* studies [28, 30-34], attention is devoted to the laboratory simulation of wear. Such studies are generally conducted to validate the formulation of a new material or a new prosthesis design prior to *in vivo* studies.

From the *in vivo* studies [26-29], it has been found that most prosthesis failures that required a revision were due to osteolysis phenomena. It was proved that the latter were linked to the reaction of macrophage toward the wear debris of the UHMWPE bearing component. The examination of explanted UHMWPE cup revealed the presence of large craters at the origin of the release of wear particles. Primarily, it was believed that these craters were due to abrasive wear mechanisms from the hard acrylic particles (bone cement). Indeed, the area surrounding the craters was generally scratched and some cement particles were found embedded in the polyethylene. Latter, it was found that craters were actually generated by the cyclic loading stresses that cause local plasticity mechanisms and fracture / fatigue crack propagation mechanisms. Local plasticity mechanisms imply first the formation of fibrils and then the breaking up of the latter, which leads to the formation of wear particles. A low fracture and/or crack propagation resistance leads to delamination and formation of large wear particles of the UHMWPE component. It is important to mention, that the smallest wear debris, that are considered as nanometric, leads to the most marked body reaction. The following Table II-3 reports the two basic wear mechanisms (fatigue wear and surface wear as shown in Figure II-14) occurring in hip prosthesis, but also in knee prosthesis.

Table II-3: Two basic wear mechanisms (fatigue and surface wear)

Type of wear mechanisms	Type of implant	Basic mechanisms description	References
Surface wear	In hip and knee implants (same proportion)	Local formation of polymer fibril due large deformation conditions, rupture of the fibrils and formation of wear particles, this phenomenon is due to the resistance of the polymer network to deformation (high strength is required)	[32, 35, 36]
Fatigue wear	Mainly in knee implant, less reported case for hip implant	Local formation of cracks below the surface, propagation and coalescence of the cracks, this phenomenon is due to a subtle combination of fracture and crack growth mechanisms	[37-39]

a) 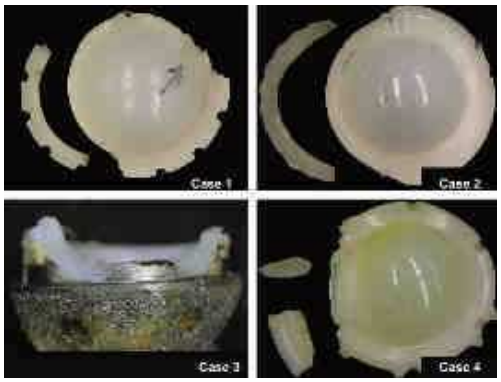

b) 

Figure II-14: a) Fatigue wear mechanism (4 reported cases corresponding to 4 different designs) [40], and b) surface wear mechanism [20, 41]

II.3 Improving wear resistance of UHMWPE

This part is focused on four aspects which dictate the chemical and mechanical durability of UHMWPE, namely oxidation, cross-linking, crystallinity and texturing. Oxidation phenomena are active during the polyethylene processing and in the human body, and significantly change the physical properties of the polymer network inducing a decrease of ductility. Such a decrease of ductility is not desirable for the wear mechanisms of UHMWPE. It is of fundamental importance to find a strategy to reduce oxidation. Regarding cross-linking, it is a method that is now well-accepted to reduce wear of UHMWPE due to an increase of the resistance to deformation of the molecular network. But, at the same time, the chemical stability, toughness and tensile strength decrease what is not suitable. To date, avoiding such drawbacks of cross-linking appears to be a scientific challenge. Last, some pioneer works [42-46] showed that acting on the initial crystallinity and orientation state of the chains (texture) can have positive effects on the mechanical strength and resistance to fracture of UHMWPE. Further research works are required regarding this last strategy.

II.3.1 Cross-linking by irradiation

Improving the wear resistance of UHMWPE through an irradiation step leads to an increase of the degree of cross-linking of the material. Cross-linking systematically occurs at high doses of gamma or electron radiation, while sterilization procedure of the cup is conducted at low irradiation doses. Note that irradiation changes the chemical structure of the polymer because of chain scission mechanisms (C-C and C-H bonds) and produces free radicals (Figure II-15). Two phenomena can then occur, namely i) a reaction between these radicals and oxygen of the environment (oxidation, Figure II-13), or ii) a reaction between radicals to form a covalent bond between adjacent chains inducing the formation of a 3D network (Figure II-16).

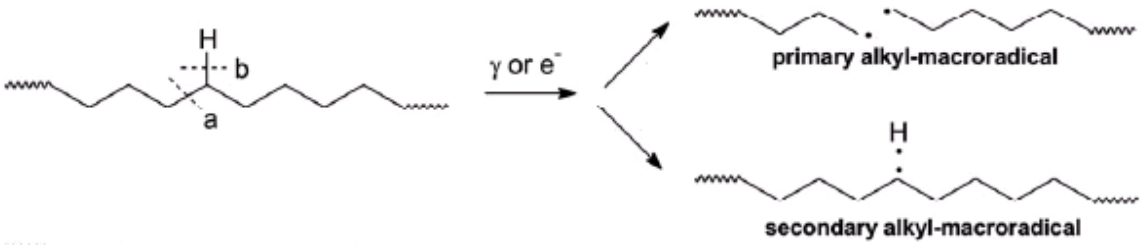

Figure II-15: The process of irradiation [16]

Figure II-16: The phenomenon of cross-linking [16]

Different authors [43, 47-53] studied the influence of irradiation and environment conditions on the physical and mechanical properties of UHMWPE. They compared for example a non-irradiated and an irradiated material (obtained by gamma irradiation) at different dose levels and found that the higher the irradiation dose was, the greater the wear resistance (Figure II-17). This was explained by a higher resistance of the molecular network to deformation, which reduces the formation of fibrils and hence of wear debris. However, other mechanical properties such as crack propagation resistance and fracture resistance decrease with increasing radiation dose. This phenomenon is explained by a lower activation of plasticity mechanisms in the case of cross-linked UHMWPE compared to the reference material (non cross-linked).

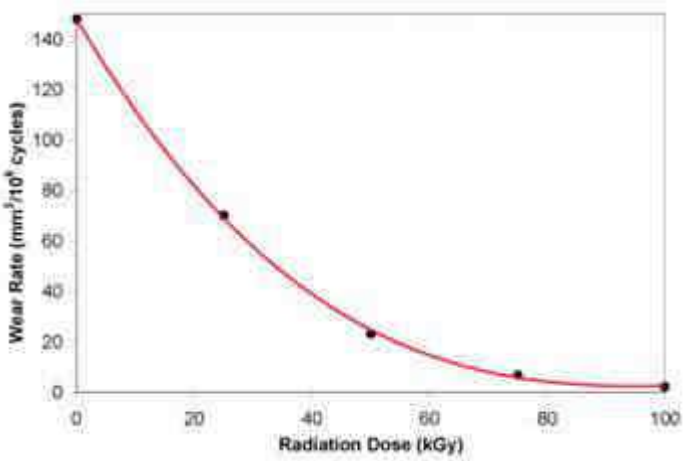

Figure II-17: Wear rate as a function of radiation dose [54]

Laurent et al.[55] characterized a UHMWPE with a high degree of cross-linking. Two samples were subjected to two different treatments, namely i) irradiation by electron beam (100 kGy) followed by annealing below the melting point and plasma sterilization (gas), and ii) sterilization by gamma irradiation. For the first sample, the absence of free radicals leads to an improvement of oxidation resistance, which is suitable regarding the stability of the mechanical properties.

Costa et al. [17] studied the initiation of oxidation by focusing on the chemical reactions created during oxidation. The aim of their work was to analyze the irradiated UHMWPE (electron beam) using different doses and in different atmospheres (vacuum / air / pure oxygen). They found an increased concentration of hydroperoxides (ROOH) as a function of irradiation dose at room temperature and in air. This increase seems to be due to the reaction of secondary alkyl macroradicals formed during irradiation with oxygen (Figure II-15). This chemical modification of UHMWPE leads to oxidation which is one of the main weak points in UHMWPE.

Dalborg et al. [56] analyzed the spatial distribution of oxidation using different characterization techniques. They studied the distribution of sites of oxidation by comparing light microscopy (staining of hydroperoxides by SO_2 (gas) and HCl (35% solution) followed by heat treatment (95 °C for 24 hours with SO_2 and 95 °C for 4 hours with HCl)), chemiluminescence and FTIR. They observed an inhomogeneity of the distribution of oxidation in the cup and noted a band of oxidation

just below the surface. They also observed an oxidation in the mass that is associated with poor consolidation of the material.

Lee et al. [57] studied in vivo the impact of irradiation (oxidation and cross-linking) on the wear resistance of UHMWPE. Irradiation increases the cross-linking density and the degree of crystallinity because the shorter chains have more mobility and can cross-link or recrystallize more easily than the initial macromolecules. At in-vivo level, oxidation and cross-linking of polyethylene are in competition to capture free radicals once created. Indeed, the authors found that the degree of oxidation (obtained by FTIR) increases with time and the degree of cross-linking (assessed by gel fraction measurements) decreases with time. They also found a decrease in wear resistance (wear test performed by unidirectional pin (UHMWPE)-on-disc (316L)) which is accompanied by the formation of a white area and a weakening of the material. The difference in behaviour between the degree of crystallinity and degree of cross-linking would imply that free radicals are still present in the material. These free radicals generate an intermolecular and intra-molecular decomposition resulting from a splitting of chains in the amorphous phase. These chains are rearranged and the degree of crystallinity (measured by DSC) increases. These changes in cross-linking, crystallinity, and oxidation obviously impact the mechanical properties. In this latter study, polyethylene wear has been associated with the existence of white strip of brittle fracture, a high degree of oxidation and a low percentage of cross-linking of the material.

The irradiation step is a source of oxidation, and therefore weakens the material, but many studies [17, 44, 45, 51-53, 57-63] have shown that irradiation is essential to obtain good tribological properties in terms of surface wear resistance. To limit the unwanted effects of cross-linking, the irradiation procedure must be associated with pre- or post-treatments of the material. To reduce or eliminate sources of free radical oxidation, the irradiated UHMWPE materials can be heated above (150 °C) or below (130 ° C) their melting temperature. Some authors, as Kurtz et al. [43, 53, 64] have shown that above the melting point (during a remelting step), the crystalline phase is destroyed and the amount of free radicals decreases because they combine to each other but the degree of crystallinity also decreases, which directly impacts the mechanical properties. Below the melting point (during an annealing step), the degree of crystallinity is not affected but free radicals are not totally eliminated, what causes oxidation. A compromise has in general to be found regarding the stabilization temperature or other treatments that are required.

These studies showed that a chemical modification of UHMWPE leads to oxidation which is one of the main weak points in hip prosthesis.

II.3.2 Addition of anti-oxidants

Some works deal with the addition of stabilizers to decrease or eliminate the oxidation process [17, 51, 65]. Oral et al. [51] introduced E-Vitamin into UHMWPE prior to irradiation. After irradiation, the splitting of the OH bond in the molecule of E-Vitamin leads to the formation of O radical and the hydrogen atom will react with the macroradical of UHMWPE as shown in Figure II-18. Oral et al. [51] indicated that less than 0.3 wt. % of E-Vitamin is recommended to preserve the wear resistance.

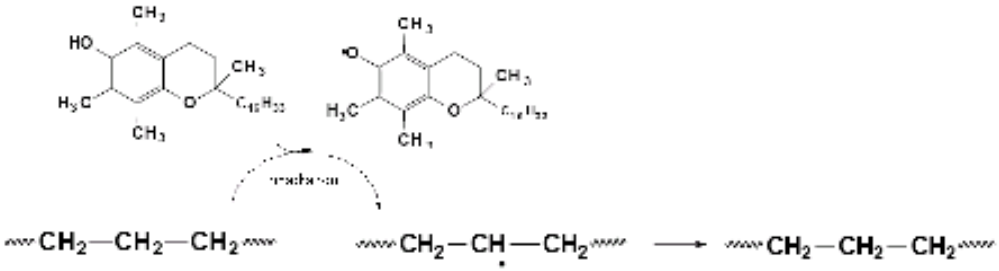

Figure II-18: Reaction between UHMWPE and vitamin E [51]

As already mentioned, the cross-linking density is an indicator of wear resistance, and it was found that cross-linking improves wear resistance. However, the cross-linking density decreases with increasing the concentration of E-vitamin. Further studies are needed to optimize the formulation and the processing of E-Vitamin / UHMWPE materials in terms of oxidation stability and surface wear resistance. It is to be highlighted that no stabilizer can be used in hip replacements according to ASTM F 648 [66]. Nevertheless, Ticona Company already supplies UHMWPE with E-vitamin for medical applications.

II.3.3 Modification of the initial microstructure

The crystallinity index is well-known to dictate most of the bulk mechanical properties of a semi-crystalline polymer as Young's modulus, yield stress, plasticity mechanisms and hence surface mechanical properties.

Karuppiah and al. [67] investigated the impact of crystallinity on the friction and wear of UHMWPE. In this context, two UHMWPE with two different degrees of crystallinity were analyzed. The degree of crystallinity was controlled by the processing of the material. In particular, the material was first slowly cooled in an air flow to promote crystal growth (high crystallinity), and in a second step the material was quenched in nitrogen to limit crystal growth (low crystallinity). The degree of crystallinity was determined by DSC: it is higher in the first case (55.1 %) than in the second case (45.6 %) and no significant variation between the skin and the core of the material was found. To analyze the influence of crystallinity on the surface mechanical behaviour of UHMWPE, different analysis techniques were used, namely:

i) The analysis of the topography by AFM showed a larger strip size when cooling is slower, and so, when the degree of crystallinity is higher (Figure II-19).

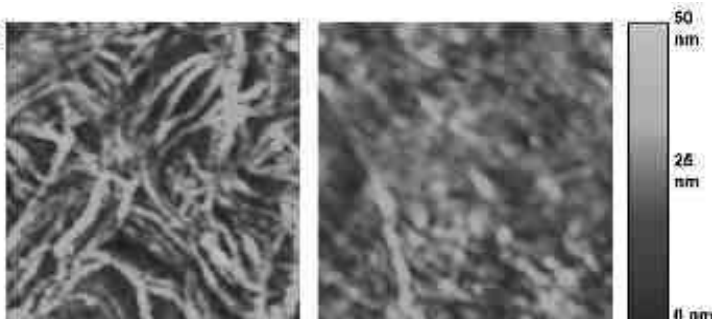

Figure II-19: Topography of samples at high (left) and low (right) index of crystallinity [67]

ii) The analysis by means of a micro-scratch tester revealed that the sample with a high degree of crystallinity has a higher scratch resistance (lower depth and width of the scratch groove)

and a higher friction force than the sample with a low degree of crystallinity. The same tendency regarding the scratch groove depth was obtained by AFM (Figure II-20).

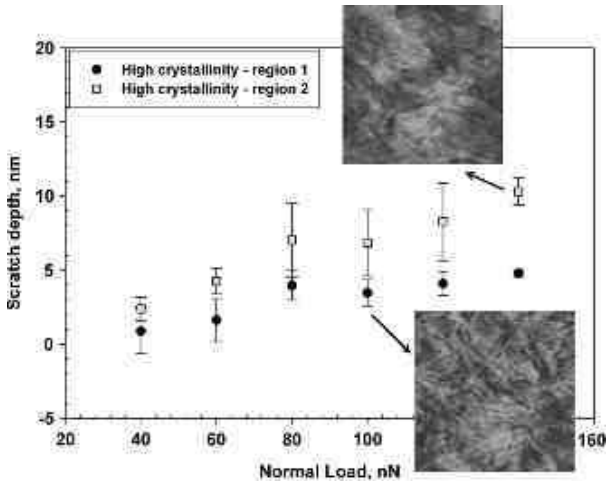

Figure II-20: Scratch depth in two different areas of the sample with a high degree of crystallinity (region 1, the blade shape of the crystalline phase is better defined than for region 2) [67]

The above points i) and ii) show that the lamellar structure affects the surface mechanical properties of the material.

UHMWPE has been recrystallized with different cooling conditions for the purpose of enhancing cross-linking extent of the polymer after γ-irradiation by Kang and Nho [68]. It was shown that the crystallinity of the irradiated samples increased with the irradiation dose. The irradiated UHMWPE after quenching had a lower sliding wear rate than the irradiated UHMWPE after recrystallization with slow cooling conditions, and the sliding wear rate of UHMWPE decreased with irradiation dose up to 250 kGy, resulting in about 40% of the wear rate of non-irradiated UHMWPE. From these experimental results, the authors expect that UHMWPE having the enhanced cross-linking after γ-irradiation will be used to extend the life time of the artificial joints.

Tribology tests [69] (reciprocating sliding, under dry conditions, done with a ball-on-plate configuration, spherical Si_3N_4 ball with a radius of ~ 1.2mm) showed that the lower the degree of crystallinity, the higher the friction force (Figure II-21). Ho and al. [69] suggested that this increase in friction with decreasing degree of crystallinity is due to the consequent decrease of the modulus of elasticity. Indeed, in semi-crystalline polymers, the crystalline phase is more rigid than the amorphous phase, what implies that the elastic modulus increases with increasing degree of crystallinity.

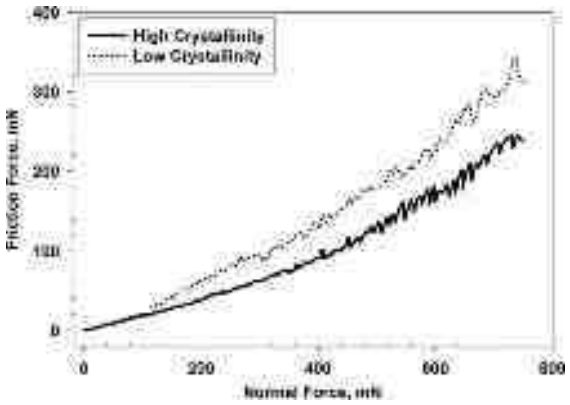

Figure II-21: Friction force as a function of normal force with a tribometer (reciprocating sliding, under dry conditions, done in a ball-on-plate configuration, spherical Si_3N_4 ball with a radius of ~ 1.2 mm) [67]

In addition, some sliding tests were conducted using the same configuration than the tribological tests (reciprocating sliding, under dry conditions, done in a ball-on-plate configuration, spherical Si_3N_4 ball with a radius of ~ 1.2 mm) and confirmed the previous tendency regarding the impact of crystallinity on frictional force.

The mechanical properties measured by nanoindentation (hardness and elastic modulus) showed that the higher the crystallinity, the higher the hardness and elastic modulus. These mechanical properties are directly related to the decrease in friction force observed by tribological testing and increased scratch resistance observed by scratch testing.

Pruitt et al. [52, 70, 71] modified the microstructure of UHMWPE by hot-pressing that leads to an increase of the crystallinity. This increase enhances the elastic modulus and hardness, improving the resistance to crack propagation by fatigue, and the tensile fracture resistance, and keeping a good wear resistance. The modification of crystallinity was associated with cross-linking. Three samples were analyzed, namely one reference sample, one hot-pressed sample (300 MPa at 180 °C for one hour), and one irradiated/stabilized/hot-pressed sample (gamma irradiation, 50 kGy, stabilization at 170 °C for 4 h and 125 °C for 48 hours, hot-pressed at 500 MPa at 240 °C for one hour with a cooling procedure carried out for 1 h at room temperature without pressure). This study demonstrated that the degree of crystallinity obtained by DSC increases with the pressure force of the hot-pressing procedure compared with the reference material. As shown by USAXS measurements, when the reference material is hot-pressed, crystal-growth is favoured with respect to crystal- nucleation. The opposite behaviour is observed when the cross-linked material is hot-pressed. Indeed, cross-linking appears as an obstacle to the growth of polyethylene crystals (the mobility of the molecules is reduced by the 3D network). In both cases, the UHMWPE was characterized by a higher crystallinity and crystal thickness than the reference material. It has been demonstrated that when the size of crystalline lamellae increases, the fatigue resistance of UHMWPE increases [52]. This result was linked to the increase in yield stress that dictates the initiation of the cracks.

Ohta et al. [44-46] studied the impact of the orientation state of the UHMWPE molecules to improve the wear properties of the material. The material was first subjected to a low dose (2.0 Mrad with γ-rays) of irradiation (cross-linking procedure). Then, the orientation state was obtained by a compression process performed at the melted state (temperature of the procedure 200 °C) by means of a ball to achieve the shape of a cup (Figure II-22). Different strain levels were reached (strain calculated by comparison between the final thickness and the initial thickness). The material was cooled down to room temperature.

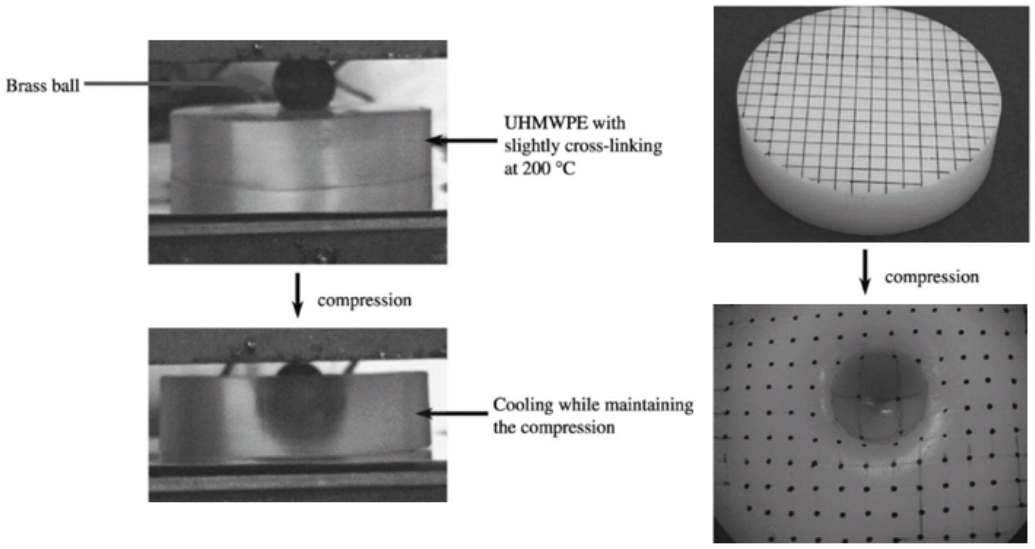

Figure II-22: Preparation of the UHMWPE sample by compression at molded state [46]

Ohta et al. [46] first examined the influence of the radiation dose on the cross-linking degree obtained by gel fraction. From a certain dose of irradiation (1.8 Mrad), the density of cross-links becomes more important and the orientation becomes more difficult to achieve. This threshold gives the optimum irradiation dose leaving sufficient mobility to the chains. The material properties assessed by DSC (melting temperature), XRD (crystallinity) and micro indentation (hardness) showed that an increase of the compression pressure causes an increase of the melting temperature, the index of crystallinity and the hardness. Wear tests were carried out in a tribometer plan (Co-Cr) - pin (UHMWPE) configured to perform reciprocating sliding tests. After the reciprocating sliding tests, the wear factor is improved for compressed samples by a factor of 5. The compressed samples appear harder than non-compressed samples in Vickers hardness measurements. It was found that what seems to improve the wear factor is not the crystallinity degree as a whole, but the crystal structure (molecular chains orientation) on the sample surface. The result indicates that the sliding wear rate decreases with increasing the compression strain. Moreover, it was found that the degree of crystallinity does not directly influence the wear resistance. What actually influences the sliding wear behaviour is the orientation state of the crystals imposed by the compression procedure, as shown by WAXD (Figure II-23). The increase in the degree of orientation leads to a decrease in the wear factor. However, little is known about these mechanisms.

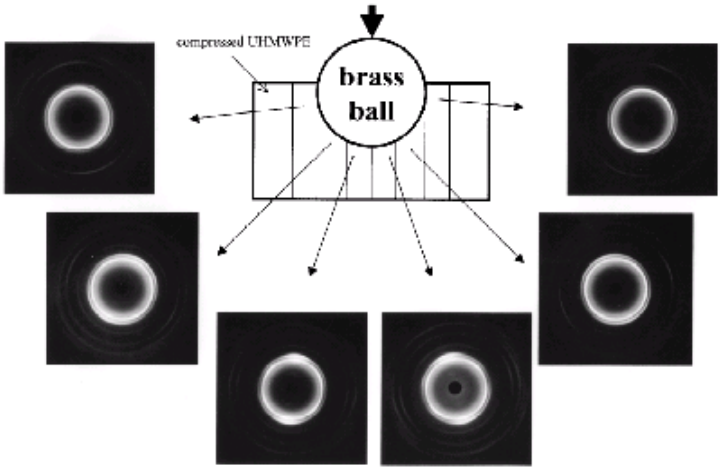

Figure II-23: Diffraction patterns depending on the point of deformation [46]

Texturing affects mechanical properties as strength, fracture resistance and fatigue crack propagation. The strength of semi-crystalline polymers is markedly affected by the orientation state of the chains (texture) that can be imposed by a solid-state deformation process. Indeed, compared to the non-deformed state, an initially-stretched UHMWPE has an increased strength when stretched parallel to the chain direction and a decreased strength when stretched perpendicular to the chain direction [10]. Therefore, textured semi-crystalline polymers can be considered as long-nanofibre polymer composites with a high number of connections between the fibres and the matrix and a high fatigue and fracture resistance in the fibre direction due to the high strength level in this direction. These new features can be appropriate for applications that require wear resistance to uniaxial tension. Thus, as suggested by Kurtz et al. [11], the cup in THA could be designed with the polar axis aligned with the texture direction. The wall of the cup at the equator and rim is hence parallel to the texture direction and may benefit to the high strength during eccentric and rim loading conditions. Nevertheless, UHMWPE component used in artificial joints are generally submitted to multiaxial loading conditions. A detailed study about the influence on the mass mechanical behaviour of the texture of such structural components is consequently required to assess whether solid-state deformation constitutes an effective treatment of UHMWPE in joint

prosthesis. Little is known about the influence of an initial molecular alignment of UHMWPE on the wear behaviour prior to cross-linking.

Li et al. [72, 73] investigated the wear behaviour of pre-compressed UHMWPE samples with a linear reciprocating tribometer using a ball-on-flat configuration. These authors showed that from a strain level of 20 %, the wear volume of pre-compressed UHMWPE significantly increased parallel to the chain direction (Figure II-24a) and decreased perpendicularly to the chain direction (Figure II-24b). Micromechanical models are used to predict the evolution of the microstructure and the improvement in wear resistance during processing. Predicted results agree well with experimental data. These models may help the materials designer to optimize processing to achieve a better sliding wear behaviour along desired directions.

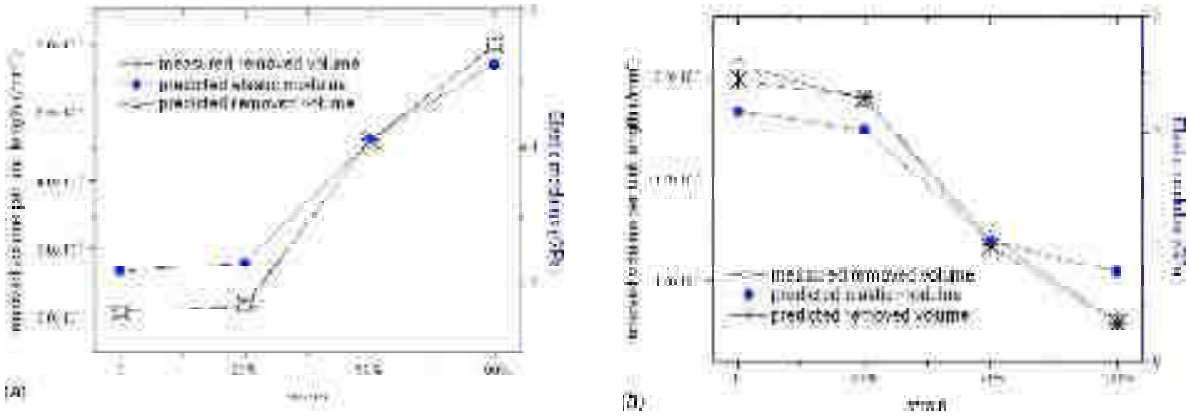

Figure II-24: Measured and predicted wear behaviour and predicted elastic modulus of UHMWPE on the plane parallel to the compression direction (a) along the direction parallel to the compression direction, and (b) along the direction perpendicular to the compression direction [72]

However, the previous study does not provide any wear mechanism in terms of dissipated energy and topographical features. Furthermore, the sliding wear tests performed in this previous study (high track length) were not representative of the relative motion in the hip (low track length due to fretting).

II.4 Conclusions

This literature review points out that the use of UHMWPE as biomaterial in THA must address numerous specifications regarding physical properties, chemical properties, bulk and surface mechanics, and biological aspects, which represents a complex topic of research. Current scientific challenges are to increase the chemical and mechanical durability of UHMWPE to decrease the revision rate of the implants due to the failure of this material. One treatment of interest for UHMWPE is texturing since i) it does not alter the chemistry of the material, ii) it is an easy and well-controlled process, and iii) texturing can increase resistance to fracture and resistance to crack propagation and hence can decrease fatigue wear. This treatment can also be suitable to increase the mechanical strength of UHMWPE in the chain direction for particular conditions, which can be favourable. Regarding surface wear mechanisms, little is known about the influence of chain orientation on the formation of wear debris. Further researches are needed to assess whether surface texturing would be a relevant treatment of UHMWPE in the context of medical implants.

II.5 References

[1] www.uhmwpe.org.

[2] K. Steven M, Chapter 1 - A Primer on UHMWPE, in: The UHMWPE Handbook, Academic Press, San Diego, 2004, pp. 1-12.

[3] F. Addiego, Caractérisation de la variation volumique du polyéthylène au cours de la déformation plastique en traction et en fluage, (2006).

[4] F. Addiego, O. Buchheit, D. Ruch, S. Ahzi, A. Dahoun, Does Texturing of UHMWPE Increase Strength and Toughness?: A Pilot Study, Clinical Orthopaedics and Related Research®, 469 (2011) 2318-2326.

[5] K. Steven M, M.K. Steven, P.D. Ph.D.A2 - Steven M. Kurtz, Chapter 2 - From Ethylene Gas to UHMWPE Component: The Process of Producing Orthopedic Implants, in: UHMWPE Biomaterials Handbook (Second Edition), Academic Press, Boston, 2009, pp. 7-19.

[6] A.A. Edidin, S.M. Kurtz, Influence of mechanical behavior on the wear of 4 clinically relevant polymeric biomaterials in a hip simulator, Journal of Arthroplasty, 15 (2000) 321-331.

[7] R. Seguela, F. Rietsch, Tensile drawing behaviour of a linear low-density polyethylene: Changes in physical and mechanical properties, Polymer, 27 (1986) 532-536.

[8] F. Detrez, S. Cantournet, R. Seguela, A constitutive model for semi-crystalline polymer deformation involving lamellar fragmentation, Comptes Rendus Mécanique, 338 (2010) 681-687.

[9] J. Petermann, J.M. Schultz, Lamellar separation during the deformation of high-density polyethylene, Journal of Materials Science, 13 (1978) 50-54.

[10] P. Ramos-Cabrer, J.P.M. van Duynhoven, A. Van der Toorn, K. Nicolay, MRI of hip prostheses using single-point methods: In vitro studies towards the artifact-free imaging of individuals with metal implants, Magnetic resonance imaging, 22 (2004) 1097-1103.

[11] G. D.W, The Williams dictionary of biomaterials, Materials Today, 2 (1999) 29.

[12] F. Langlais, N. Belot, M. Ropars, H. Thomazeau, J.C. Lambotte, G. Cathelineau, Antibiotic cements in articular prostheses: current orthopaedic concepts, International Journal of Antimicrobial Agents, 28 (2006) 84-89.

[13] Rixrath, Contributions numériques à l'étude de l'usure des prothèses totales de hanche, (2008).

[14] T. Masaoka, I.C. Clarke, K. Yamamoto, J. Tamura, P.A. Williams, V.D. Good, H. Shoji, A. Imakiire, Validation of volumetric and linear wear-measurement in UHMWPE cupsâ€"a hip simulator analysis, Wear, 254 (2003) 391-398.

[15] G. Lewis, Polyethylene wear in total hip and knee arthroplasties, Journal of Biomedical Materials Research, 38 (1997) 55-75.

[16] L. Costa, P. Bracco, M.K. Steven, P.D. Ph.D.A2 - Steven M. Kurtz, Chapter 21 - Mechanisms of Crosslinking, Oxidative Degradation and Stabilization of UHMWPE, in: UHMWPE Biomaterials Handbook (Second Edition), Academic Press, Boston, 2009, pp. 309-323.

[17] L. Costa, I. Carpentieri, P. Bracco, Post electron-beam irradiation oxidation of orthopaedic Ultra-High Molecular Weight Polyethylene (UHMWPE) stabilized with vitamin E, Polymer Degradation and Stability, 94 (2009) 1542-1547.

[18] L. Costa, M.P. Luda, L. Trossarelli, E.M. Brach del Prever, M. Crova, P. Gallinaro, Oxidation in orthopaedic UHMWPE sterilized by gamma-radiation and ethylene oxide, Biomaterials, 19 (1998) 659-668.

[19] C. J, The tribology of natural and artificial joints: J.H. Dumbleton, Tribology International, 14 (1981) 246-247.

[20] J. L.Tipper, L. Richards, E. Ingham, J. Fisher, M.K. Steven, P.D. Ph.D.A2 - Steven M. Kurtz, Chapter 27 - Characterization of UHMWPE Wear Particles, in: UHMWPE Biomaterials Handbook (Second Edition), Academic Press, Boston, 2009, pp. 409-422.

[21] http://en.wikipedia.org/wiki/Wear.

[22] R.M. Gul, F.J. McGarry, C.R. Bragdon, O.K. Muratoglu, W.H. Harris, Effect of consolidation on adhesive and abrasive wear of ultra high molecular weight polyethylene, Biomaterials, 24 (2003) 3193-3199.

[23] N.S.M. El-Tayeb, Abrasive wear performance of untreated SCF reinforced polymer composite, Journal of Materials Processing Technology, 206 (2008) 305-314.

[24] H. John, The friction and lubrication of solids: F. P. Bowden and D. Tabor; published by Clarendon Press, Oxford, U.K., 1986; 374 pp.; price, Â£17.50, Wear, 130 (1989) 385.

[25] K. Steven M, M.K. Steven, P.D. Ph.D.A2 - Steven M. Kurtz, Chapter 5 - The Clinical Performance of UHMWPE in Hip Replacements, in: UHMWPE Biomaterials Handbook (Second Edition), Academic Press, Boston, 2009, pp. 43-53.

[26] J.M. Dowling, J.R. Atkinson, D. Dowson, J. Charnley, The characteristics of acetabular cups worn in the human body, J Bone Joint Surg Br, 60-B (1978) 375-382.

[27] D. Veigl, M. Slouf, E. Pavlova, I. Landor, Comparison of in vivo characteristics of polyethylene wear particles produced by a metal and a ceramic femoral component in total knee replacement, 78 (2011) 49-55.

[28] S. Affatato, L. Cristofolini, W. Leardini, P. Erani, M. Zavalloni, D. Tigani, M. Viceconti, A New Method of In Vitro Wear Assessment of the UHMWPE Tibial Insert in Total Knee Replacement, Artificial Organs, 32 (2008) 942-948.

[29] P.G. Ren, A. Irani, Z. Huang, T. Ma, S. Biswal, S.B. Goodman, Continuous infusion of UHMWPE particles induces increased bone macrophages and osteolysis, Clinical Orthopaedics and Related Research, 469 (2011) 113-122.

[30] S. Affatato, W. Leardini, M. Zavalloni, Hip Joint Simulators: State of the Art, in: Bioceramics and Alternative Bearings in Joint Arthroplasty, 2006, pp. 171-180.

[31] C.R. Bragdon, D.O. O'Connor, J.D. Lowenstein, M. Jasty, S.A. Biggs, W.H. Harris, A new pin-on-disk wear testing method for simulating wear of polyethylene on cobalt-chrome alloy in total hip arthroplasty, The Journal of Arthroplasty, 16 (2001) 658-665.

[32] C.R. Bragdon, D.O. O'Connor, J.D. Lowenstein, M. Jasty, W.H. Harris, Development of a new pin on disk testing machine for evaluating polyethylene wear, in: Transactions of the Annual Meeting of the Society for Biomaterials in conjunction with the International Biomaterials Symposium, 1996, pp. 788.

[33] O.K. Muratoglu, B.R. Burroughs, C.R. Bragdon, S. Christensen, A. Lozynsky, W.H. Harris, Knee Simulator Wear of Polyethylene Tibias Articulating against Explanted Rough Femoral Components, Clinical Orthopaedics and Related Research, 428 (2004) 108-113.

[34] M.A. Wimmer, C. Sprecher, R. Hauert, G. TÃ¤ger, A. Fischer, Tribochemical reaction on metal-on-metal hip joint bearings: A comparison between in-vitro and in-vivo results, Wear, 255 (2003) 1007-1014.

[35] M. Jasty, D.D. Goetz, C.R. Bragdon, K.R. Lee, A.E. Hanson, J.R. Elder, W.H. Harris, Wear of polyethylene acetabular components in total hip arthroplasty. An analysis of one hundred and twenty-eight components retrieved at autopsy or revision operations, Journal of Bone and Joint Surgery - Series A, 79 (1997) 349-358.

[36] C.R. Bragdon, D.O. O'Connor, J.D. Lowenstein, M. Jasty, W.D. Syniuta, The importance of multidirectional motion on the wear of polyethylene, Proceedings of the Institution of Mechanical Engineers, Part H: Journal of Engineering in Medicine, 210 (1996) 157-165.

[37] H. Shoji, R.D. D'Ambrosia, P.R. Lipscomb, Failed polycentric total knee prostheses, Journal of Bone and Joint Surgery - Series A, 58 (1976) 773-777.

[38] D.L. Scott, P.A. Campbell, C.D. McClung, T.P. Schmalzried, Factors contributing to rapid wear and osteolysis in hips with modular acetabular bearings made of hylamer, Journal of Arthroplasty, 15 (2000) 35-46.

[39] C.H. Geerdink, B. Grimm, R. Ramakrishnan, J. Rondhuis, A.J. Verburg, A.J. Tonino, Crosslinked polyethylene compared to conventional polyethylene in total hip replacement: Pre-clinical evaluation, in-vitro testing and prospective clinical follow-up study, Acta Orthopaedica, 77 (2006) 719-725.

[40] J. Furmanski, M. Anderson, S. Bal, A.S. Greenwald, D. Halley, B. Penenberg, M. Ries, L. Pruitt, Clinical fracture of cross-linked UHMWPE acetabular liners, Biomaterials, 30 (2009) 5572-5582.

[41] L. Richards, C. Brown, M.H. Stone, J. Fisher, E. Ingham, J.L. Tipper, Identification of nanometre-sized ultra-high molecular weight polyethylene wear particles in samples retrieved in vivo, Journal of Bone and Joint Surgery - Series B, 90 (2008) 1106-1113.

[42] S.M. Kurtz, D. Mazzucco, C.M. Rimnac, D. Schroeder, Anisotropy and oxidative resistance of highly crosslinked UHMWPE after deformation processing by solid-state ram extrusion, Biomaterials, 27 (2006) 24-34.

[43] P. Lisa A, Deformation, yielding, fracture and fatigue behavior of conventional and highly cross-linked ultra high molecular weight polyethylene, Biomaterials, 26 (2005) 905-915.

[44] M. Ohta, S.-H. Hyon, Y.-B. Kang, S. Murakami, S. Kohjiya, M. Oka, S. Tsutsumi, Effect of the compression ratio on wear properties of slightly cross-linked ultra-high molecular weight polyethylene, crystallized under uniaxial compression, Wear, 250 (2001) 145-151.

[45] M. Ohta, S.-H. Hyon, M. Oka, S. Tsutsumi, Wear resistance of lightly cross-linked ultrahigh-molecular-weight polyethylene crystallized from the melt under uniaxial compression, Wear, 225-229 (1999) 312-318.

[46] M. Ohta, S.-H. Hyon, S. Tsutumi, Control of crystalline orientation to enhance the wear resistance of ultra-high molecular weight polyethylene crystallization cups for artificial joints, Wear, 255 (2003) 1045-1050.

[47] S. Kurtz, F.J. Medel, M. Manley, (iii) Wear in highly crosslinked polyethylenes, Current Orthopaedics, 22 (2008) 392-399.

[48] S.M. Kurtz, O.K. Muratoglu, M. Evans, A.A. Edidin, Advances in the processing, sterilization, and crosslinking of ultra-high molecular weight polyethylene for total joint arthroplasty, Biomaterials, 20 (1999) 1659-1688.

[49] J.M. Martell, J.J. Verner, S.J. Incavo, Clinical performance of a highly cross-linked polyethylene at two years in total hip arthroplasty: a randomized prospective trial, The Journal of Arthroplasty, 18 (2003) 55-59.

[50] O.K. Muratoglu, C.R. Bragdon, D.O. Connor, M. Jasty, W.H. Harris, R. Gul, F. McGarry, Unified wear model for highly crosslinked ultra-high molecular weight polyethylenes (UHMWPE), Biomaterials, 20 (1999) 1463-1470.

[51] E. Oral, C. Godleski Beckos, A.S. Malhi, O.K. Muratoglu, The effects of high dose irradiation on the cross-linking of vitamin E-blended ultrahigh molecular weight polyethylene, Biomaterials, 29 (2008) 3557-3560.

[52] K.S. Simis, A. Bistolfi, A. Bellare, L.A. Pruitt, The combined effects of crosslinking and high crystallinity on the microstructural and mechanical properties of ultra high molecular weight polyethylene, Biomaterials, 27 (2006) 1688-1694.

[53] M.C. Sobieraj, S.M. Kurtz, C.M. Rimnac, Large deformation compression induced crystallinity degradation of conventional and highly crosslinked UHMWPEs, Biomaterials, 26 (2005) 6430-6439.

[54] S. Kurtz, Advances in UHMWPE. Society for Biomaterials Tutorial: Advances in Highly Crosslinked UHMWPE for Hip and Knee Replacement.

[55] M.P. Laurent, T.S. Johnson, R.D. Crowninshield, C.R. Blanchard, S.K. Bhambri, J.Q. Yao, Characterization of a Highly Cross-linked Ultrahigh Molecular-Weight Polyethylene in Clinical Use in Total Hip Arthroplasty, The Journal of Arthroplasty, 23 (2008) 751-761.

[56] M. Dalborg, K. Jacobson, S. Jonsson, Methods for determining the spatial distribution of oxidation in ultra-high molecular-weight polyethylene prostheses, Polymer Degradation and Stability, 92 (2007) 437-447.

[57] K.-Y. Lee, K.H. Lee, Wear of shelf-aged UHMWPE acetabular liners, Wear, 225-229, Part 2 (1999) 728-733.

[58] S. Affatato, B. Bordini, C. Fagnano, P. Taddei, A. Tinti, A. Toni, Effects of the sterilisation method on the wear of UHMWPE acetabular cups tested in a hip joint simulator, Biomaterials, 23 (2002) 1439-1446.

[59] I. Carpentieri, V. Brunella, P. Bracco, M.C. Paganini, E.M. Brach del Prever, M.P. Luda, S. Bonomi, L. Costa, Post-irradiation oxidation of different polyethylenes, Polymer Degradation and Stability, 96 (2011) 624-629.

[60] S.J. Gencur, C.M. Rimnac, S.M. Kurtz, Fatigue crack propagation resistance of virgin and highly crosslinked, thermally treated ultra-high molecular weight polyethylene, Biomaterials, 27 (2006) 1550-1557.

[61] O.K. Muratoglu, D.O. O'Connor, C.R. Bragdon, J. Delaney, M. Jasty, W.H. Harris, E. Merrill, P. Venugopalan, Gradient crosslinking of UHMWPE using irradiation in molten state for total joint arthroplasty, Biomaterials, 23 (2002) 717-724.

[62] M.C. Sobieraj, S.M. Kurtz, A. Wang, M.M. Manley, C.M. Rimnac, Notched stress-strain behavior of a conventional and a sequentially annealed highly crosslinked UHMWPE, Biomaterials, 29 (2008) 4575-4583.

[63] A. Wang, A. Essner, V.K. Polineni, C. Stark, J.H. Dumbleton, Lubrication and wear of ultra-high molecular weight polyethylene in total joint replacements, Tribology International, 31 (1998) 17-33.

[64] H. McKellop, F.-w. Shen, B. Lu, P. Campbell, Development of an extremely wear-resistant ultra high molecular weight polythylene for total hip replacements, Journal of Orthopaedic Research, 17 (1999) 157-167.

[65] D. Molina-Manso, E. Sandoval, J. Cordero, J. Esteban, Evaluation of the effect of vitamin e doped UHMWPE on biofilm development and infection using an in vivo experimental model, Journal of Physics: Conference Series, 252 (2011).

[66] ASTM F648 - 10a Standard Specification for Ultra-High-Molecular-Weight Polyethylene Powder and Fabricated Form for Surgical Implants.

[67] K.S. Kanaga Karuppiah, A.L. Bruck, S. Sundararajan, J. Wang, Z. Lin, Z.-H. Xu, X. Li, Friction and wear behavior of ultra-high molecular weight polyethylene as a function of polymer crystallinity, Acta Biomaterialia, 4 (2008) 1401-1410.

[68] P. Hyun Kang, Y. Chang Nho, The effect of irradiation on ultra-high molecular weight polyethylene recrystallized under different cooling conditions, Radiation Physics and Chemistry, 60 (2001) 79-87.

[69] S.P. Ho, R.W. Carpick, T. Boland, M. LaBerge, Nanotribology of CoCr-UHMWPE TJR prosthesis using atomic force microscopy, Wear, 253 (2002) 1145-1155.

[70] L. STEPHEN, Process of manufacturing ultrahigh molecular weight linear polyethylene Patents, E. I. Du Pont de Nemours and Company (US 500053 A 23-Mar-1990).

[71] S.L. A.R. Champion, K. Saum, E. Howard and W. Simmons,, The effect of crystallinity on the physical properties of UHMWPE, Trans Orthop Res Soc, 19 (1994) p. 585.

[72] D.S. Li, H. Garmestani, S. Ahzi, M. Khaleel, D. Ruch, Microstructure Design to Improve Wear Resistance in Bioimplant UHMWPE Materials, Journal of Engineering Materials and Technology, 131 (2009) 041211.

[73] D. Li, H. Garmestani, A. Chu, H. Ahzi, G. Alapati, M. Khatonabadi, O. Es-Said, M. Siniawski, L. Matrisciano, S. Ahzi, Wear resistance and microstructure in annealed ultra high molecular weight polyethylenes, Polymer Science Series A, 50 (2008) 533-537.

Chapter III

Experimental section

This chapter describes the UHMWPE used in this study, the procedure selected to consolidate and to texture UHMWPE, and the characterization techniques used in this study. In particular, characterization is focused on the chemical, microstructural, topographical, bulk and surface mechanical properties of the tested materials.

III.1 Preparation of UHMWPE

III.1.1 Consolidation by compression-moulding

The UHMWPE powder used in this study was produced by Ticona (Ticona GmbH, Oberhausen, Germany) under the reference GUR1050 (molecular weight of 5×10^6 g/mol). The powder having a particle size comprised between 100 µm and 200 µm was consolidated by compression moulding. A specific mould was designed to ensure a high consolidation and a homogeneous microstructure. To this end, a cylindrical mould made of brass was machined. Brass was selected due to its good thermal and mechanical properties (resistance to high pressure). Concerning the pressure control, the dimensions of the different parts of the mould as shown in Figure III-1 avoid a direct contact between the upper and central part of the mould, ensuring thus that the applied pressure is well transmitted to the polymer. By means of this mould, it is possible to obtain plates having different thickness ranging between 3 mm and 10 mm. A schematic representation of the designed mould is given in Figure III-1.

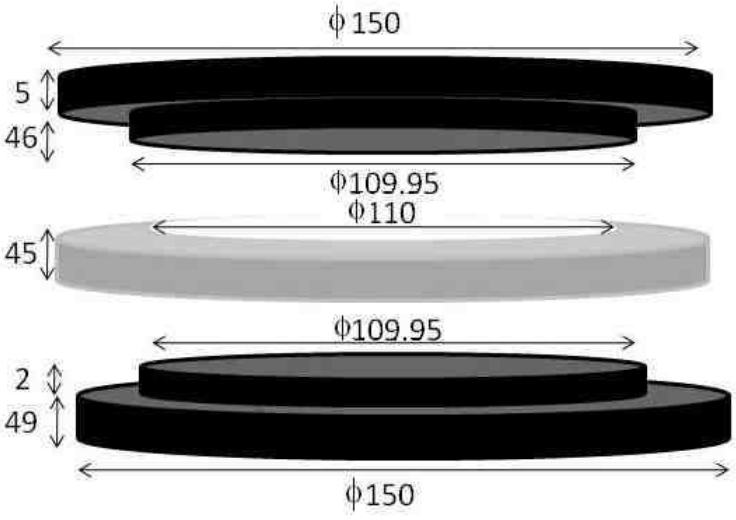

Figure III-1: Schematic representation of the designed mould (all the dimensions are in mm)

The specific mould was placed in a Carver laboratory press (Carver Inc, Wabash, IN, USA) equipped was heating plates (Figure III-2). The hot-pressing procedure consisted of a heating step performed at 240 °C during 30 min at a low pressure of 2.5 bars to facilitate inter-particle diffusion. Then, the pressure was set at 20 bars to increase the consolidation degree during 15 min at 240 °C. Subsequently, the material was cooled down to 23 °C at 20 bars using a water circulation within the press plates, and then the pressure was released. The final disc was 4 mm thick and 110 mm in diameter.

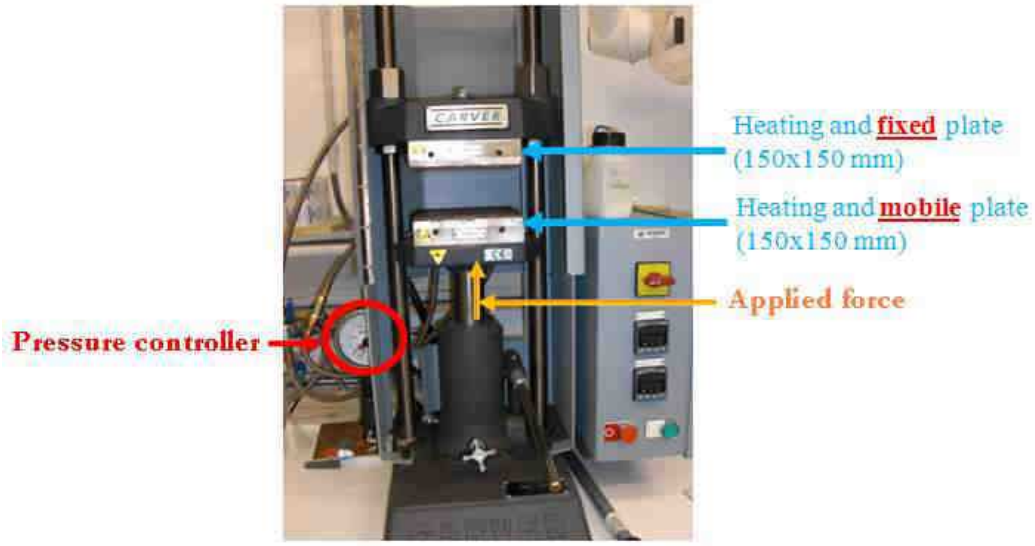

Figure III-2: Carver press equipped with heating plates

III.1.2 Texturing by uni-axial stretching

Texturing of UHMWPE was done by a uni-axial stretching procedure up to different strain levels. Rectangular tensile specimens with dimensions of 60 × 25 × 4 mm^3 (Figure III-3) were machined from the compressed disks using a computer-controlled milling machine (CharlyRobot CRA4). Note that the width of the central part of the specimens was reduced to 24 mm to localize deformation in this zone during the tensile tests. Due to the extremely high length of UHMWPE

chains, we expect a low necking process in contrast to the one occurring on HDPE which is very marked.

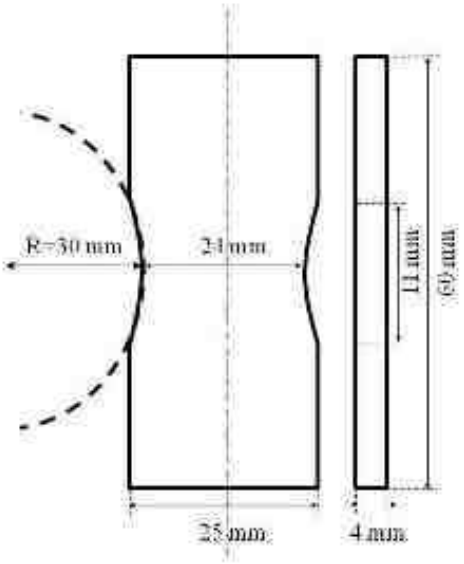

Figure III-3: Initial tensile specimen referred to as non-textured UHMWPE

The axial and transverse strains were accurately measured with an optical extensometer VidéoTraction system developed by Apollor SA (now ProVisys, INPL, Nancy, France) [1, 2]. This extensometer enables to measure the true axial strain (Hencky's definition), the true transverse strains assuming a transversal isotropy of the deformations, and the true axial stress. Moreover, a specific algorithm gives access to the local axial strain in the centre of the tensile specimen, although the axial strain localization is expected to be low for UHMWPE. It is important to mention that the VidéoTraction system allows to perform tests at constant axial strain rate by controlling the actuator of the tensile machine based on the real-time measurement of the axial strain. More details about this technique can be found in the paper by Addiego et al. [1]. This procedure is based on the monitoring of seven dot markers made of flexible fluorescence ink, printed on the front flat face of the sample as shown in Figure III-4. Five of these dots are aligned and equally spaced in the tensile direction, while the two others are aligned with the central dot along the transverse direction.

Figure III-4: Monitoring of markers printed on a tensile specimen
by means of VidéoTraction extensometer

The mechanical tests are carried out with a servo-hydraulic testing machine (MTS 810). The seven fluorescent markers are illuminated by an UV lamp, and monitored in real-time during the tensile test by means of a CCD camera (resolution 800 × 600 pixels) interfaced to a microcomputer through a video interface board (Genesis, Matrox, Canada). The used software calculated the centre of gravity of each marker and subsequently calculated four partial axial deformations between successive couples of axial dots, and two transverse deformations from the two successive couples of transverse dots. The axial strain is obtained from an interpolation of the deformations of the axial dots, while the transverse strain is the average of the deformations of the transverse dots. Also, the load cell and the actuator of the tensile machine are interfaced with the microcomputer to record the applied load, F_N, and to regulate the speed of the actuator, respectively, (Figure III-5). The tensile tests were done at 30 °C and at constant true strain rate 10^{-3} s^{-1}.

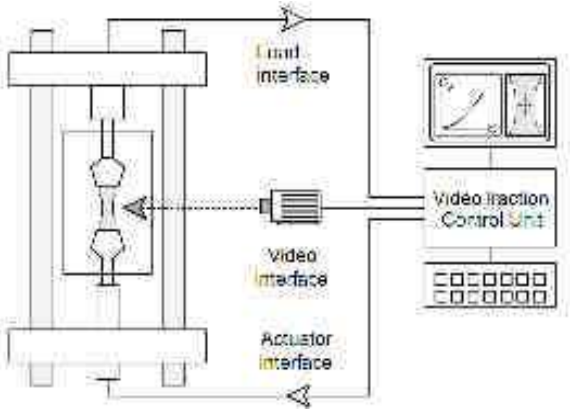

Figure III-5: General diagram of the VidéoTraction system [3]

It is important to note that we used a second stretching procedure for extremely high deformations (ε = 4) that could not be reached with the VidéoTraction system. To this end, tensile tests were conducted on an INSTRON testing machine equipped (model 8031) with an INSTRON strain gauge extensometer operated at a strain rate of 10^{-3} s^{-1} and at room temperature.

III.2 Characterization of UHMWPE

III.2.1 Chemical analysis by FTIR

Analysis by Fourier transform infrared spectroscopy provides information about the nature of chemical groups from the vibration of chemical bonds present in the material. This technique is commonly used in the case of UHMWPE to follow vibrational groups related to oxidation functions [4, 5]. A Bruker Optics Tensor 27 spectrometer in reflection mode (ATR) was used in this study (Figure III-6).

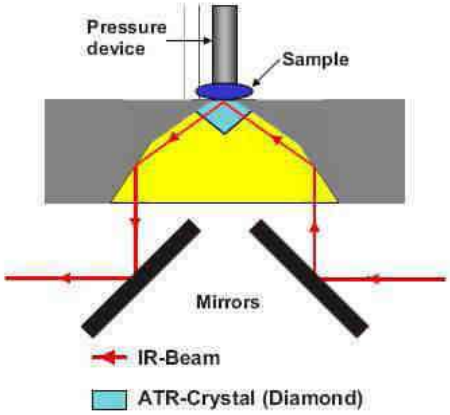

Figure III-6: Principle of the ATR mode

50 scans with a nominal resolution of 4 cm^{-1} from 400 cm^{-1} to 6500 cm^{-1} were recorded and averaged. A summary of the technical parameters used in this work is given in Table III-1.

Table III-1: Technical specifications

ATR crystal	Diamond Type IIa Diamond 45°, 2 mm × 2 mm
Wave number range	6500 - 400 cm^{-1}
ATR plate **Active Sampling Area**	Diamond brazed into, Tungsten Carbide Disc 0.8 mm in diameter
Depth of penetration	2.0 µm (for refractive index 1.5 material at 1000 cm^{-1})
Anvil **Aperture**	Sapphire having a width of 3.8 mm diameter 6 mm

III.2.2 Structural characterization by SEM, XRD and DSC

III.2.2.1 Scanning electron microscope

In a first step, the morphology evolution of the materials resulting from the texturing process was studied. For this purpose, samples were polished and etched for 18 h. Note that primarily the etching solution was set-up by Olley et al. [6] and then improved by Olley and Basset [7] to create nanometric topography by eliminating amorphous layer between crystalline lamellae for SEM observations. This solution consists of concentrated sulphuric acid (H_2SO_4, 98 %), pure orthophosphoric acid (H_3PO_4, 85 %) and potassium permanganate ($KMnO_4$) in quantities mentioned in Table III-2.

Table III-2: Composition of the etching solution

Components	**% weight**	**% volume**	**ρ (g/cm^3)**	**V (mL) for 120 mL**	**m (g) for 120 mL**
H_2SO_4 (98%)	65.8	65	1.83	78	-
H_3PO_4 (85%)	32.9	35	1.7	42	-
$KMnO_4$	1.3	-	-	-	2.81

This mixture produces an active substance O_3MnOSO_3H, while the orthophosphoric acid eliminates the artefacts formed on the polyethylene surface during the etching. The sample remains for 18 hours in the solution under stirring. Then the sample is rinsed to totally remove the residue of the etching solution. This procedure consists of rinsing the polymer sample as follows:

- rinsing in cooled and diluted (8 times) H_2SO_4
- rinsing in distilled water in ultrasonic bath
- rinsing in hydrogen peroxide H_2O_2
- rinsing in distilled water in ultrasonic bath
- rinsing in methanol

After etching, samples were carefully air dried.

Samples were characterized by WLI and SEM without conductive coating using a water pressure of 150 Pa.

In a second step, we analyzed the wear tracks features on non-textured and textured materials. Hereto, samples were gold sputtered prior to the observation in order to use the high-vacuum mode of the SEM. Such a procedure enables to use a low magnification (this is not possible with the pressure-controlled mode), and hence to visualize a large area which is the case for wear tracks.

The working distance is about 10 mm. The acceleration voltage is 10 kV and the pressure is about 10^{-3} Pa when samples are coated and is 6 kV and 150 Pa when samples are etched.

III.2.2.2 Small- and wide-angle x-ray scattering

The structural periodicities of UHMWPE in the range 0.1 nm – 100 nm were studied by small- and wide-angle x-ray scattering (SAXS/WAXS) using a Panalytical X'Pert Pro MPD configured with the transmission mode. The beam was generated at 40 kV and 45 mA by means of an x-ray tube equipped with a copper anode which enables to analyze the material periodicities with the Kα copper radiation (wavelength λ = 1.54 Å). As incident optics, we used a focusing mirror, and as secondary optics we utilized the PIXcel detector. A spinner was used as sample-holder which enables to analyze different azimuthal angles. The optics was used with specific slits to get a high signal of the sample and a low background in the 2θ angular range of interest. Table III-3 reports the detailed configuration of the equipment for the two methods.

Table III-3: Configuration of SAXS and WAXS experiments

Methods	SAXS	WAXS
Incident optics	**Focusing mirror** Divergent slit: 1/8° Antiscatter slit: 1/32° Mask : 4 mm	**Focusing mirror** Divergent slit : 1/2° Soller slit: 0.04 rad Antiscatter slit: 1/2° Mask : 2 mm
Sample holder	**Spinner** used with ϕ = 0°, 45° and 90°	**Spinner** used with ϕ = 0°, 15°, 30°, 45°, 60°, 75° and 90°
Secondary optics	**PIXcel detector** Mode receiving, 1 channel Antiscatter slit: 1/16°	**PIXcel detector** Mode scanning, 255 channels Soller slit: 0.04 rad (large) Antiscatter slit: 1/32°
Acquisition	2θ Range: 0.04° - 1° Step: 0.01° Time/step: 50 s Test duration: 1h20	2θ Range: 10° - 55° Step: 0.026° Time/step: 250 s Test duration: 30 min.

The experimental set-up is represented in Figure III-7. It has to be noted that the specimen is mounted on the spinner with tensile axis first perpendicular to the detection direction. This first position is called ϕ = 0°. Then, a rotation of the specimen is performed to analyze other azimuthal angles. The specific configuration of this equipment indicates that for each azimuthal angle, we record the scattering signal in the perpendicular direction.

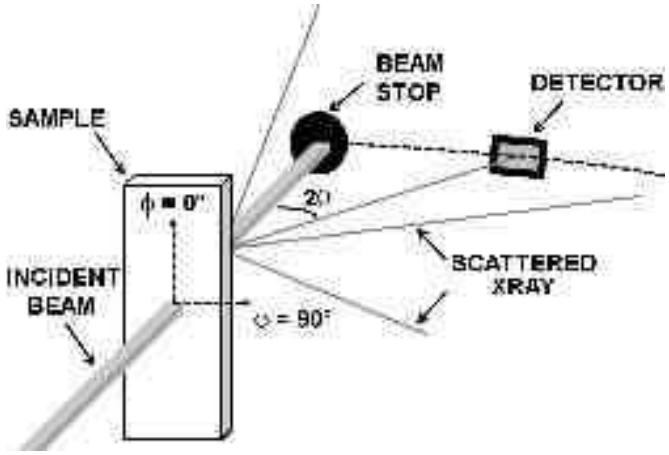

Figure III-7: Graphical representation of experimental set-up of SAXS and WAXS tests [8]

The analysis of WAXS diffractograms provides information about the crystalline structure of UHMWPE, and in particular information about the weight index of crystallinity X_{cw}, and the orientation state of the diffracting planes. In particular, X_{cw} was calculated based on the following relationship:

$$X_{cw} = \frac{C}{C + A} \qquad \text{III-1}$$

where C is the total area of the peaks resulting from crystalline plane reflection, and A is the area of the amorphous bump deduced from the analysis of WAXS diagrams.

Concerning SAXS curves, they provide information on the long spacing L_p of the crystalline lamellae / amorphous layers that depends on L_c, the thickness of crystalline lamellae, and L_a, the thickness of amorphous layers (Equation II-1).

The long spacing is deduced from the first order scattering peak position q_p of the crystalline lamellae on SAXS curves (scattering intensity Iq^2 vs. scattering vector q). The scattering vector q is calculated from the relationship:

$$q = \frac{4\,\pi \sin\theta}{\lambda} \qquad \text{III-2}$$

L_p is obtained from the equation:

$$L_p = \frac{2\pi}{q_p} \qquad \text{III-3}$$

The lamellae thickness can be calculated from the following relationship:

$$L_c = L_p \times X_{cv} \qquad \text{III-4}$$

where X_{cv} is the volume index of crystallinity. This parameter is assessed from the equation:

$$X_{cv} = X_{cw} \times \frac{\rho_c}{\rho} \qquad \text{III-5}$$

where ρ_c and ρ are the density of the material and of crystalline phase, respectively. As density of crystalline phase, we take ρ_c = 0.997 g/cm^3 [9]. The density of the material is calculated based on the relationship:

$$\rho = X_{cw} \times (\rho_c - \rho_a) + \rho_a \qquad \text{III-6}$$

where ρ_a is the density of amorphous phase that is equal to 0.854 g/cm^3 [9]. Note that for a homogeneous spatial distribution of the scattering dipoles (crystalline planes or crystalline lamellae), the values of L_p and X_{cw}, and hence of L_c calculated for one spatial direction ϕ can be representative of the overall material. But, in the case of textured materials, the latter assumption is no longer valid. Based on the work of Addiego et al. [1, 3], an averaged value of the index of crystallinity $<X_{cw}>$ of a textured polyethylene can be assessed as follow:

$$< X_{cw} > = \frac{\int_0^{90} X_{cw}(\phi) \times \sum I_c(\phi) \times \sin(\phi)}{\int_0^{90} \sum I_c(\phi) \times \sin(\phi)} \qquad \text{III-7}$$

where $X_{cw}(\phi)$ is the weight index of crystallinity calculated from a given azimuthal angle ϕ, and $\sum I_c(\phi)$ corresponds to the sum of the intensity (i.e. the amplitude) of all the peaks resulting from crystalline planes and amorphous bump on a WAXS diagram for a given azimuthal angle ϕ. The same procedure is used to calculate the average long spacing $<L_p>$:

$$< L_p > = \frac{\int_0^{90} L_p(\phi) \times I_p(\phi) \times \sin(\phi)}{\int_0^{90} I_p(\phi) \times \sin(\phi)} \qquad \text{III-8}$$

where $L_p(\phi)$ is the long spacing calculated for a given azimuthal angle ϕ, and $I_p(\phi)$ corresponds to the intensity (i.e. the amplitude) of the first order scattering peak of the lamellae on a SAXS diagrams for a given azimuthal angle ϕ.

Once known, $<L_p>$ and $<X_{cw}>$ are used to calculate $<X_{cv}>$, ρ and then $<L_c>$ based on the equations III-4, III-5 and III-6.

SAXS and WAXS diagrams recorded along a given azimuthal angle are treated by means of the software PeakFit.

The SAXS curves were treated as follows: i) absorption correction by means of Beer-Lambert approach:

$$I = I_o \times exp\left(\frac{\mu \times t}{cos(2\theta)}\right) \qquad \text{III-9}$$

where I is the corrected intensity, I_o is the uncorrected intensity, μ is the absorption coefficient of polyethylene taken equal to 3.85 cm^{-1} [1] and t is the specimen thickness, ii) plot of scattering intensity I vs. scattering vector q, Lorentz correction (plot of Iq^2 vs. q), and iii) deconvolution of the curves using Gaussian functions for the scattering peaks and for the background. An example of deconvolution of SAXS curve is shown in the Figure III-8 in the case of non-textured UHMWPE. The two Gaussian functions centred at q = 0.193 nm^{-1} and q = 0.386 nm^{-1} represent the first and second order scattering of the crystalline lamellae, respectively. The other Gaussian functions (one is centred at q = 0 nm^{-1}, a second is centred at 0.134 nm^{-1}, and a third is centred at 0.54 nm^{-1}) represent the background. The software PeakFit gives access to the equation of each Gaussian function, and hence, to the position q_p and amplitude I_p of the function corresponding to the first lamellae scattering peak.

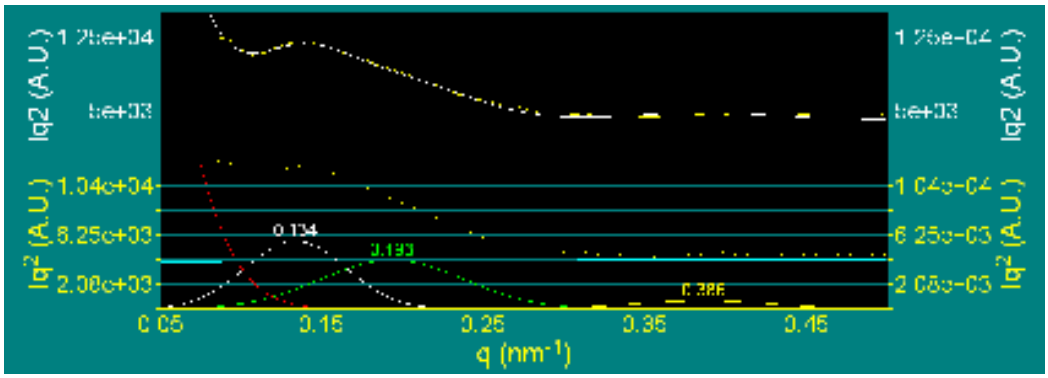

Figure III-8: Example of deconvolution of SAXS curve in the case of non-textured UHMWPE

WAXS diagrams are treated as follows: i) absorption correction based-on the Beer-Lambert approach (Equation III-8), ii) background-correction and iii) deconvolution of the curves by means of Gaussian function to fit the reflection peak of the crystalline planes and the scattering bump of amorphous phase [1]. An example of deconvolution is shown in the Figure III-9 in the case of non-textured UHMWPE. This example is focused on the main crystalline peak of polyethylene in terms of intensity that is in the 2θ range 15°-25°. It can be noted that in addition to the crystalline peaks of orthorhombic system (110) centred at 21.6° and (200) centred at 24°, we considered crystalline peaks of monoclinic phase (001) centred at 19.8° and (200) centred at 23°.

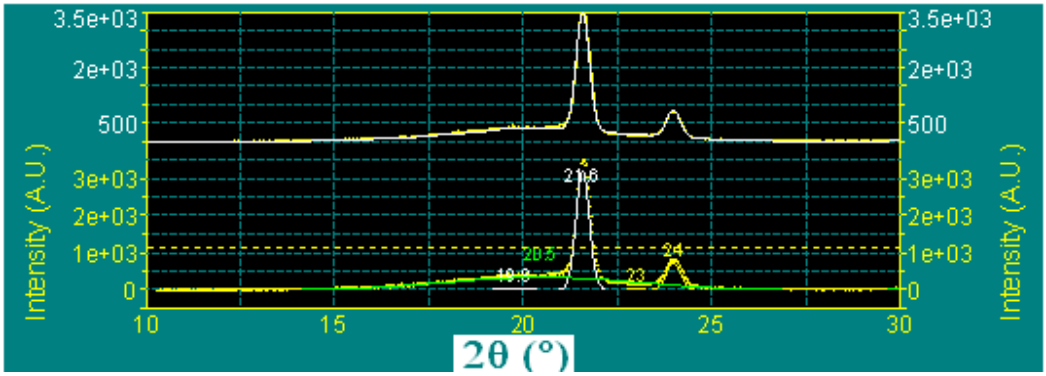

Figure III-9: Example of deconvolution of WAXS curve in the case of non-textured UHMWPE

III.2.3 Topographical characterization by WLI

The surface topography was analyzed with a white light interferometer (WLI) Wyko NT 3300 (Veeco Metrology Inc, Tucson, AZ, USA) on unworn and worn (after reciprocating sliding test) areas for non-textured and textured UHMWPE. By means of WLI, we get information about texturing mechanisms and wear/sliding mechanisms of UHMWPE. The principle of this technique consists of a vertical movement of the interferometer objective, i.e. perpendicularly to the measured surface and is represented in Figure III-10.

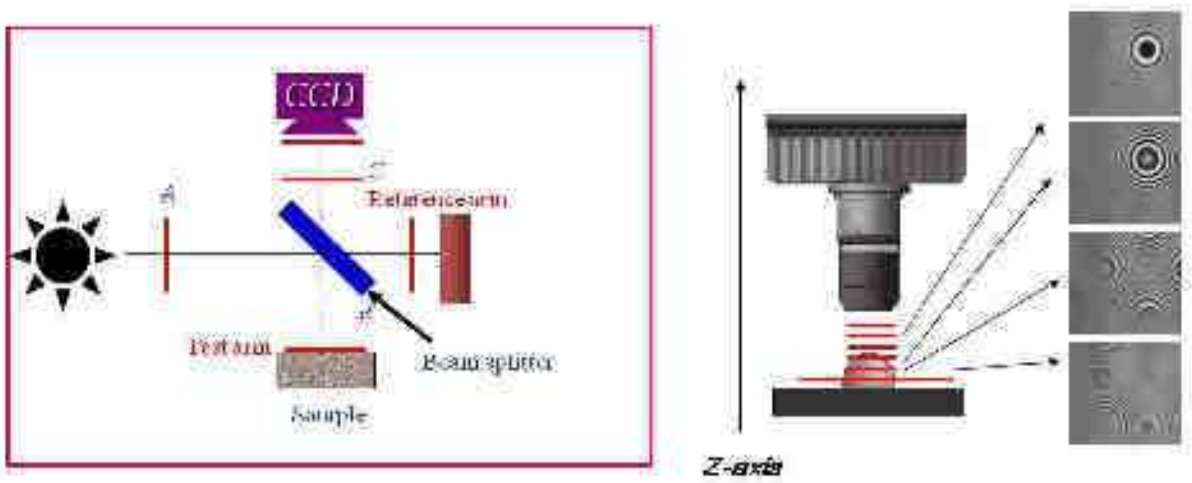

Figure III-10: White light interferometer principle

A CCD camera continuously records the light intensity of every measured point of the surface in the field of view. The recorded light intensity is a consequence of the combination of the light reflected on the surface with the light reflected on a reference mirror, and hence, it contains information about the height of the point (theory of the measurement can be found in Michelson interferometry principle). Light intensity is recorded every 40 nm vertical step and a mathematical modelling enables an accuracy for the height of the point as low as 10 nm. The surface roughness parameters considered in this work are reported in Table III–4, while the experimental parameters used with the WLI are listed in Table III–5.

Table III-4: Definition of the surface roughness parameters used in this study ("R" stands for parameters calculated in 2D, while "S" stands for parameters calculated in 3D)

Roughness parameters		Description
Amplitude	Ra/Sa	Arithmetic mean of absolute amplitude values
	Rq/Sq	Quadratic mean of amplitude values
	Rp/Sp	Height of the highest peak
	Rv/Sv	Depth of the deepest valley
	Rz/Sz	Mean height difference between the five highest peaks and the five deepest valleys
Symmetry	Rsk/Ssk	Symmetry of the amplitude distribution function relatively to the profile/surface mean line/plane, also called skewness
	Rku/Sku	Spikiness of the amplitude distribution function relatively to the profile/surface mean line/plane, also called kurtosis
Spacing	RSm	Horizontal distance between two peaks
	RTp/Smr	Bearing ratio at a given height (1/4 Rz here)
	RHSc/Spd	Peaks density
Hybrid	Rda/Sdq	Mean quadratic slope of the profile/surface
	Rlo/Sdr	Developed interfacial area ratio
	Ssc	Arithmetic mean curvature of the peaks

Table III-5: WLI parameters for unworn/worn material and wear track analysis

Wyko analysis by VSI mode	Objective	Analyzed area (mm^2)	Stitched area (mm^2)	Overlap (%)	Lateral resolution (μm)	Vertical resolution (nm)
Unworn material	×20; ×0.5	0.62 × 0.47	5 × 0.47	20	0.99	10
Worn material + wear track	×5; ×1	1.24 × 0.94	1.6 × 1.6	20	2.31	10

The choice of two different objectives was done based on the size of the unit area to be analyzed and subsequently to be stitched. This allows a characterizing unworn material along a small rectangular area (ISO 4288 procedure), while the worn area was characterized including some unworn area. For this last case, no standard procedure exists. To unravel the surface topography of the worn area, a filtering was carried out to remove the waviness from the profile due to the low wear resulting from the sliding test. The procedure consisted of acquiring the micro-relief in the wear track. To this end, data were treated with a Gaussian filter using a cut-off length of 8 µm with the software Mountains Map 5.1 (Digital Surf Company, Besançon, France). This software proposed a filter between 0.00576 and 0.797 mm. After a debucking, it was observed by eye that the worn surface started to be detected at around 0.02 mm. Then, step by step (0.001 by 0.001 mm), the best rationale that allowed to separate the waviness from the roughness and to observe all the worn areas was 0.008 mm. Focus was on the residue of the filtering to access and to characterize only the micro-relief of the surface. 2D-parameters were determined on unworn material as an average of 484 profiles. 3D topographical parameters of worn areas were determined through three measurements. Standard deviations for each topographical parameter are provided. It should be noted that only representative images are shown in the thesis manuscript.

III.2.4 Viscoelastic characterization by DMA

Viscoelastic properties of non-textured and textured UHMWPE were determined by dynamic mechanical analysis (DMA). DMA experiments were carried out by using a Netzsch DMA 242C equipment. Samples with dimensions 10x5x1 mm^3 were cut from UHMWPE samples (tensile specimen before and after stretching) and analyzed in tensile mode. The DMA experiments were performed from -180 °C to 120 °C at a heating rate of 1 $K.min^{-1}$, at frequencies of 0.1 Hz, 1 Hz, 10 Hz and 100 Hz and the samples underwent cyclic strain with fixed amplitude of displacement equal to 10 µm (dynamic force of 7 N, and static force of 0.2 N).

The two extreme parts of the specimen are clamped in a fixed and a moving clamp respectively. The measurements were repeated three times. The storage modulus and loss modulus (respectively E’ and E’’) were measured as a function of temperature and frequency. The storage modulus corresponds

to the stored energy, representing the elastic part of the mechanical response and the loss modulus corresponds to the energy dissipated into heat, representing the viscous part. The damping factor (tan δ) is the ratio of the loss modulus (E'') over the storage modulus (E').

III.2.5 Tribological characterization by reciprocating sliding

The tribological behaviour of non-textured and textured UHMWPE was studied in a reciprocating fretting mode which is one of the most representative motions in THA. In this context, the oscillatory motions responsible for friction are often induced by cyclic accelerations, cyclic stresses, acoustic noises, or by thermal cycling. The displacement used is a linear trajectory. A detailed representation of the fretting mode I is presented in Figure III-11.

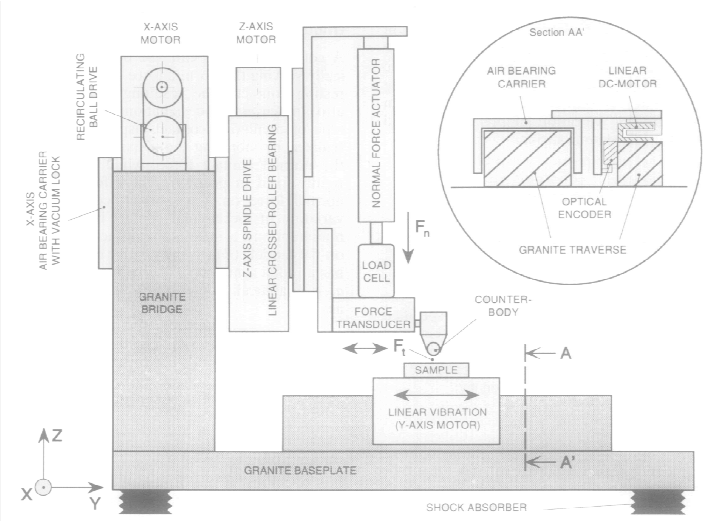

Figure III-11: Detailed representation of a tribometer configurated with the fretting mode I [10]

The hardware of the present fretting simulation device consists of an X-Y-Z positioning system, including an actuation mechanism for linear contact vibrations, and a control unit. A software terminal is implemented giving access to all hardware functions and processing the acquired

mechanical data on-line during fretting testing. The normal force pressing the counterbody against the sample is built up by compressing a double spring system having an effective stiffness of 1.06 N/mm. Accordingly, the normal force can be varied with increments of around 10^{-3} N up to a maximum of 20 N. The actual force magnitude is monitored by a precision load cell (type FGP FN3030). The counterbody is horizontally linked to the stage by a quartz force transducer (type Kistler 9203). This transducer is oriented parallel to the Y-axis and measures the friction force developed in the fretting contact. A schematic representation of the tribometer is shown in Figure III-12 for a ball-on-flat contact condition.

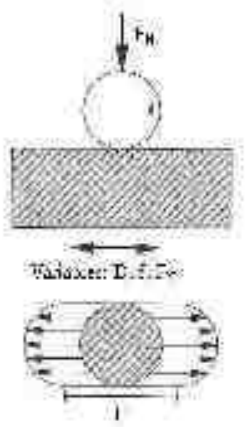

Figure III-12: Schematic representation of ball-on-flat contact geometry [11]

In mode I, friction is induced by a small amplitude displacement with constant frequency. The imposed normal force (F_N), displacement amplitude (D), and vibration frequency (f) are the external mechanical variables in such vibrating contacts. The contact displacement in fretting mode I can be “partial-slip” or “gross-slip”. In partial-slip regime, sliding is confined to an outer ring shaped zone called “slip annulus”, whereas the inner contact zone called “stick zone” deforms elastically. In gross-slip regime, sliding between mating solids occurs across the whole contact area. Laboratory fretting experiments reported in literature are mainly related to this fretting mode I testing.

The evolution of the mechanical contact response is monitored by acquiring force-displacement hysteresis loops at closely spaced time intervals during reciprocating sliding tests. There are six force-displacement coordinates of interest as indicated in Figure III-13.

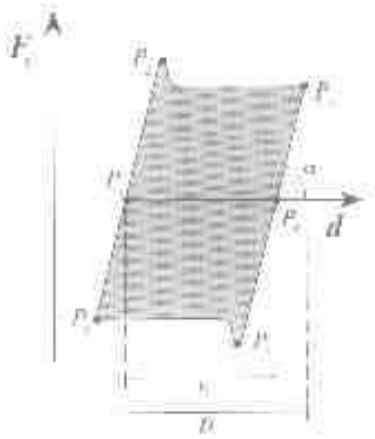

Figure III-13: Schematic representation of the hysteresis loop between the tangential force (F_t) and the contact displacement (d) observed in reciprocating sliding experiments [11].

The corresponding values for the displacement d and the tangential force f are selected from the loop data set by a straightforward search algorithm. This algorithm discriminates the minima (min) and maxima (max) of the displacement and tangential force values and also detects the two successive zero-crossings of the force signal. The six force-displacement coordinates are defined as:

$P_1 = [d, F_t = 0]$ $P_2 = [d, \max(F_t)]$
$P_3 = [\max(d), F_t]$ $P_4 = [d, F_t = 0]$ III-10
$P_5 = [d, \min(F_t)]$ $P_6 = [\min(d), F_t]$

The coordinate P7 consists of the loop area and the average normal force. The loop area is calculated by numerical integration of the n force-displacement data set as:

$$E_d = \sum_{i=2}^{n} \frac{1}{2}\left(d_{(i)} - d_{(i-1)}\right)\left(F_{t(i)} + F_{t(i-1)}\right) \quad \text{III-11}$$

The interdependence between the dissipated energy and the generation of surface damage has already been pointed out. Dissipated energy data can be further used to estimate the contact temperature during reciprocating sliding test and to evaluate the mechanical damping capacity of a vibrating contact. The coefficient of sliding friction (COF) is then defined as the ratio of the mean sliding force and the average normal force during a reciprocating sliding cycle.

III.3 Conclusions

We reported here the consolidation and the texturing procedures used to prepare test samples made of UHMWPE. The latter is conducted by uni-axial tensile testing using the VideoTraction extensometer system allowing an accurate measurement of the local deformation state of UHMWPE. The texturing mechanisms induce in this area can be identified by a multiphysical approach combining SEM, SAXS/WAXS, DMA, DSC and WLI. In particular, attention is focused on the index of crystallinity, long spacing, lamellae thickness, relaxation mechanisms, and topographical parameters. The textured samples will be subjected to reciprocating sliding testing to understand the impact of texture on the tribological behaviour. The wear behaviour will be analyzed by FTIR, WLI and SEM to assess the wear mechanisms and the wear volume.

III.4 References

[1] F. Addiego, A. Dahoun, C. G'Sell, J.-M. Hiver, Characterization of volume strain at large deformation under uniaxial tension in high-density polyethylene, Polymer, 47 (2006) 4387-4399.

[2] C. G'Sell, J.M. Hiver, A. Dahoun, A. Souahi, Video-controlled tensile testing of polymers and metals beyond the necking point, Journal of Materials Science, 27 (1992) 5031-5039.

[3] F. Addiego, Caractérisation de la variation volumique du polyéthylène au cours de la déformation plastique en traction et en fluage, (2006).

[4] P. Bracco, E.M. Brach del Prever, M. Cannas, M.P. Luda, L. Costa, Oxidation behaviour in prosthetic UHMWPE components sterilised with high energy radiation in a low-oxygen environment, Polymer Degradation and Stability, 91 (2006) 2030-2038.

[5] L. Costa, I. Carpentieri, P. Bracco, Post electron-beam irradiation oxidation of orthopaedic Ultra-High Molecular Weight Polyethylene (UHMWPE) stabilized with vitamin E, Polymer Degradation and Stability, 94 (2009) 1542-1547.

[6] R.H. Olley, A.M. Hodge, D.C. Bassett, A permanganic etchant for polyolefines, Journal of Polymer Science: Polymer Physics Edition, 17 (1979) 627-643.

[7] R.H. Olley, D.C. Bassett, An improved permanganic etchant for polyolefines, Polymer, 23 (1982) 1707-1710.

[8] F. Addiego, O. Buchheit, D. Ruch, S. Ahzi, A. Dahoun, Does Texturing of UHMWPE Increase Strength and Toughness?: A Pilot Study, Clinical Orthopaedics and Related Research®, 469 (2011) 2318-2326.

[9] B. Wunderlich, Crystal Structure, Morphology, Defects, Macromolecular Physics, Vol. 1, Academic Press, New York (1973).

[10] H. Mohrbacher, J.P. Celis, J.R. Roos, Laboratory testing of displacement and load induced fretting, Tribology International, 28 (1995) 269-278.

[11] H.M. Zahedul, Tribological behaviour of advanced titanium nitride-based mono- and multilayered coatings in vibrating contacts, (2001).

Chapter IV
Non-textured and textured UHMWPE: characteristics and performance under reciprocating sliding experiments

The study of friction and the resulting wear of a material is very complex since it depends on numerous parameters including i) the intrinsic properties of the two contacting materials (design, mechanical properties, topographical properties, chemical resistance…), ii) the friction conditions (load, temperature, rate/frequency, sliding geometry), and iii) the environment (use of a lubricant or not, relative humidity…). Thus, it is of fundamental interest to identify first the intrinsic properties of UHMWPE resulting from a texturing process. Then, the influence of several relevant experimental conditions on the sliding behaviour of UHMWPE is investigated. The attention is focused on the effect of normal load, initial surface roughness of UHMWPE, and deformation state of UHMWPE on the sliding behaviour of UHMWPE. After selecting the optimal conditions in terms of correlation with the human body conditions (load) and reduced dissipated energy, an in-depth study of the sliding behaviour of UHMWPE is conducted with attention devoted to the determination of sliding/wear mechanisms.

IV.1 Impact of solid-state deformation on the physical and mechanical properties of UHMWPE

IV.1.1 Solid-state deformation of UHMWPE

Texturing was carried out up to 4 tensile strain levels in the viscoplastic deformation stage that correspond to the true strains of 0.3, 0.6, 0.9 and 1.3. The latter are the maximum deformation levels reached by the specimen before unloading. Unfortunately, it was not possible to record the evolution of the specimen strain during the unloading procedure and eventually during a recovery period because of a slipping of the specimens in the tensile machine jaws just after starting the unloading. The real deformation state of the specimens is hence lower than that considered in this work due to the unloading and to the viscoelastic recovery. The true strain - true stress curves for the 4 different strain levels are shown in Figure IV-1, while the different samples studied in this section are referenced in Table IV-1.

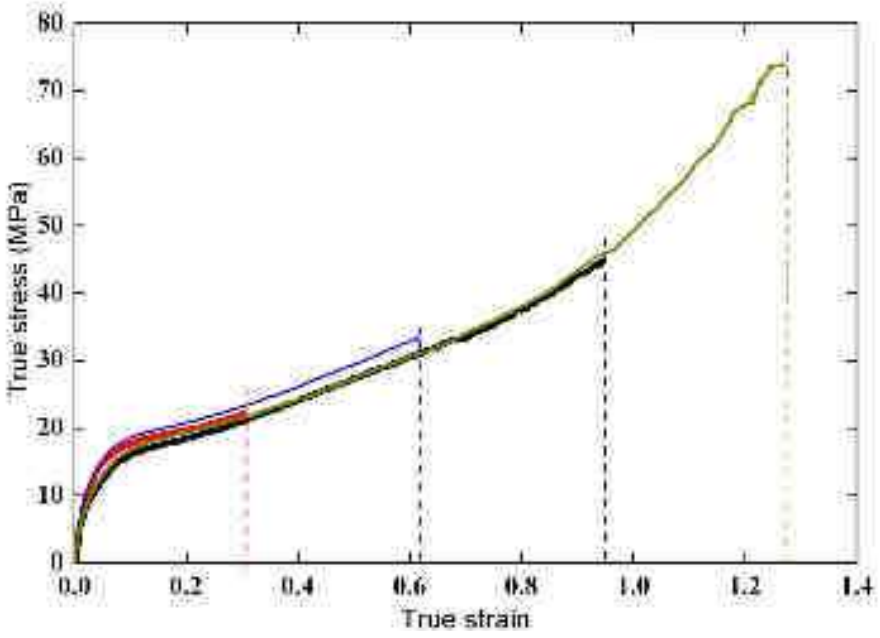

Figure IV-1: Stress-strain curves recorded using VidéoTraction

Table IV-1: Summary of the different samples

Name		Description
Non-textured samples	Non-textured	As hot-compressed specimens
Textured samples	Textured-0.3	Specimens stretched up to a true strain of 0.3 and then unloaded
	Textured-0.6	Specimen stretched up to a true strain of 0.6 and then unloaded
	Textured-0.9	Specimens stretched up to a true strain of 0.9 and then unloaded
	Textured-1.3	Specimens stretched up to a true strain of 1.3 and then unloaded

For example, the tensile specimens prior to the deformation and after a true axial strain up to 1.3 are given in Figure IV-2. One notes a marked reduction of the section of the tensile specimen, and a quite homogeneous sample width at the deformation state. Using the Instron device, the sample, called textured-4 is studied in the prospects, where the deformation level is higher.

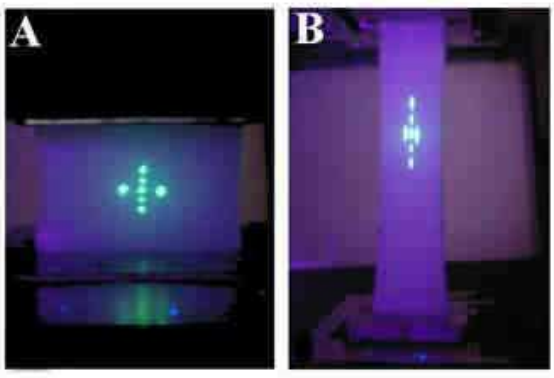

Figure IV-2: Follow-up of markers printed in the central zone of a tensile specimen a) prior to the deformation, and b) after a true axial strain $\varepsilon = 1.3$

IV.1.2 Evolution of structural properties with WAXS, SAXS and SEM

IV.1.2.1 WAXS investigation

The evolution of WAXS diffractogram of UHMWPE as a function of the azimuthal angle (ϕ) and the strain level is given in Figure IV-3. For each azimuthal angle, we provide the crystallinity based on the equation III-1 [1].

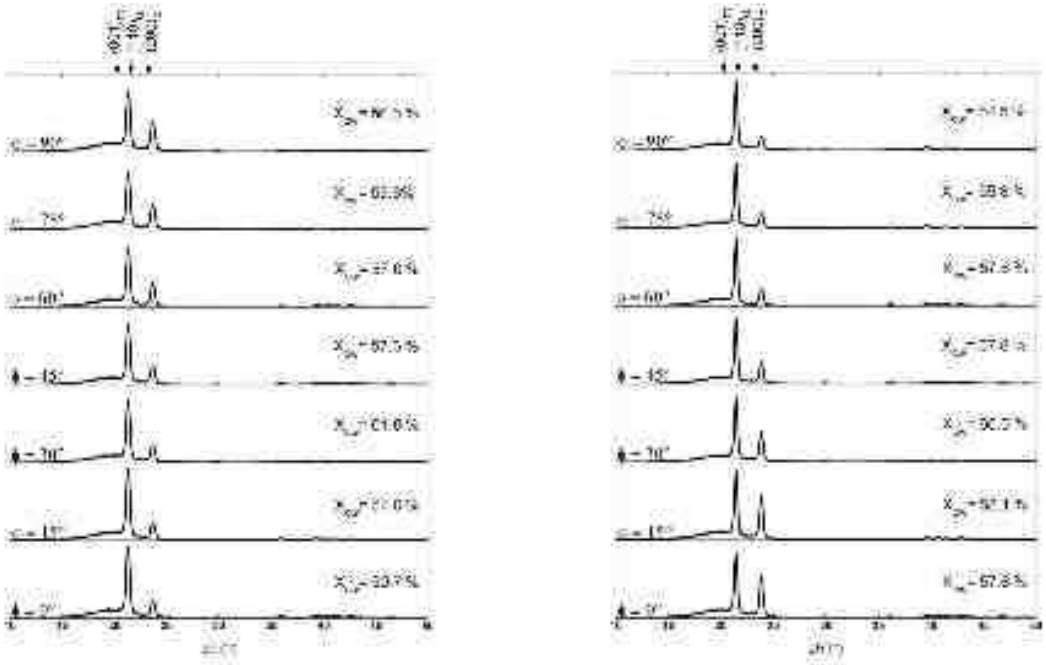

a) **ε = 0** b) **ε = 0.3**

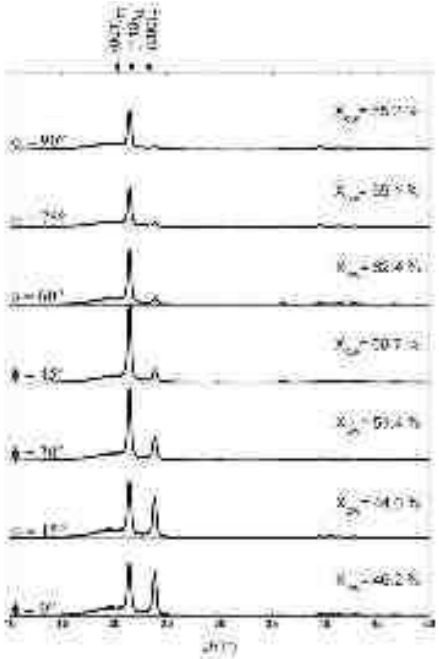

c) **ε = 0.6**

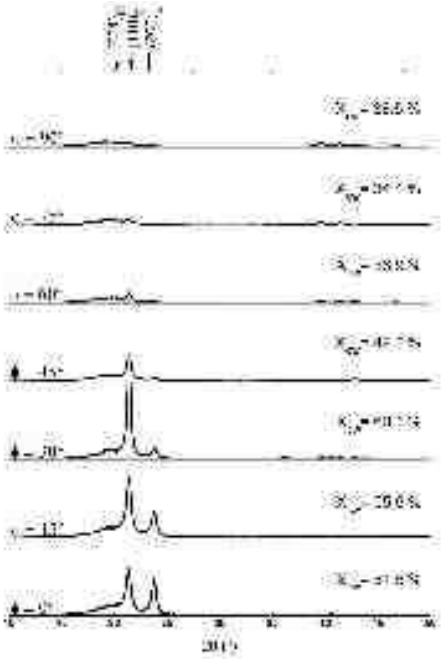

d) **ε = 0.9**

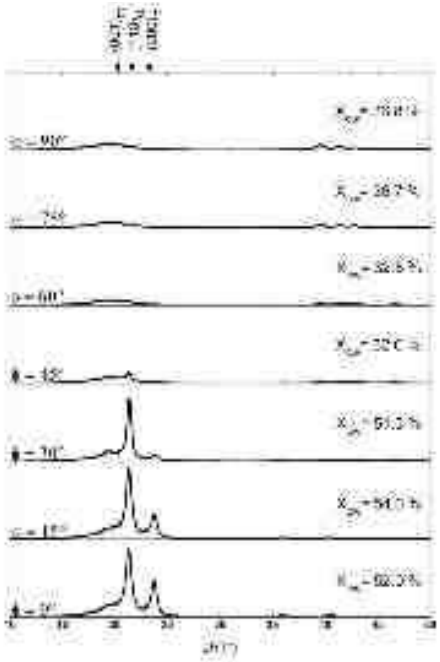

e) **ε = 1.3**

Figure IV-3: WAXS diffractograms for different azimuthal angles ϕ as a function of the axial strain ε

Before interpreting the WAXS diagrams, it should be noted that the WAXS mode of the equipment used does not allow us to record a signal at 2θ angles above 60°. As a result, the $(001)_o$ reflection of orthorhombic system centred at 75° could not be observed. The main observed peaks correspond to the planes $(110)_o$ and $(200)_o$ of the orthorhombic phase, and $(001)_m$ of the monoclinic phase.

The presence of $(001)_m$ peak of monoclinic phase centred at 2θ= 19° points out a partial martensitic transformation of the orthorhombic phase under stress or under fast cooling rates [2]. This phase transformation may be due in this study to the compression procedure. For the non-textured material and textured (ε = 0.3 and ε = 0.6), a homogeneous scattering intensity is obtained for both amorphous and crystalline phases in the two azimuthal angles of interest. This indicates a random spatial orientation of amorphous and crystalline scattering dipoles of non-textured material. For higher strain levels, the scattered intensity varies with the azimuthal angle, indicating preferred orientation phenomena. In particular, we note a gradual intensification of the scattered intensity at the azimuthal angle ϕ = 0° and on the contrary, a decrease of scattering intensity at ϕ = 90°. This result indicates a progressive orientation of polymer chain in the tensile direction.

We also observe a crystalline peak broadening with increasing deformation state, demonstrating a lowering of the crystalline lamellae size. SAXS analyses were used to accurately determine the crystalline lamellae size evolution of UHMWPE with deformation level. From these diffractograms and using the equation III-7, the average index of crystallinity was determined and plotted in Figure IV-4.

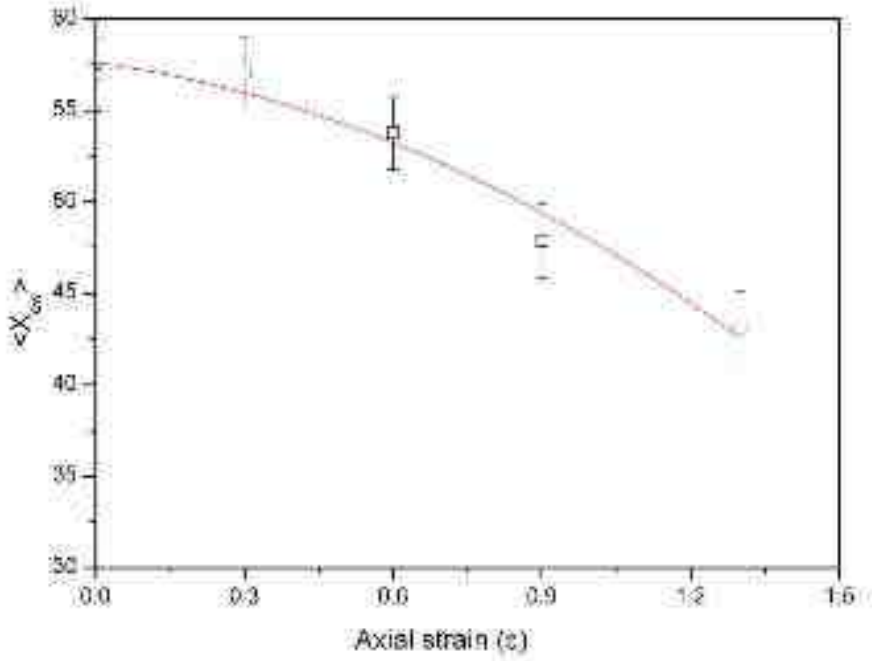

Figure IV-4: Average index of crystallinity $<X_{cw}>$ as a function of the strain level obtained from the analysis of WAXS diffractograms

For the non-textured UHMWPE (as hot-compressed), the index of crystallinity average is about X_{cw} = 57 %. With increasing strain level, the average crystallinity gradually decreases up to 43 % for ε = 1.3, which correspond to drop of about 25 %.

IV.1.2.2 SAXS investigation

The evolution of the SAXS diagrams of UHMWPE as a function of the azimuthal angle (ϕ) and axial strain (ε) is given Figure IV-5. During the deformation of the polyethylene, SAXS diagrams show the scattering by the crystalline lamellae when no cavitation occurs [3]. Before describing the curves, it is important to mention that what appears as the scattering peak of crystalline lamellae at q = 0.16 nm^{-1} for non-textured state Figure IV-5-a, is in reality the superposition of a background peak centred at 0.134 nm^{-1} and of the lamellae scattering peak centred at 0.193 nm^{-1} (see Figure IV-58). The background peak can be also observed in SAXS diagrams of stretched specimens

(Figure IV-5-d and e), while the scattering peak of the crystalline moved to higher q values, and hence, it is no longer superposed with the background peak. It can be seen that the SAXS diagrams are quite similar for the three azimuthal angles up from the non-textured state to the deformation state 0.6. We however note the lamellae peak recorded at $\phi = 90°$ slightly move to lower q value indicating an increase of the long spacing. For higher strain levels, the scattering peaks of the lamellae become more visible (no longer superposed with the background peak) and move to higher q value indicating a decrease in long spacing.

Regarding the intensity of lamellae scattering, it can be observed that for the highest deformation level:

- it is not equal to 0 at $\phi = 0°$ demonstrating the presence of lamellae oriented parallel to tensile direction
- it is maximum at $\phi = 90°$ showing that an important proportion of crystalline lamellae are oriented perpendicular to tensile direction
- a scattering intensity is recorded at $\phi = 45°$ indicating the presence of lamellae oriented at 45° with respect to the tensile direction.

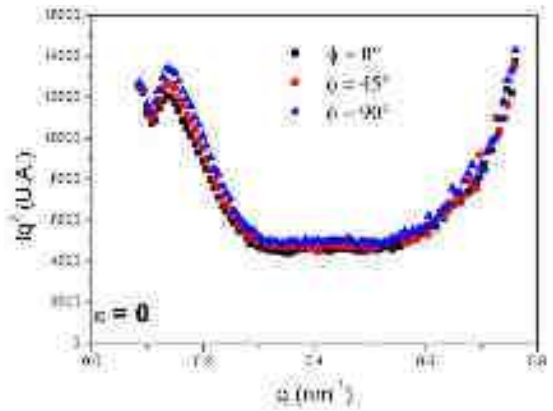

a)

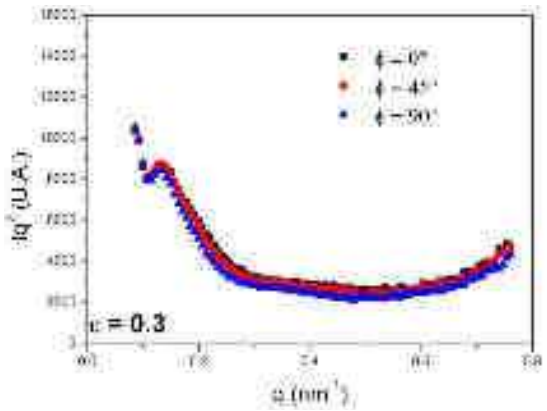

b)

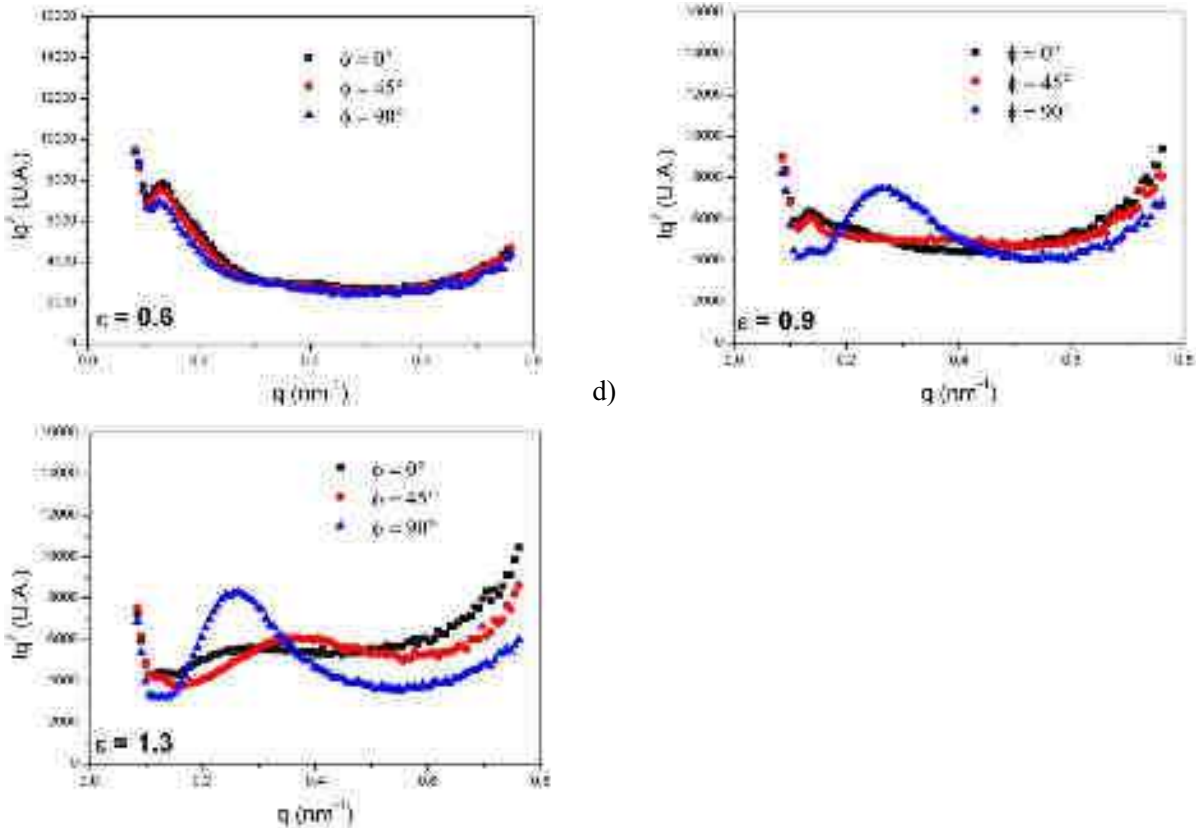

c) d) e)

Figure IV-5: Scattered intensity lq^2 as a function of scattering vector q for 3 different azimuthal angles in the case of non-textured (ε = 0), b) strained up to ε = 0.3, c) strained up to ε = 0.6, d) strained up to ε = 0.9 and e) strained up to ε = 1.3

From these SAXS diagrams and equations III-3, III-4 and III-8, the long spacing (or long period) at 3 tilt angles and the lamellae thickness as function of the axial strain (ε) are calculated and plotted in Figure IV-6. At the undeformed state, $<L_p>$ and $<L_c>$ are equal to 32.5 nm and 20 nm, respectively. The average long spacing and lamellae thickness lamellae are quite constant till ε = 0.6, then they both constantly decrease with the strain. For the highest deformation state ε = 1.3, the average long spacing is equal to 22 nm, which indicate an overall decrease of 32 %, while the average lamellae thickness is equal to about 10 nm, which corresponds to an overall decrease of 50 %.

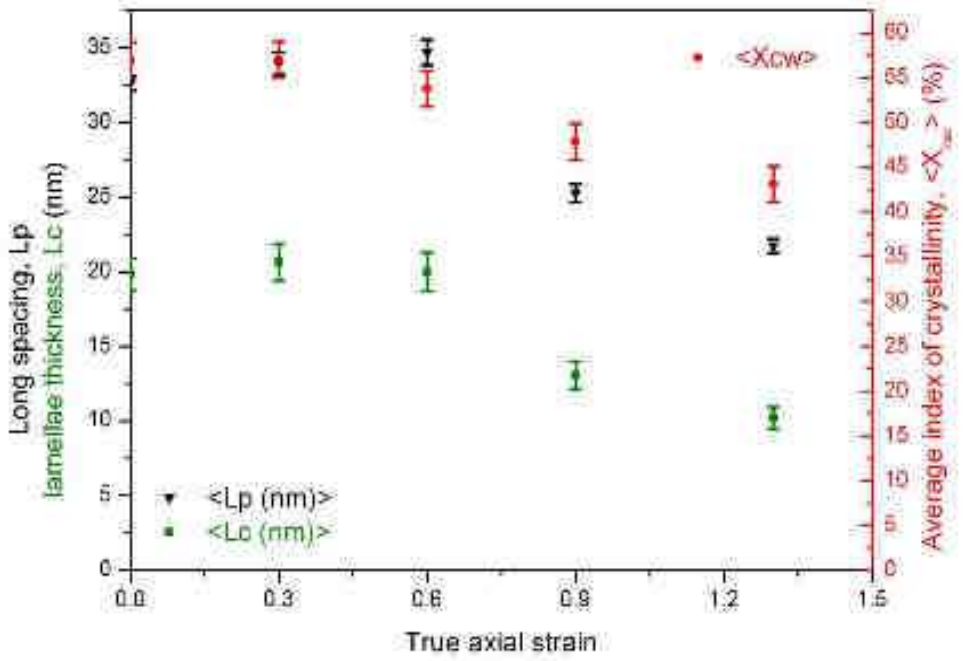

Figure IV-6: Long spacing, L_p (at 3 azimuthal angles ϕ), average long spacing $<L_p>$ and average lamellae thickness $<L_c>$ as a function of the axial strain (ε)

IV.1.2.3 SEM investigation

SEM pictures after etching (protocol described in 0, page 56) of the non-textured and the textured materials is shown in Figure IV-7.

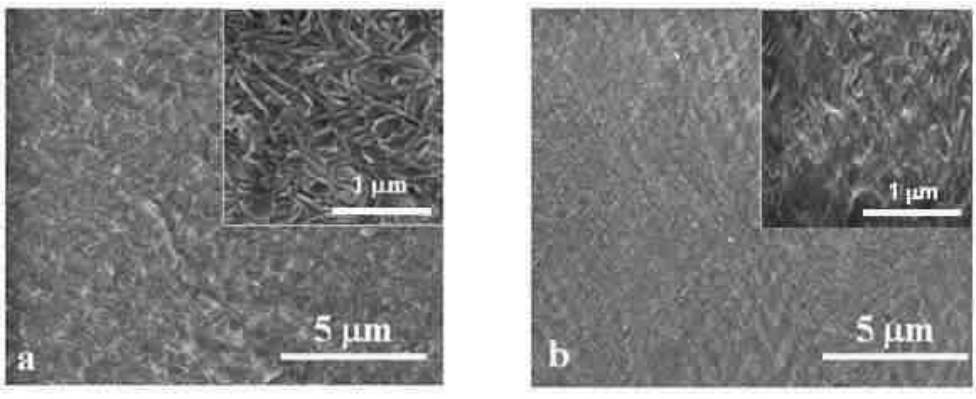

Figure IV-7: SEM micrographs (water pressure of 150 Pa) of a) non-textured UHMWPE, and b) textured UHMWPE.

Prior to stretching, the material is characterized by randomly oriented intertwined lamellae (Figure IV-7a). After the texturing process, lamellae fragments forming a chevron-type pattern (Figure IV-7b), are detected. We also note the presence of small lamellae fragments. These results are in line with SAXS measurements:

i) the lamellae forming chevrons explain the scattering signal at the azimuthal angle 45° and at 0° in the case of lamellae totally bended and hence oriented along stretching direction,

ii) the presence of lamellae fragments may result from the gradual orientation, shear, and fragmentation of the lamellae (Figure II-10) which give rise to crystalline blocks oriented perpendicular to tensile direction. This explains the scattering signal at the azimuthal angle 90°.

It is important to notice that no cavitation mechanism occurs in UHMWPE which implies that the tensile process does not generate damage as is for example observed in the case of in high-density polyethylene [4, 5].

IV.1.2.4 Summary

Based on SAXS, WAXS and SEM results, the microstructure of textured UHMWPE appears as a pseudo-microfibrillar morphology consisting of i) highly oriented amorphous chains in the tensile direction, ii) lamellae forming chevrons, iii) lamellae totally bended oriented in the tensile direction and iv) lamellae blocks oriented perpendicular to tensile direction resulting from fragmentation mechanisms. In the extreme deformation level, the overall lamellae thickness is 50 % smaller than the initial one. Based on these results, the microstructure of UHMWPE before and after the texturing procedure can be represented as in Figure IV-8.

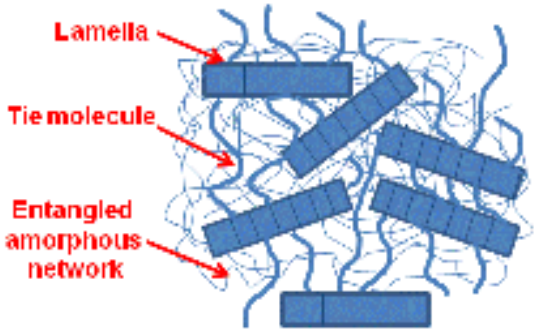

a)

b)

Figure IV-8: a) initial microstructure of UHMWPE, b) textured microstructure of UHMWPE

Since the amorphous phase is rubbery at the texturing process temperature of 30 °C, the deformation starts with conformational changes and a gradual orientation of the amorphous chains between entanglements in the elongation direction [6, 7]. At lamellae scale, the initial viscoelastic deformation stage is characterized by an interlamellar separation (Figure IV-9a) if lamellae are oriented perpendicular to tensile direction, by an interlamellar compression if lamellae are oriented in the tensile direction (Figure IV-9c), and for the other cases, by an interlamellar shear (Figures IV-9b and d). Interlamellar separation mechanisms may explain the weak but significant increase in long spacing on SAXS diagrams recorded at $\phi = 90°$ (Figures IV-5 and IV-6) for low deformation levels.

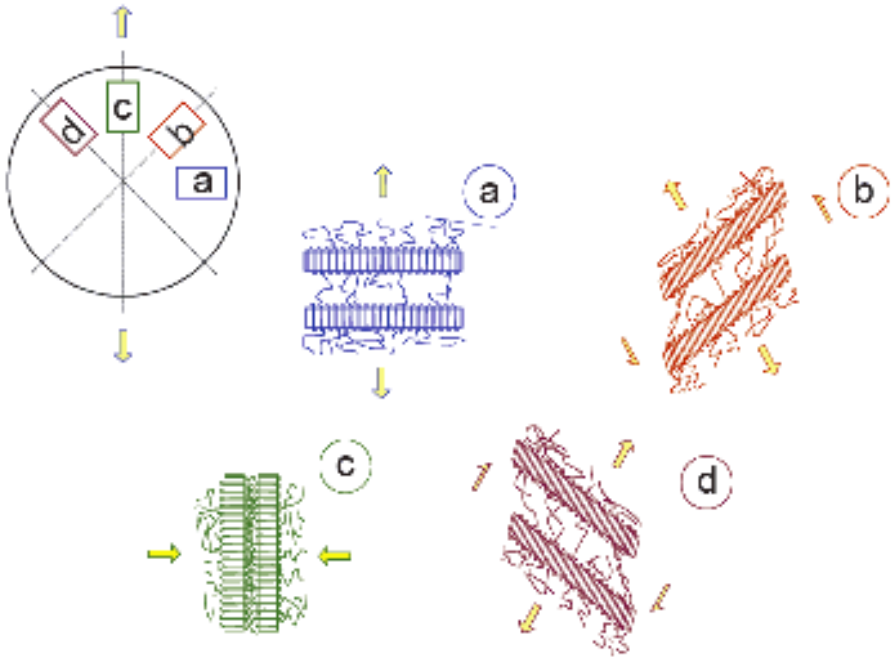

Figure IV-9: Deformation mechanisms of UHMWPE as a function of lamellae orientation with respect to tensile direction occuring below the yield point [6, 8]

The high number of entanglements and the high number of tie molecules in UHMWPE [9-11] imply a quick stress transfer from amorphous phase to crystalline lamellae. In UHMWPE, this stress transfer occurs at a lower stress level than in high-density polyethylene due to the higher number of connections between amorphous and crystalline phases. At this state of the deformation, the yield point is reached. At this state of the deformation, we suppose that viscoplastic mechanisms imply two different process, namely i) lamellae rotation, tilt, shear and fragmentation leading to the formation of lamellae blocks oriented perpendicular to tensile direction [7, 12] (Figure IV-9), and ii) a partial lamellar shear and then lamellar bending leading to the fragmentation (Figure IV-10) and to the formation of lamellae chevrons and totally bended lamellae (Figure IV-11) [10, 13].

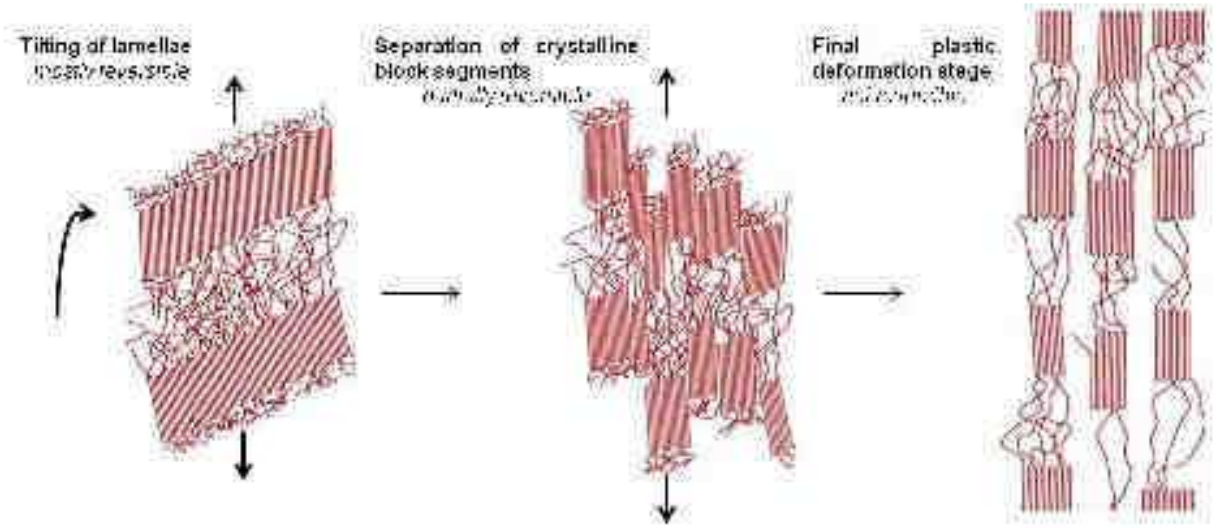

Figure IV-10: Deformation mechanisms of UHMWPE after the yield point without lamellae bending (adapted figure from [14])

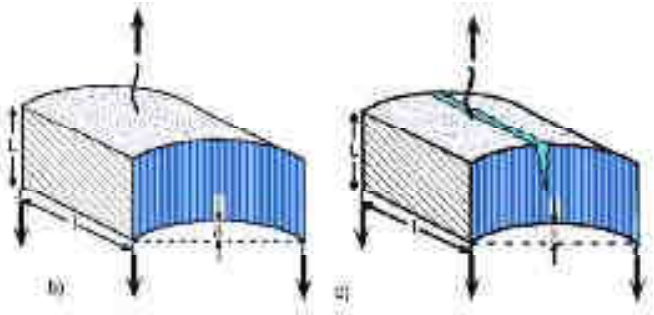

Figure IV-11: Deformation mechanisms of UHMWPE after yield point with lamellae bending [1]

Indeed, due to the high initial lamella thickness and the limited mobility of UHMWPE amorphous chains (highly entangled), the fragmentation of crystalline lamellae is not totally achieved in some area. We consider that these two types of mechanisms are active in our material. The drop in the long spacing and lamellae thickness occurring between $\varepsilon = 0.6$ and $\varepsilon = 0.9$ can be explained by the initiation of fragmentation and/or the initiation of the lamellae bending. Further research works are required to check this hypothesis.

IV.1.3 Evolution of topographical properties with WLI

The topographical parameters measured by WLI on non-textured and textured materials are plotted in Figure IV-12.

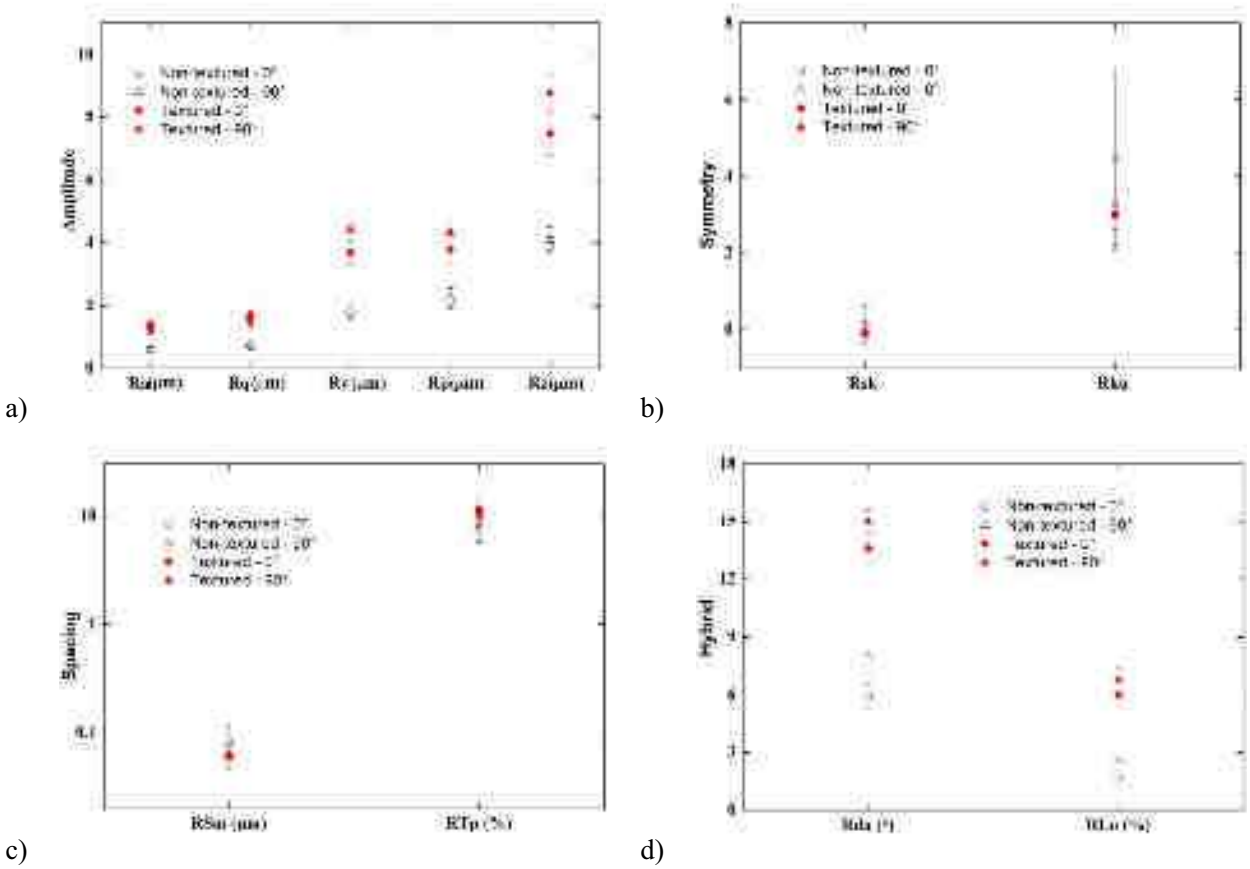

Figure IV-12: (a) Amplitude parameters, (b) symmetry parameters, (c) spacing parameters (semi-log), and (d) hybrid parameters of non-textured and textured UHMWPE measured along the azimuthal angles 0° and 90°, prior to sliding tests (with standard deviations).

It can be seen that the amplitude parameters (Figure IV-12a) increase by a factor of about 2 from the non-textured to the textured material. Regarding the symmetry parameters (Figure IV-12b), Rsk has similar values for the two materials whatever the azimuthal angles. The surface of the materials is symmetrical (Rsk#0) with respect to the mean plane what means that peaks and valleys are comparable in amplitude and number. The height distribution (Rku#3) is almost Gaussian on

textured material with no peculiar peaks or valleys. The height distribution for non-textured material is high even if the range is high. Regarding spacing parameters (Figure IV-12c), the distance between two peaks, RSm, is similar whatever the deformation state and the azimuthal direction. The material ratio at ¼ Rz, RTp, increases after elongation in both directions. The peak density, RHSc, is constant in the azimuthal direction 0°, and decreases in the azimuthal direction 90° after elongation. The higher range in the spacing parameters does not allow any conclusion. Regarding the hybrid parameters (Figure IV-12d), the surface curvature, Rda, and the developed length RLo are 2 and 3 times higher for textured UHMWPE compared to non-textured UHMWPE, respectively. In any case, the WLI investigation showed that the texturing process increases amplitude, symmetry, and hybrid parameters on UHMWPE. This indicates that the surfaces contain more pronounced peaks and valleys after elongation. Some authors attributed this phenomenon to a plastic deformation of surface asperities [15, 16]. These asperities can subsequently detach when the yield point is reached causing a further increase in surface roughness. It is also thought that this increase in roughness can be due to an ejection mechanism of the crystalline lamellae from the polymer surface during the texturing process.

IV.1.4 Evolution of viscoelastic properties with DMA

Figure IV-13 shows the temperature dependence of the loss factor (tan δ) for different strains. Measurements were done at frequencies ranging from 0.1 Hz to 100 Hz.

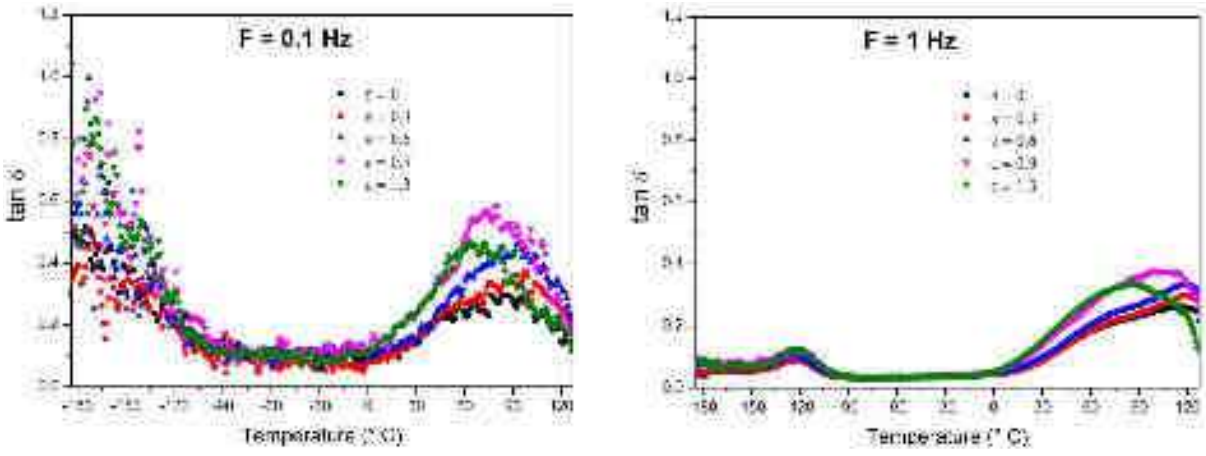

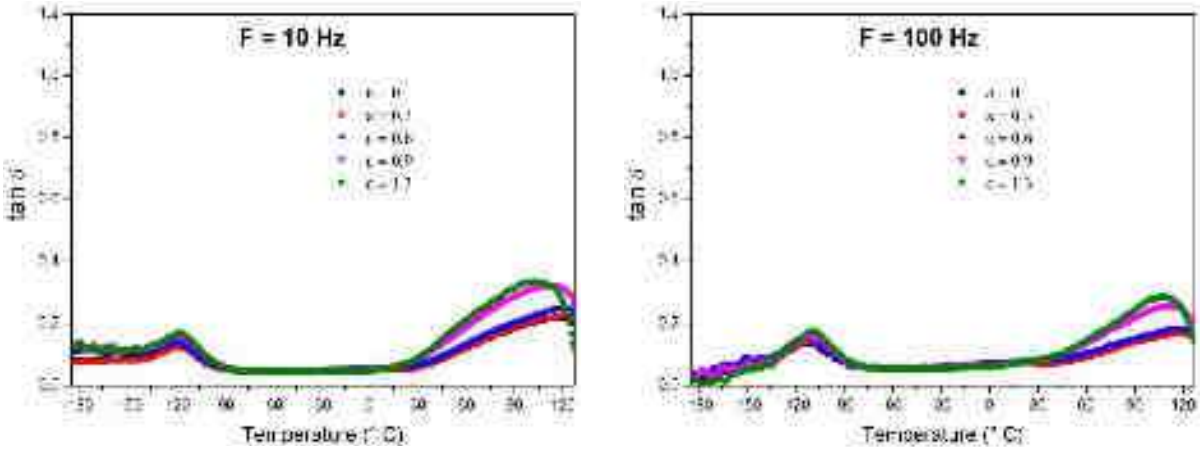

Figure IV-13: Loss factor (tan δ) as function of the temperature recorded at different frequencies (0.1, 1, 10 and 100 Hz) for non-textured (ε = 0) and textured UHMWPE (ε = 0.3, 0.6, 0.9 and 1.3)

Two main relaxation processes are observed at increasing temperature, namely γ-relaxation and an α-relaxation. The γ–relaxation occuring at around -120 °C, is associated with the glass transition of the amorphous phase [17]. We do not observe an influence of the deformation level on this relaxation phenomenon. Concerning the α-relaxation, it characterizes movements of the crystalline phase induced by an interlamellae shear and/or intralamellar shear mechanisms [17-22]. It can be seen that an increase of the deformation level leads to a decrease of the α-relaxation temperature. This result indicates that the α-relaxation mechanisms involve a lower characteristic time and/or smallest molecular units with increasing deformation level.

The α-relaxation of the materials is analyzed by means of the Arrhenius approach to determine the activation energy [23, 24]. The Arrhenius plots of this relaxation are shown in Figure IV-14. The slope of each line is equal to $-E_a/R$ where E_a is the activation energy of α-relaxation and R = 8.314 $J.mol^{-1}.K^{-1}$ is the gas constant. The activation energy for the α-relaxation of non-textured (ε = 0) and textured UHMWPE up to ε = 0.3 and 0.6 is quite similar and is comprised between 584 and 591 $kJ.mol^{-1}$. At higher deformation states, the activation energy is about 262 $kJ.mol^{-1}$ at ε = 0.9 and about 99 $kJ.mol^{-1}$ at ε = 1.3.

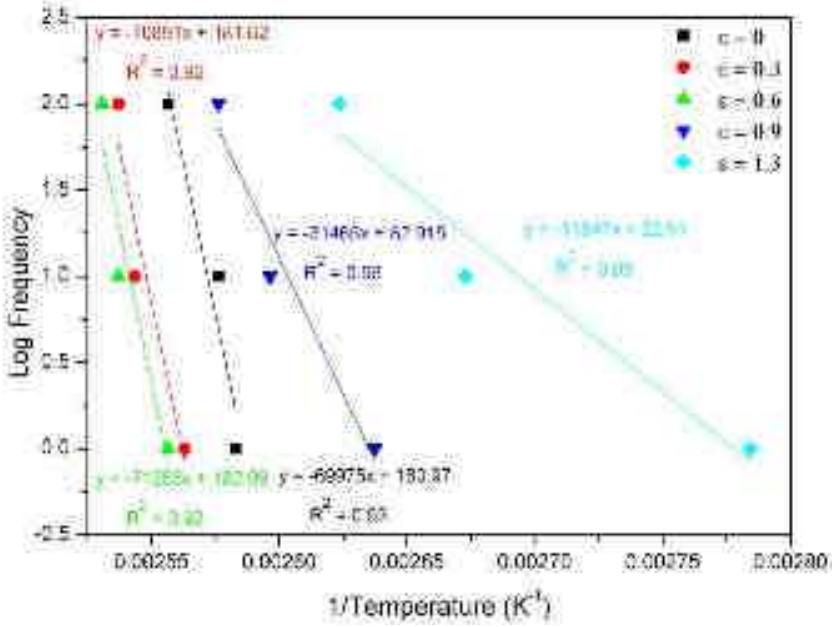

Figure IV-14: Arrhenius plot: temperatures of α-relaxation

DMA also provides information about the β-relaxation (Figure IV-15) that is less marked than the γ and α relaxation processes.

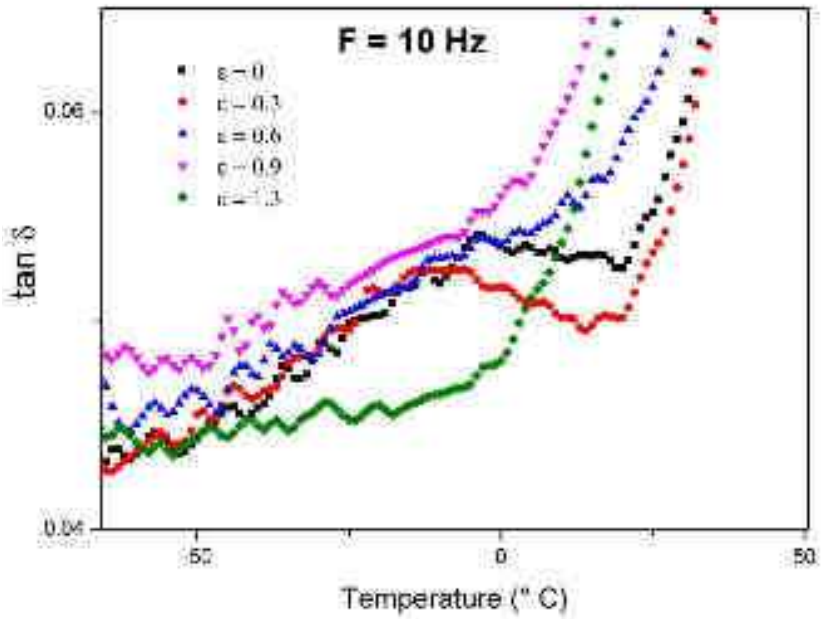

Figure IV-15: Zoom-in β–relaxation recorded at 10 Hz for non-textured (ε = 0) and textured UHMWPE (ε = 0.3, 0.6, 0.9 and 1.3)

According to literature, the origin of β-relaxation is quite unclear. It may be due to movements of loops or amorphous chain segments in the interfacial regions [17, 25, 26]. Other authors attributed this relaxation to changes in the amorphous regions due to branching, ordering of amorphous chains, cross-links, oxidation, tie-molecules or may be linked to glass transition [27]. Figure IV-15 indicates that the intensity of the β-relaxation disappears for ε = 0.9 and for ε = 1.3, which seems to be linked to the evolution of long spacing and lamellae thickness (Figure IV-5 and Figure IV-6). In particular, the drop in long spacing and lamellae thickness coincides with the disappearance of the β-relaxation. From a general point of view, we consider that the disappearance of b-relaxation with high strain levels indicates a disappearance of chain mobility that was localized in the amorphous phase or in the interfacial region.

IV.2 Set-up of the tribological investigation

IV.2.1 Effect of the normal load on friction

Reciprocating sliding tests under mode-I were performed at 22 °C in ambient air of 50 % relative humidity on non-textured and textured UHMWPE. Corundum balls with a diameter of 10 mm, a surface roughness (R_a) of 0.2 μm, and an elastic modulus of 300 GPa were loaded on surface of the UHMWPE samples at normal loads of 2 N, 5 N and 10 N. Hertz theory was used to calculate the contact pressure at the surface of UHMWPE as a function of the normal load. Such loads correspond to a maximum Hertzian pressure of approximately 26 MPa, 36 MPa, and 45 MPa, respectively (calculated based on an elastic modulus of 900 MPa and a Poisson's ratio of 0.4 for non-textured material). The selected deformation state corresponds to a strain level of 1.3 (elongation of about 300 %) obtained by tension as mentioned in III.1.2 (30 °C, strain rate of 10^{-3} s^{-1}). Before starting sliding tests, the samples were cleaned with distilled water and air dried. The UHMWPE samples were oscillated against the rigid fixed counter-body. The oscillations imposed consisted of a linear displacement stroke of 200 μm at a frequency of 5 Hz, resulting in gross slip regime. For hip joints, the maximum pressure generated during daily activities on the hip joint has been estimated at 12 MPa in acetabular cups [28]. By considering a safety factor of 3, the maximum pressure used in this

study was 36 MPa. In some reported studies, the expected pressure was approximated to a very high value of 375 MPa, to accelerate the expected wear events [29]. The evolution of the dissipated energy performed under 50,000 cycles according to the three different normal loads is shown in Figure IV-16 for the non-textured and textured UHMWPE along the azimuthal direction 0°.

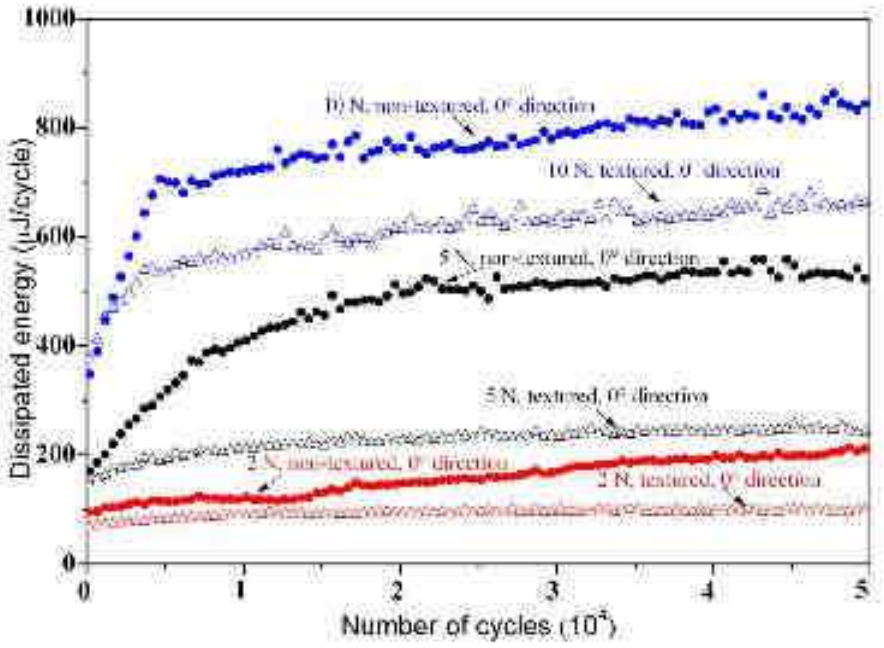

Figure IV-16: Dissipated energy as function of the number of cycles on non-textured and textured (strain level of 1.3) UHMWPE at 0° (along texture direction) for different normal loads (2N, 5N and 10N)

The initial sliding stage is characterized by an increase of the dissipated energy as a function of the number of cycles, and this is observed at loads of 5 N and 10 N. This stage can be considered as a running-in stage, and is characterized by a gradual adaptation of the surfaces to each other by removing surface defects and creating new physical interactions. After the running-in stage, the dissipated energy reaches a steady-state. At a normal load of 10 N the highest steady-state dissipated energy is noticed, while at 2 N the lowest one is recorded. A decrease of the dissipated energy with decreasing deformation level is systematically observed when comparing non-textured with textured UHMWPE whatever the load. The dissipated energy decreases from 846 µJ on non-

textured UHMWPE to 665 µJ on textured UHMWPE (-21 %) at a normal load of 10 N and 50,000 cycles. At 5 N, a decrease of the dissipated energy is noticed from 522 µJ down to 245 µJ (-53 %) at 50,000 cycles for non-textured and textured UHMWPE respectively. At a normal load of 2 N and 50,000 cycles, the dissipated energy decreases from 210 µJ down to 101 µJ (-52 %) for non-textured and textured UHMWPE respectively. Overall, it appears that the impact of deformation on the dissipated energy is more marked at a normal load of 5 N on comparing non-textured and textured UHMWPE.

These preliminary results indicate that the normal load and the initial texture state have an important effect on the sliding behaviour of UHMWPE. Concerning the load, it seems clear that the sliding dissipated energy increases with normal load. An increase of the normal load increases the tangential load and hence, the area of the hysteresis loops (tangential force vs. displacement). The increase of the tangential force may be explained as follows. If we consider that an increase of the normal load on the corundum ball corresponds to an increase of the local deformation at the surface of the polymer, the polymer network resistance in terms of local stress increases. This mechanism is highlighted by the continuous increase of stress with strain (the imposed local deformation by increasing the ball normal load) in the case of a simple tensile test on UHMWPE. In this case, there is no impact of other variables like initial roughness or physical interaction, since these two variables do not evolve with the normal load of the ball. We also consider that the contact area increases with increasing normal load, which implies a higher volume of polymer involved in the friction, and hence, more interactions between the ball and polymer surfaces, resulting in a higher tangential load. As regards the influence of texture, tangential force appears to be reduced by the texture during the sliding. This point will be discussed in the next sections.

IV.2.2 Effect of the initial roughness of UHMWPE on friction

In this investigation, experimental data are reported on the impact of the surface roughness on the friction behaviour of UHMWPE evaluated by fretting mode I tests. Two different surface roughnesses have been prepared in this study. The first one was the as hot-compressed specimen.

The second one was treated after the compression-moulding step. In particular, the second sample was first finely polished and then etched by an oxidative solutions made of acids and potassium permanganate. The polishing procedure was done to reduce the sample roughness down to several microns. The chemical etching was conducted to further reduce the roughness. This procedure is given in III.2.2.1.

Topographical parameters measured by WLI are plotted in Figure IV-17.

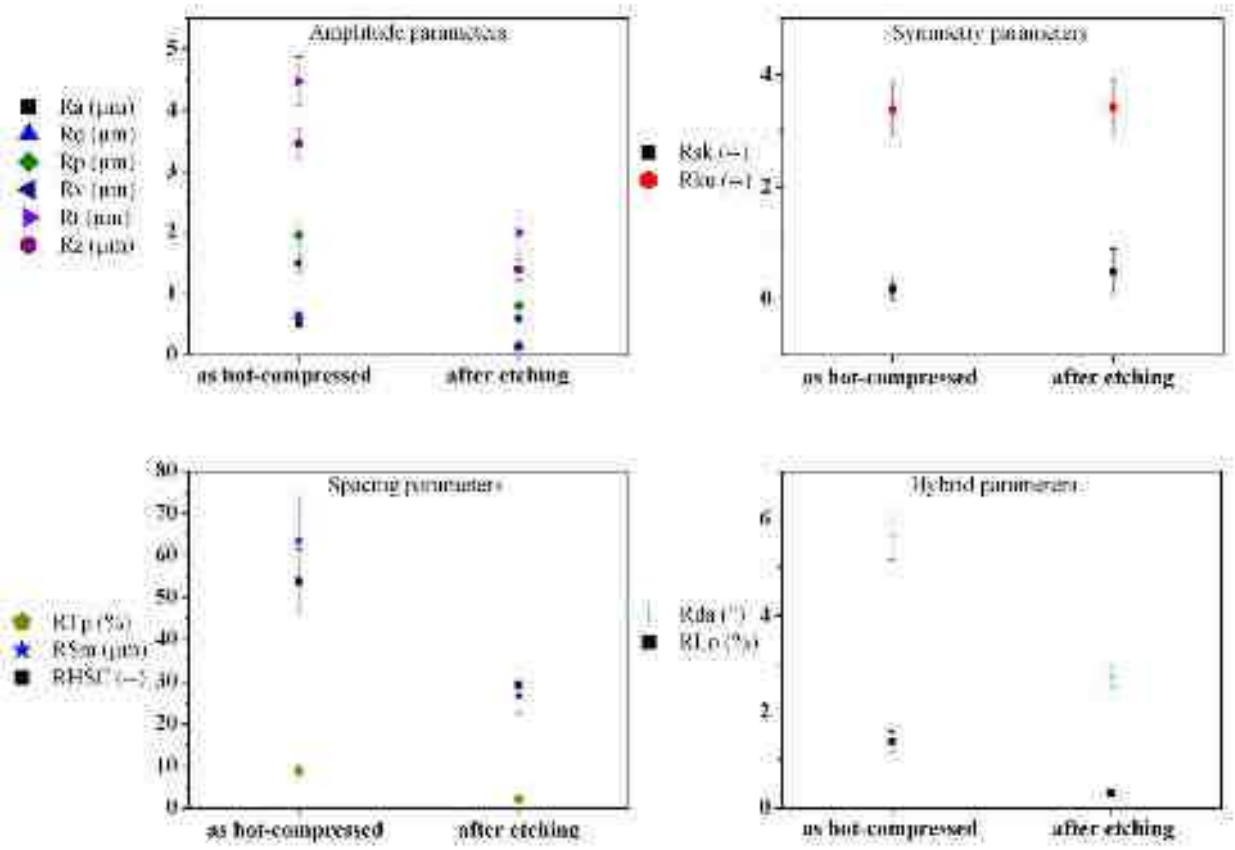

Figure IV-17: Topographical parameters for non-textured UHMWPE (as hot-compressed and after etching)

It can be seen that the amplitude, spacing and hybrid parameters decrease significantly after the treatment by a factor of two. The surface becomes smoother with a lower peak density, less marked slopes and complexity.

Friction was investigated under the sets of parameters described in the previous paragraph on hot-compressed UHMWPE samples and after etching). The evolution of the dissipated energy as a function of the number of cycles is shown in Figure IV-18.

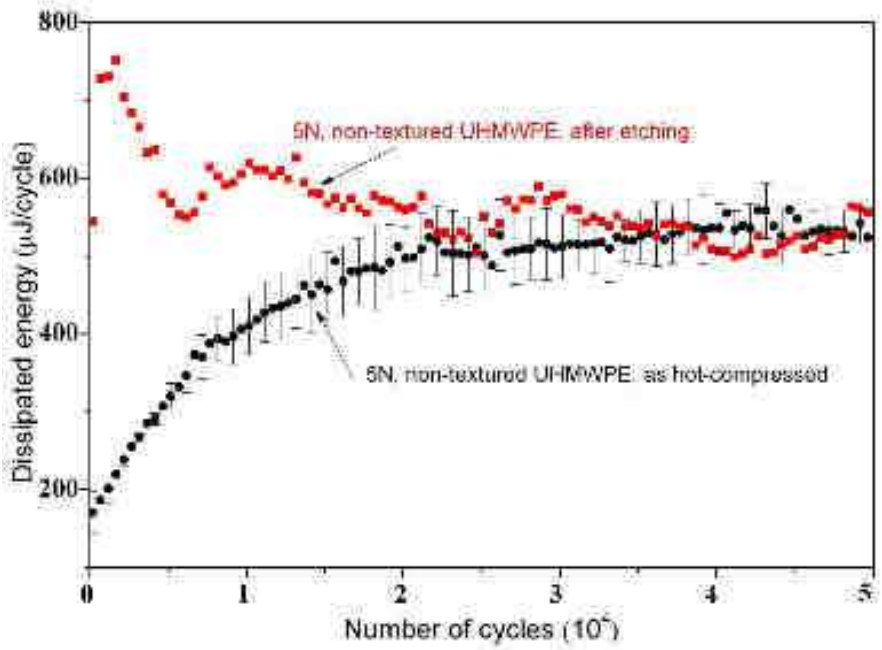

Figure IV-18: Evolution of the dissipated energy as a function of number of cycles for non-textured UHMWPE (without treatment and etching)

As expected, in the case of the hot-compressed sample, the dissipated energy increases at increasing number of cycles during the running-in period till it reaches a steady-state value. On the treated sample, a very fast increase of the dissipated energy is noticed followed by a gradual decrease during the running-in period. It has also to be mentioned that the steady state of the dissipated energy curves is very similar for the two samples. The reduction of roughness induced by the combination of polishing and chemical etching may create some new physical interactions between the corundum ball and the UHMWPE. This new physical interactions can be due to the presence of new chemical species derived from the used chemicals absorbed at the surface of the polymer. We also hypothesize that the presence of nanometric topography may possibly increase the interactions between the ball and the polymer. These two possible new interactions are overwhelming the

running-in stage what explains the decrease of the dissipated energy in the case of the treated UHMWPE. After this initial stage, there is no effect of the initial surface roughness anymore. Since it is our main interest to study the sliding wear behaviour of UHMWPE occurring at a large number of sliding cycles, it was decided to pursue the research work using hot-pressed samples without any post-treatment.

IV.2.3 Effect of the initial deformation level of UHMWPE on friction

Reciprocating sliding tests under mode-I were performed in ambient air at 22 °C and 50 % RH on these 5 types of samples against corundum ball with a diameter of 10 mm at a normal load of 5 N. The linear displacement stroke and the frequency imposed were 200 µm and 5 Hz. A typical evolution of the dissipated energy is shown in Figure IV-19 for non-textured and textured UHMWPE at different deformation levels, sliding along the tensile direction, 0°, and in Figure IV-20 when sliding perpendicular to the tensile direction, 90°.

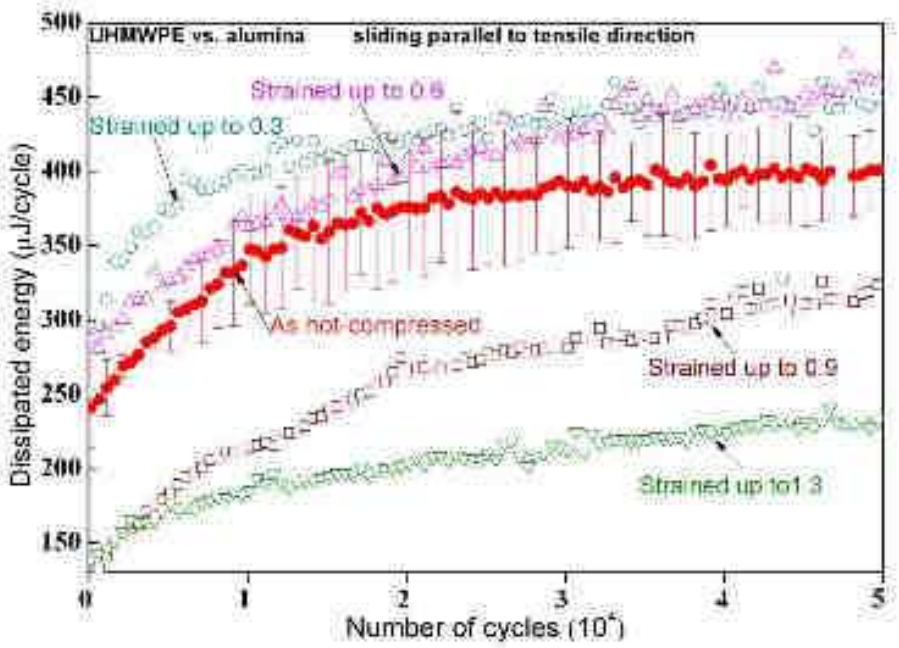

Figure IV-19: Dissipated energy as function of the number of cycles for non-textured and textured UHMWPE at different deformation levels. Sliding tests along the tensile direction, 0°

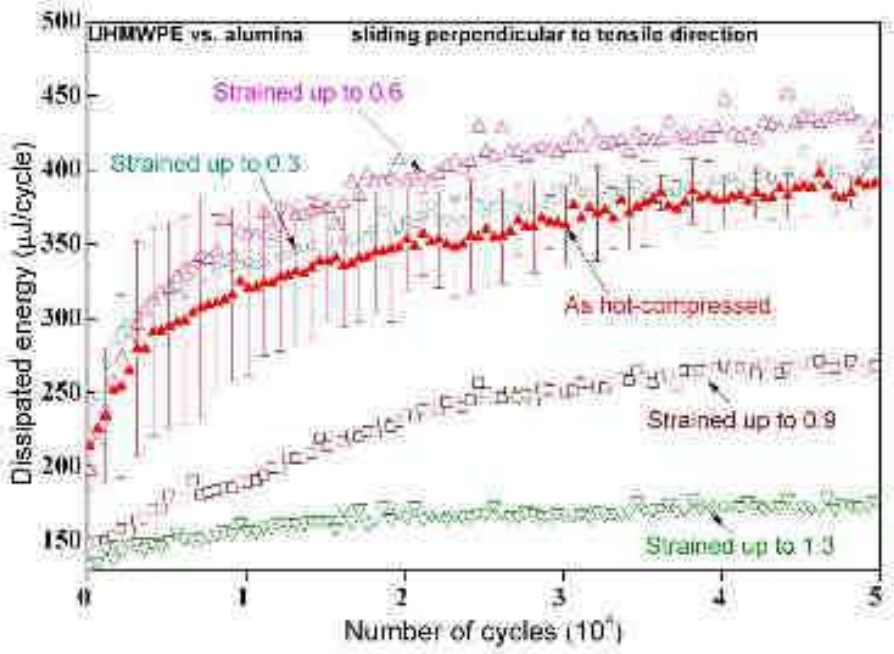

Figure IV-20: Dissipated energy as function of the number of cycles for non-textured and textured UHMWPE at different deformation levels. Sliding tests perpendicular to the tensile direction, 90°

At 0° and 90°, the dissipated energy on non-textured and textured samples at true strains of 0.3, 0.6, 0.9 and 1.3, increases during the initial sliding cycles corresponding to the running-in stage, and then reaches a steady-state value. Among the different deformation levels, it can be clearly observed that the friction behaviour is related to the deformation level once the strain level reaches 0.9. The dissipated energy on non-textured, strained up to 0.3, and strained up to 0.6 is quite similar, while at higher deformation level, the dissipated energy decreases with increasing deformation (see strained up to 0.9 and strained up to 1.3). It has to be mentioned that at the two highest deformation levels namely 0.9 and 1.3, the dissipated energy recorded at 90° is slightly lower than the one recorded at 0°.

IV.3 Sliding performance of non-textured and textured UHMWPE

IV.3.1 Reciprocating sliding behaviour of non-textured and textured UHMWPE

Three sliding tests were carried out for each investigated case and we provide hereafter values with standard deviations for two cases (non-textured and strained up to 1.3).

An overall aim of this study was to investigate the effect of the texture of UHMWPE on the wear behaviour under reciprocating sliding. The contact displacement and tangential (frictional) force were monitored in real-time to derive the coefficient of friction for the tested materials. Typical evolutions of the tangential force *vs.* displacement hysteresis semi-log loops with the number of cycles are plotted in Figure IV-21 for non-textured and textured UHMWPE.

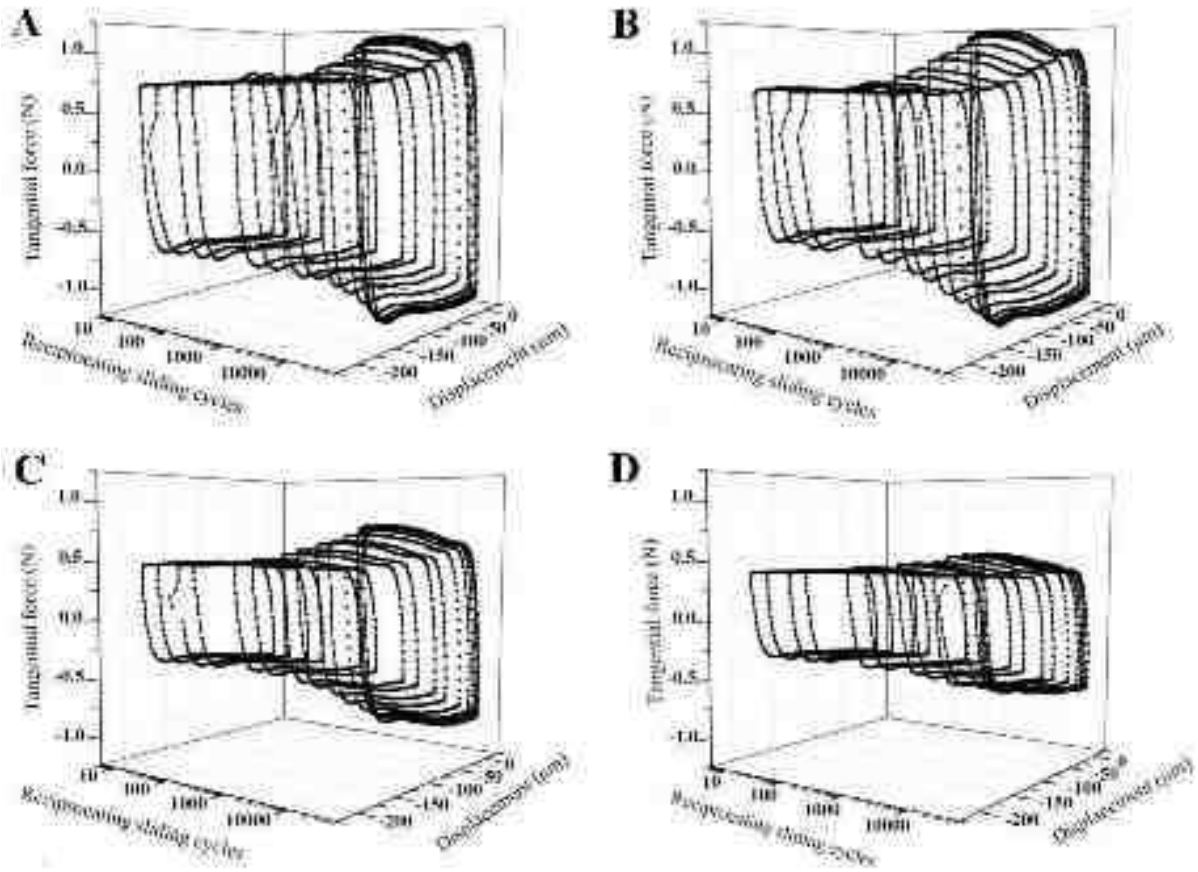

Figure IV-21: Plots of tangential force-displacement semi-log hysteresis loops of (a,b) non-textured UHMWPE and (c,d) textured UHMWPE measured along 0° and 90°.

The parallelogram-shaped hysteresis loops reveal that gross slip test conditions are achieved on both materials. The length over which gross slip sliding takes place at low number of cycles is relatively larger on non-textured than textured material. This could be due to mechanical properties shifting (e.g. viscoplastic pattern) with creep or adhesion causing sticking at the ends of the wear track area. Indeed significant static tangential force values were recorded on non-textured rather than on textured UHMWPE at the onset of sliding. The consolidation of the hysteresis loops at low number of cycles provides a further insight into the behaviour of tests at high number of cycles.

A running-in phase is noticed on non-textured UHMWPE up to 10,000 to 14,000 cycles during which the tangential force increases and reaches a high value (1.0 N) at which it stabilizes during the remaining test cycles. The hysteresis loops area on non-textured material increase gradually with the number of cycles and that along the two azimuthal angles (0° and 90°). On textured material, only a slight increase of the hysteresis loop area is noticed along the azimuthal angle 0° with increasing number of cycles, while it remains quite constant along the azimuthal angle 90°. The area of each hysteresis loop corresponds to the friction energy dissipated during each reciprocating sliding cycle. The area of the hysteresis loop is the smallest in the running-in stage, and then gradually increases with increasing number of cycles particularly in the case of non-textured material.

The evolution of the dissipated energy and its standard deviation as a function of number of cycles is shown in Figure IV-22.

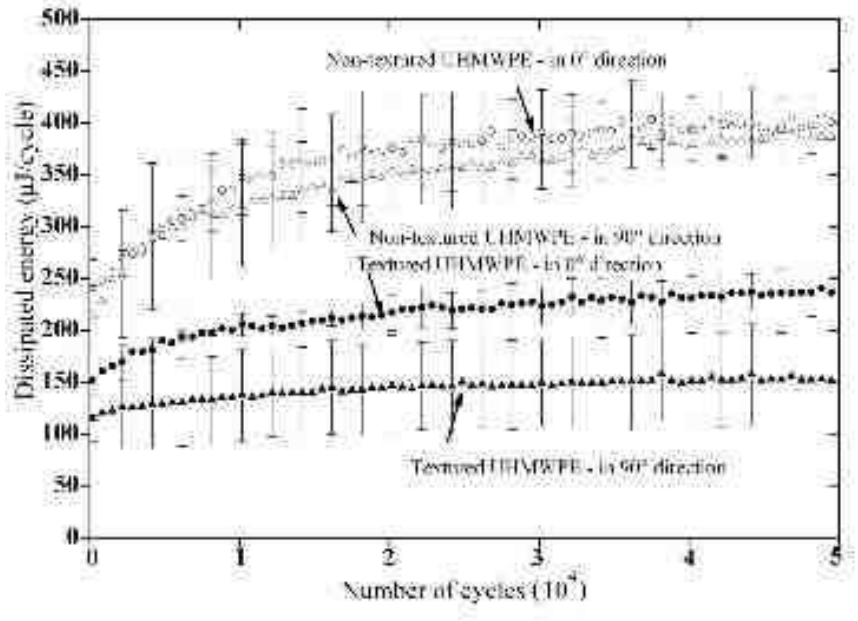

Figure IV-22: Dissipated energy as a function of reciprocating sliding cycles for non-textured and textured UHMWPE recorded along 0° and 90° (with standard deviations).

Such a monitoring offers the possibility to get real-time mechanistic information of the underlying sliding mechanisms. The dissipated energy increases rapidly during the first 15,000 cycles for non-textured material along the two azimuthal angles 0° and 90°, and during the first 7,000 to 10,000 cycles for textured material along the two azimuthal angles 90° and 0°, respectively. At 50,000 cycles, the dissipated energy stabilizes at about the same value between 380 and 420 µJ for non-textured material along the two azimuthal angles 90° and 0° respectively. On the contrary, on textured material the dissipated energy is only 160 µJ along the azimuthal angle 90°, while it is equal to 260 µJ along the azimuthal angle 0°. These observations are consistent with our results on friction variation (Figure IV-21).

The limited number of reciprocating sliding cycles performed up to now induced a quite small wear volume that can't be determined accurately. One generally accepted fact in literature is that the wear volume loss increases with the dissipated energy, often in a linear manner [30, 31]. If that would be the case for UHMWPE, the wear volume loss of both non-textured and textured materials would be directly proportional to the dissipated energy, and decreases from non-textured material (0°) ~ non-textured material (90°) > textured material (0°) > textured material (90°).

Since it was not possible to quantify directly the wear volume loss, and assuming that the wear depth is rather constant with respect to the current mode of wear (e.g. viscoplastic), we can calculate the projected area of the wear track, based on SEM observations (Figure IV-25) and correlate it to the shear energy work dissipated in the contact zone. A modified classical Archard's wear coefficient, K ($\mu m^2/J$), is thus considered to compare the reciprocating sliding wear resistance of the investigated materials. The extension of the wear track area, *A*, is compared to the product of the tangential force, F_T, and the cumulated sliding distance, s, or in other words the cumulated dissipated energy (ΣE_d). After 50,000 sliding cycles, we found that ΣE_d decreases from 18,250-17,600 J for non-textured UHMWPE to 11,700 and 6,700 J for textured UHMWPE, along azimuthal angles $\phi = 0°$ and 90°, respectively. The contact area A was measured from SEM images. The wear resistance of the material can be expressed by an energy wear coefficient $K = A / \Sigma E_d$. Surprisingly, our above assumption is confirmed by the proposed dissipated energy approach as can be seen in Figure IV-23, where the wear track area at 50,000 cycles evolves linearly with the cumulative dissipated energy in the contact.

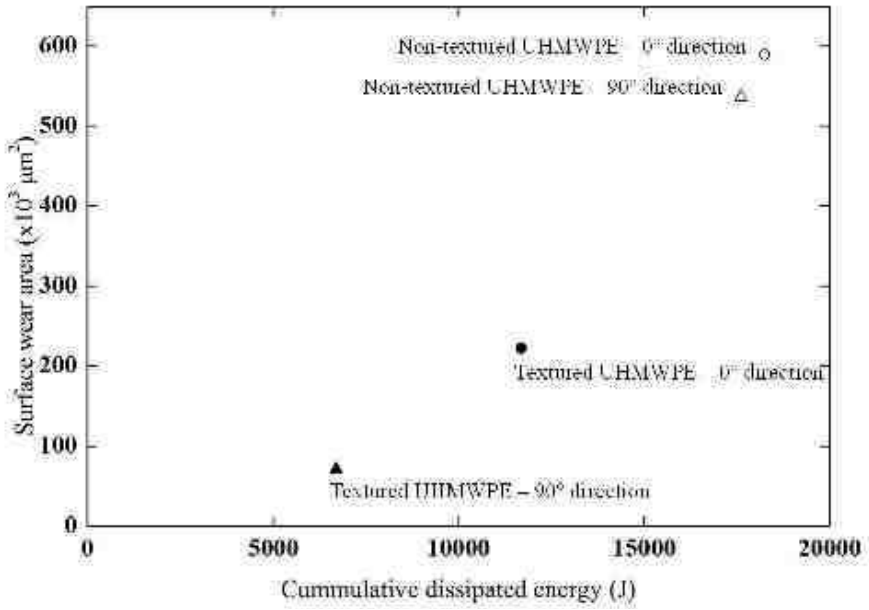

Figure IV-23: Evolution of wear area of textured and non-textured UHMWPE as a function of cumulated dissipated energy, after 50,000 sliding cycles.

A slope K = 7.83 $\mu m^2/\mu J$ is found, which represents a unique common characteristic of the friction couple corresponding to its resistance to wear independently of the applied displacement amplitude as in classical Archard's wear coefficient. This global wear energy approach can be used to predict the durability of the materials independently of any particular displacement amplitude used under field conditions. Accordingly, textured UHMWPE (90°) will achieve higher anti-wear properties along, and perpendicular to the texture direction compared to non-textured UHMWPE. Hence, the texturing process of UHMWPE may represent a worthwhile cross-linking pre-treatment for cup applications in THA, namely i) it may increase strength for applications requiring resistance to uniaxial tension, and ii) it may increase wear resistance. Obviously, in order to verify the generality of this new anti-wear property, other conditions must be tested like for example higher number of cycles, other sliding directions than 0° and 90° (15°, 30°, and 45°), and sliding under wet conditions e.g. in physiological serum.

IV.3.2 Analysis of wear scar by FTIR, SEM and WLI

The friction energy during reciprocating sliding can be dissipated through different mechanisms as oxidation, a rise in temperature, the formation of wear particles, entropy changes associated to viscoelastic and viscoplastic deformation, and noise generation [32-34]. Initial tests on the powder, and surface/bulk compressed UHMWPE studied by FTIR are presented in Figure IV-24. These analyses in the UHMWPE surface and bulk in comparison with the initial powder showed no appearance of peaks related to oxidation. Moreover, during the processing of the UHMWPE, the up and down plates of the press were at 240 °C. Due to limited heat conduction and taking into account the thickness of the mould (brass, 25 mm) a lower temperature will be reached within the material.

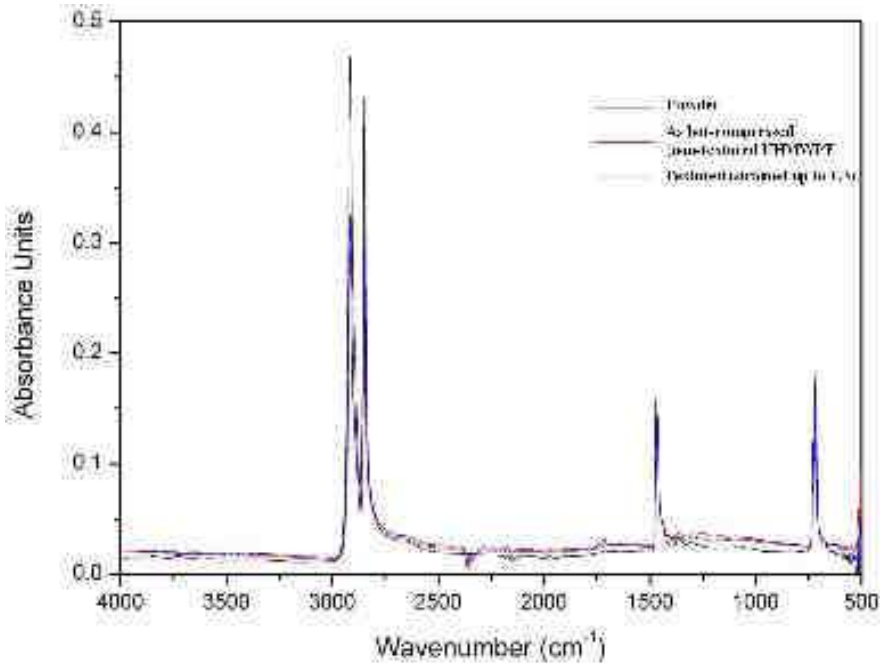

Figure IV-24: FTIR spectra of the initial UHMWPE powder and compressed UHMWPE

We consider that noise generation is negligible during reciprocating sliding tests performed on UHMWPE. Therefore, the wear mechanisms are a combination of viscoelastic/viscoplastic deformation, wear particles generation, and possibly temperature increase. Let's consider first the two first cited types of mechanisms. These two types of mechanism were carefully analyzed by SEM and WLI. It has to be noted that we tried to analyze wear tracks by atomic force microscope (AFM), but it was not possible to distinguish between unworn and worn surfaces. This is probably due to the low number of reciprocating sliding cycles performed in our work. Therefore, the sliding behaviour is mainly induced by viscoelastic/viscoplastic mechanisms, as was shown in a previous study [34], although the nominal contact pressure was lower than that selected in the present study (10.6 MPa vs. 36 MPa).

SEM images of the wear tracks are shown in Figure IV-25. A circular wear scar with a diameter of approximately 1 mm is observed on both materials independently of the sliding direction. It has to be noted that the wear track area is continuous on non-textured UHMWPE (Figure IV-25 a and b), while it is discontinuous on textured UHMWPE (Figure IV-25 c and d). By using the software CorelDraw graphics Suite X3 (Corel Corporation, Ottawa, Canada), we measured the contact area,

A, on the two materials through the following procedure applied on SEM images: i) wear scars were detected as individual objects, and ii) the software provided the contact area A by summing the surface of each individual wear scars. A is comprised between 589 and 536×10^3 μm^2 on non-textured UHMWPE. Regarding textured UHMWPE, A is equal to 222×10^3 μm^2 parallel to texture direction and equal to 71×10^3 μm^2 perpendicular to texture direction. Some scratches were observed on the two tested materials in the two sliding directions highlighting the severity of the sliding wear. At higher magnification, on non-textured UHMWPE, the wear track is characterized by the presence of parallel waves or ripples oriented perpendicular to the sliding direction, with an average thickness of about 2 μm (Figure IV-26a and b).

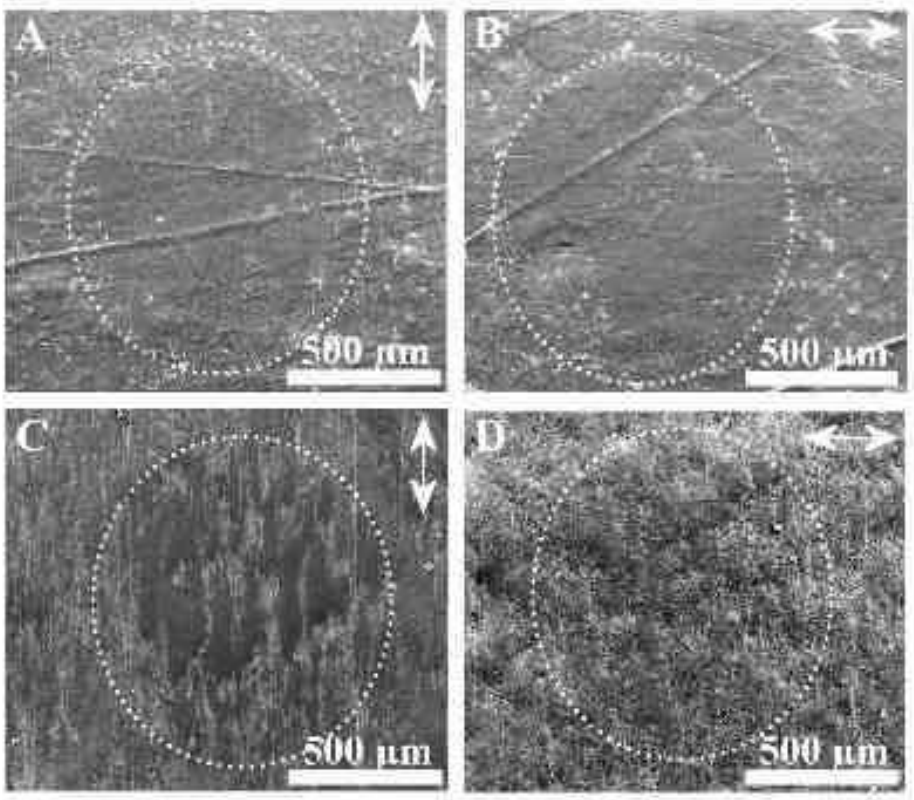

Figure IV-25: SEM micrographs (observations done under high vacuum conditions) of wear track generated on (a,b) non-textured UHMWPE and (c,d) textured UHMWPE along azimuthal angle (a,c) 0° and (b,d) 90°, after 50,000 sliding cycles (wear track area is delimitates by a circle, while a double arrow indicates the sliding direction).

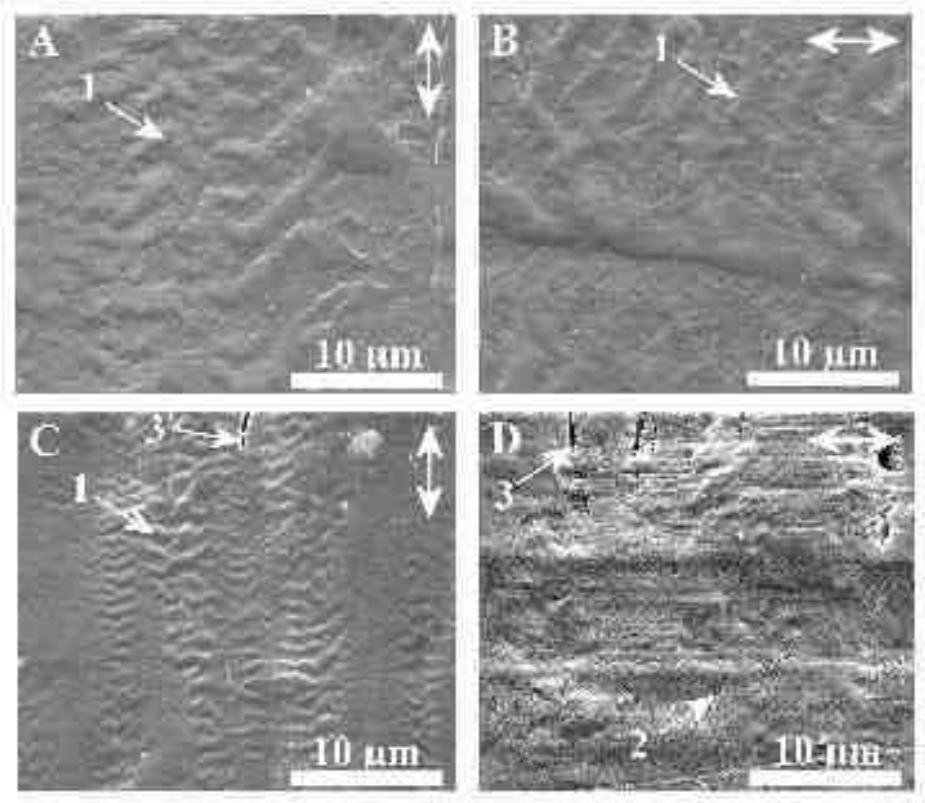

Figure IV-26: Zoom-in views (observations done under high vacuum conditions) of wear track generated on (a,b) non-textured UHMWPE and (c,d) textured UHMWPE along azimuthal angle (a,c) 0° and (b,d) 90°, after 50,000 sliding cycles (sliding direction is indicated by a double arrow; 1: waves, 2: submicron cracks, 3: cracks).

Due to the periodicity of the data acquisition that was set to 2 µm during the sliding tests, it is not possible to observe the influence of waves on the tangential force during one cycle. Regarding textured UHMWPE, we note thinner waves (thickness of about 1 µm) compared to non-textured UHMWPE when sliding tests were carried out along the texture direction (Figure IV-26c). Wear tracks measured perpendicular to the sliding direction (Figure IV-26d), contain two types of crack, namely i) submicron cracks and ii) larger cracks, oriented perpendicular to sliding direction. Little or no waves are noted in this case. Last, no significant evidence of wear debris was obtained for all the investigated materials.

We developed a specific methodology to obtain quantitative information on the wear tracks by means of WLI. To unravel the surface topography of the worn area, a filtering was carried out to

remove the waviness from the profile due to the low wear resulting from the sliding test. The procedure consisted of acquiring the micro-relief in the wear track. To this end, data were treated with Gaussian filter using a cut-off length of 8 µm with the software Mountains Map 5.1 (Digital Surf Company, Besançon, France). This software proposed a filter between 0.00576 mm and 0.797 mm. After a debucking, we observed by eye that the worn surface started to be detected at around 0.02 mm. Then, step by step (0.001 mm by 0.001 mm), the best rationale that allowed to separate the waviness from the roughness and to observe all the worn areas was 0.008 mm. Focus was on the residue of the filtering to access and to characterize only the micro-relief of the surface. 2D-parameters were determined on unworn material as an average of 484 profiles. 3D topographical parameters of worn areas were determined through three measurements. We provided standard deviations for each topographical parameter. Thus, the quantitative assessment of the 3D topographical parameters inside and outside wear tracks was done based on WLI data recorded on both textured and non-textured materials after reciprocating sliding tests.

Figure IV-27 shows a typical surface reconstruction of an area localized outside (Figure IV-27a) and an area localized inside (Figure IV-27b) wear track of non-textured UHMWPE.

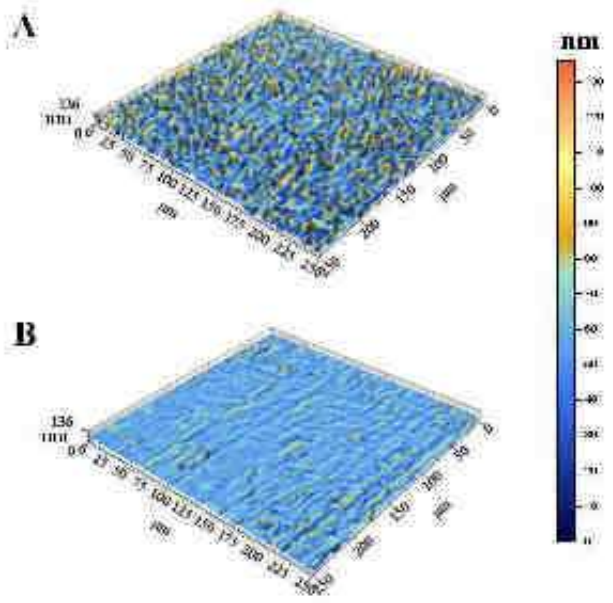

Figure IV-27: 3D representation of (a) outside wear track, and (b) inside wear track for non-textured UHMWPE, after 50,000 sliding cycles.

As expected, a rough surface is noticed outside the wear track area (Figure IV-27a). Inside the wear track, one notes a surface that is smoother than outside the wear track. The corresponding topographical parameters are displayed in Figure IV-28 inside and outside the wear tracks for both materials.

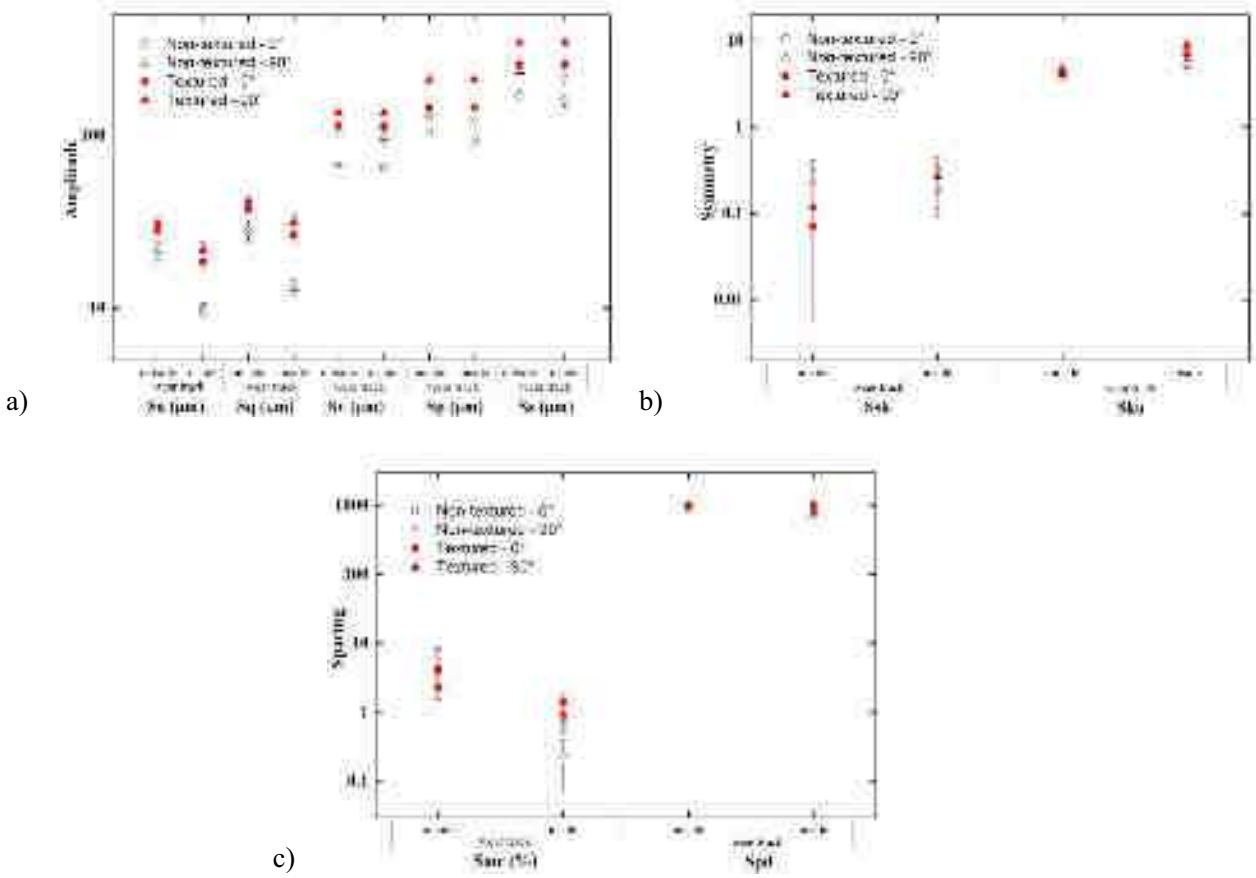

Figure IV-28: a) Amplitude, b) symmetry, and c) spacing parameters of non-textured and textured UHMWPE recorded along the azimuthal angles 0° and 90°, inside and outside wear tracks, after 50,000 sliding cycles (with standard deviations).

The main differences observed are related to the amplitude parameters Sa and Sq. These parameters significantly decrease on both tested materials after the reciprocating sliding tests. The arithmetic amplitude, Sa, decreases by 50% on non-textured materials, but only by 30% on textured materials after reciprocating sliding. This indicates that the peak heights reduced, and valleys became less

deep. The skewness values, Ssk, inside and outside the wear track area on both tested materials along both azimuthal angles 0° or 90° are quite similar (Ssk#0; peaks and valleys have approximately the same amplitude). Hence, the surfaces remain symmetrical regarding the mean plane even after reciprocating sliding tests. The kurtosis parameter, Sku, is between 3 and 5 before reciprocating sliding tests on both materials while it increases up to 5 and 9 after reciprocating sliding tests. This however indicates that the height distribution of peaks is more confined to a certain range, which is linked to the affected worn area (planes) as highlighted by SEM. For spacing parameters, the material ratio, Smr, which is the intercepted surface area at ¼ Sz micrometers above the mean plane, is significantly lower on textured material (between 0 and 1) than on non-textured material. On the contrary, the density of peaks, Spd, is less important after reciprocating sliding tests carried out on non-textured material but remains quasi-constant for textured material. When comparing the hybrid parameters, the developed surface, Sdr, which is the slope of the surfometry, Sdq, and the curvature of the peaks, Ssc, have values that are near to zero (not shown here) after the tests, indicating that the surfaces are nearly flat on both tested materials. It can be concluded that the reciprocating sliding tests smoothen the UHMWPE surface (mainly Sa, and Sq are affected), this being more marked on non-textured than on textured materials.

The limited low dissipated energy during sliding did not result in the formation of debris on textured UHMWPE as confirmed by SEM, but mainly in topographical changes due to viscoelastic-plastic deformation. On non-textured UHMWPE, the contact zone on sliding is continuous and comparable to the apparent contact area. This area contains wave due to stick-slip, and underwent some plastic deformation. This stick-slip displacement accommodation process gradually increases the tangential force with the number of cycles, and consequently the dissipated energy during sliding. The waves observed on non-textured UHMWPE surfaces as well as the thickness values obtained are in good agreement with that reported in literature for explanted UHMWPE cups [30]. This validates the current mechanical testing procedure. On textured UHMWPE, the contact zone on sliding against alumina is discontinuous due to the initial rough surface generated by the texturing process (Figure IV-12a and Figure IV-25). Moreover, the dissipation of sliding stresses is different from that on non-textured UHMWPE, and strongly depends on the sliding direction.

IV.3.3 Analysis of wear volume by WLI

Previously, it was shown that the texturing mechanism have an influence on the dissipated energy. We put forward that this dissipated energy is proportional to the wear volume. Now, we will verify here whether this assumption is valid or not. In this chapter, we report on a quantitative analysis by the determination of the wear volume on non-textured and textured UHMWPE at strain level up to 1.3. In order to be able to measure the wear volume, the reciprocating sliding test was conducted for 500,000 cycles. Fretting tests under mode-I were performed in ambient air (22 °C and 50 % RH) against corundum ball with a diameter of 10 mm and loaded at a normal load of 5 N. The ball was initially cleaned in acetone and ethanol to remove residues or greases. The evolution of the mechanical contact response is monitored by acquiring force-displacement hysteresis loops at closely spaced time intervals during reciprocating sliding tests. The energy dissipated was calculated from the hysteresis loops (tangential force vs. displacement). The sliding tests were repeated three times on each material. The evolution of the dissipated energy with the number of sliding cycles is shown in Figure IV-29.

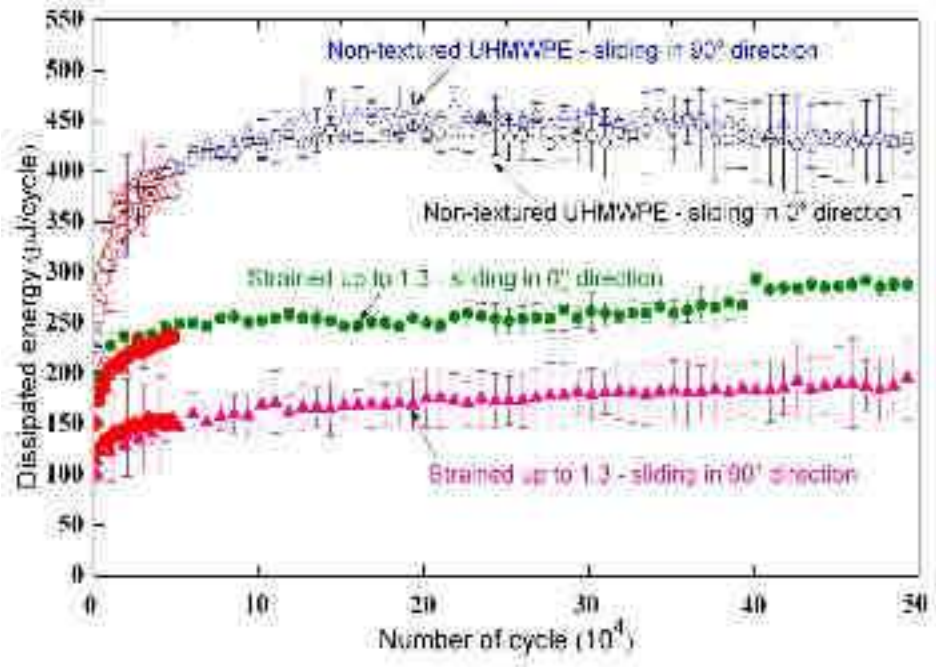

Figure IV-29: Plots of dissipated energy as a function of reciprocating sliding cycles for non-textured and textured UHMWPE (strain of 1.3) recorded along azimuthal angles 0° and 90° up to 50,000 cycles and 500,000 cycles (with standard deviations)

The dissipated energy recorded during reciprocating sliding tests done until 50,000 cycles, are also given in Figure IV-29 (in red). The dissipated energy for textured samples is lower than for non-textured samples. In particular, the dissipated energy decreases by a factor of about 2 when the sliding is done perpendicular to the tensile direction and by a factor of about 1.5 when sliding is performed along the tensile direction. The effect of texturing is maintained even at higher numbers of sliding cycles. The mechanisms proposed when reciprocating sliding tests were done up to 50,000 cycles can be similar to the ones active during reciprocating sliding tests performed up to 500,000 cycles.

The high number of cycles (500,000) allows us to determine the wear volume by post mortem observations using WLI. We used the software Mountain Map to binarize the surface (threshold in the altitude z), and hence, to easily determine the wear volume. Figure IV-30, Figure IV-31 and Figure IV-32 show the 3D representations of the wear track obtained with WLI.

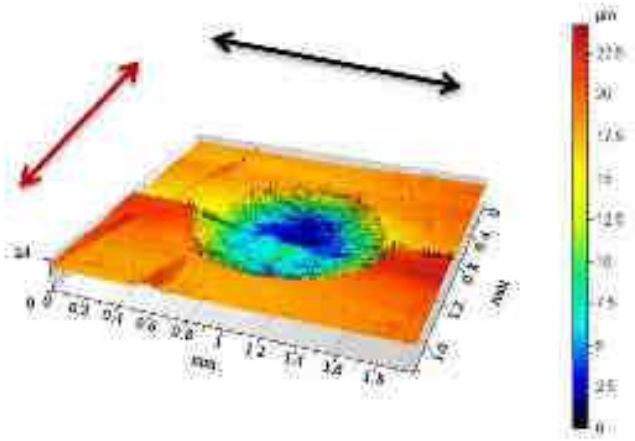

Figure IV-30: 3D representation of the wear track of the non-textured UHMWPE when sliding is performed along the direction 90° (black: sliding direction, red: stretching sliding)

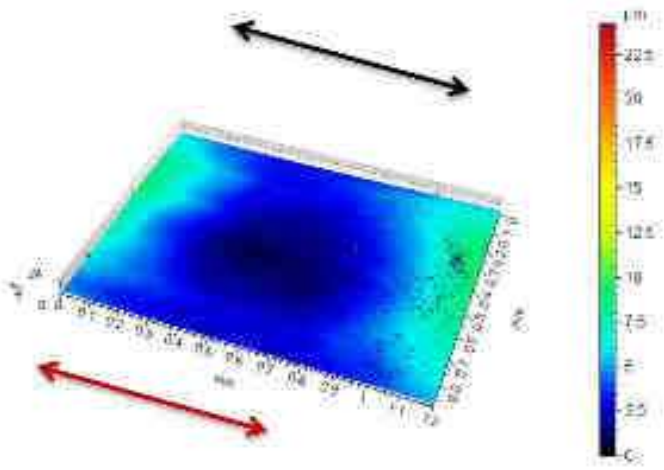

Figure IV-31: 3D representation of the wear track of the textured UHMWPE up to 1.3 when sliding is performed along the direction 0° (black: sliding direction, red: stretching sliding)

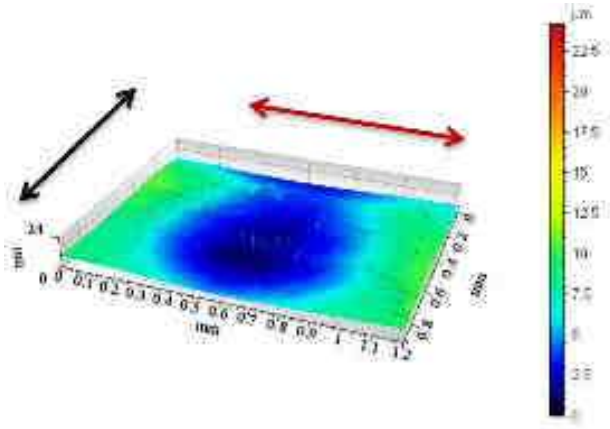

Figure IV-32: 3D representation of the wear track of the textured UHMWPE up to 1.3 when sliding is performed along the direction 90° (black: sliding direction, red: stretching sliding)

Figure IV-33 shows the wear tracks of non-textured at 0° and textured UHMWPE up to 1.3 at 0° and 90°. It was found that the wear volume on non-textured samples at 0° and 90° is about 6 x 10^{-3} mm^3, whereas on the strained sample at 0° is about 1.86 x 10^{-3} mm^3 and 90°, even lower is 0.32 x 10^{-3} mm^3.

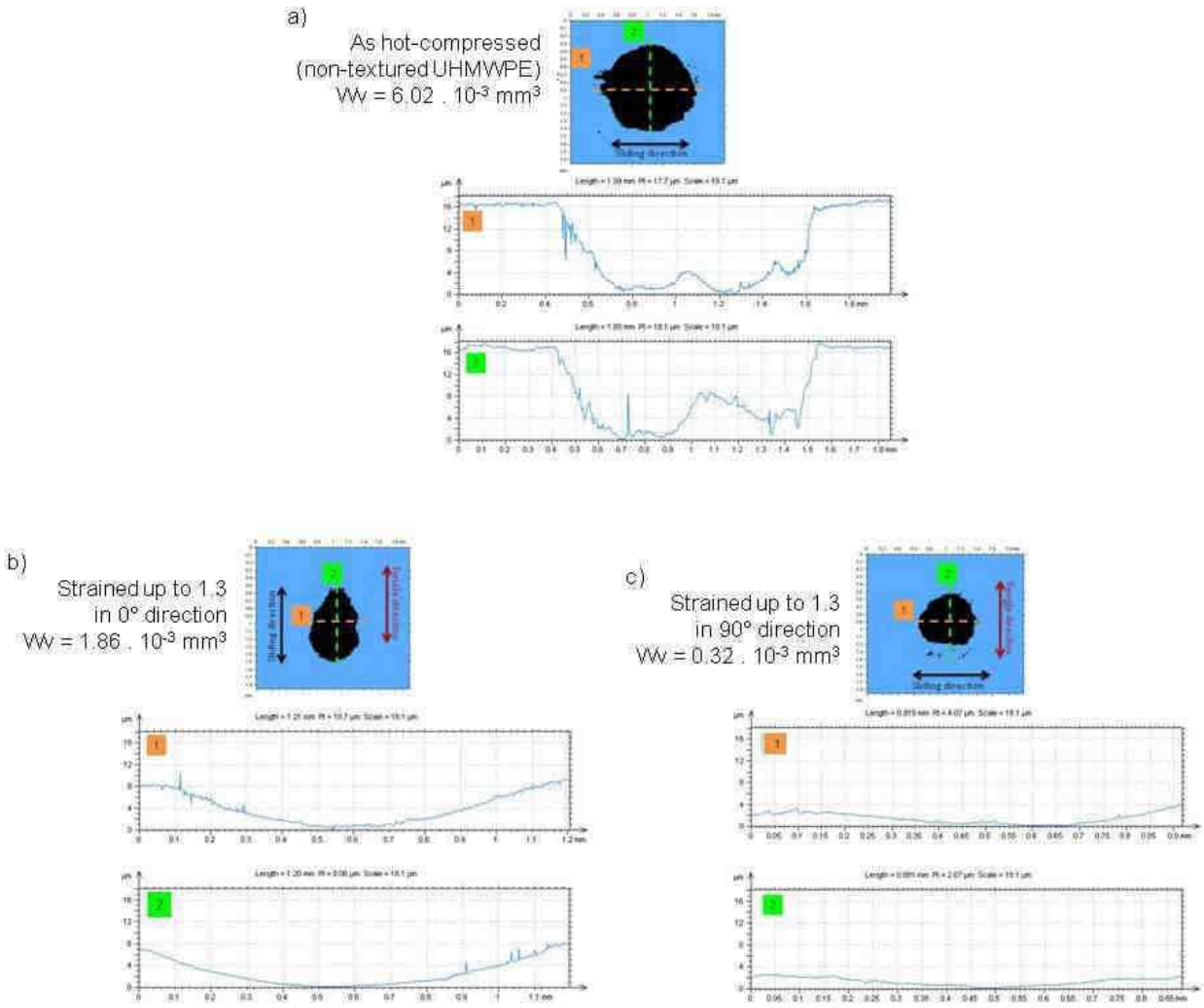

Figure IV-33: Post-mortem observations of wear tracks after sliding up to 500,000 cycles obtained by means of white light interferometer. a) non-textured UHMWPE, b) textured up to 1.3 UHMWPE when sliding is performed along tensile direction (0 °), c) textured up 1.3 UHMWPE when sliding is conducted perpendicular to tensile direction (90 °)

The worn area on non-textured UHMWPE is circular, i.e. isotropic, while on textured UHMWPE, we can observe that the worn area is anisotropic. This anisotropy is attributed to the fact that oriented polymers have a high strength in the texture direction, and on the contrary a low strength perpendicular to the texture direction. The anisotropic strength of UHMWPE influences the wear track shape which is also anisotropic. The orientation of the chains and the hardening of the network

after elongation led to a lower wear volume compared to non-textured UHMWPE, whatever the sliding direction is (decrease by a factor of 3 at 0° and 6 at 90°). This result demonstrates that the low strength of the textured material perpendicular to the chain direction is not detrimental concerning the wear volume. But, we can observe some wear particles on the sample deformed at 90° (Figure IV-33c). At 90° the sample underwent a plastic deformation resulting in some cracks, and at a high number of cycles these cracks may result in the release of wear particles (Figure IV-25). The plastic strain most likely accumulated at a certain depth and leads eventually to a shearing of the top layer. The wear mechanisms developed for sliding cycles up to 50,000, may be even valid at sliding cycles of 500,000. The wear volume and debris suggest that, within the distance tested, the primary mechanism was a viscoplastic deformation, and this evidence could suggest that at higher number of cycles (above 500,000 sliding cycles) the samples regardless their treatment would continue to behave similarly at extended sliding distance. However, from the WLI images of the worn surface, differences could be found in the number of particles outside the wear tracks (Figure IV-33c). In that area plastic strain accumulates and folds of the sample surface might retain particles. Therefore, this is an indication that materials that underwent the same reciprocating sliding conditions and surface deformation, can at longer sliding distances, undergo a delamination wear.

IV.4 Relationship between texturing and wear

To get a more precise insight of the sliding mechanisms of non-textured and textured UHMWPE, it is important to list here all the microstructural, topographical and mechanical aspects of these materials. Figure IV-25 reports all the features obtained at macroscopic and microscopic scales. Based on WAXS, SAXS, SEM, WLI, and DMA investigations, it appears that the initial texture has a marked effect on the polymer roughness, strength (pseudo-microfibrillar morphology), lamellae thickness, shape and orientation (coupled with the change in activation energy of α–relaxation), and mobility of amorphous chains in the interfacial region or amorphous phase (disappearance of β-relaxation).

<table>
<tr><th colspan="3">Non-textured</th></tr>
<tr><td rowspan="2"> 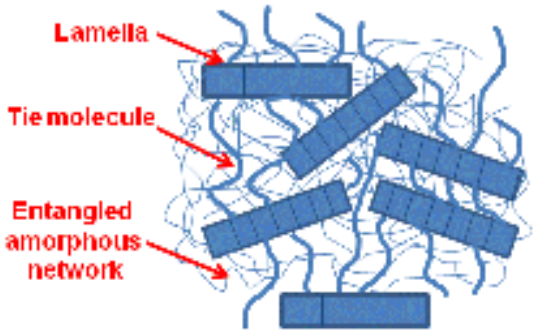
</td><td>Microscopic scale</td><td>Initial microstructure
No preferred orientation, important density of tie molecules and entanglements
Index of crystallinity ++
Lamellae thickness ++
Roughness +
Tg ++ Tβ +++ Tα ++++
Ea (α) +++

Sliding behaviour
Continuous wear track
Stick-slips ++
Cracks +
Final roughness +</td></tr>
<tr><td>Macroscopic scale</td><td>Sliding dissipated energy +++
Strength +</td></tr>
<tr><th colspan="3">Textured</th></tr>
<tr><td rowspan="2"> 
</td><td>Microscopic scale</td><td>Initial microstructure
Micro-fibrils with lamellae chevrons, lamella blocks and a stretched network of tie molecules and entangled chains
Index of crystallinity ++
Lamellae thickness +
Roughness ++
Tg ++ Tβ Tα +++
Ea (α) +

Sliding behaviour
Discontinuous wear track
Cracks at 0°+ / at 90° +
Stick-slips at 0° + / at 90 ° +
Final roughness +</td></tr>
<tr><td>Macroscopic scale</td><td>Sliding dissipated energy at 0° ++ / at 90° +
Strength at 0° ++ / at 90° +</td></tr>
</table>

Figure IV-34: General aspects of texturing prior and after sliding tests

Based on the review of Briscoe [35], two general categories of wear mechanisms, are active in the case of polymers: interfacial wear mechanisms and cohesive wear mechanisms. These two mechanisms are represented in the Figure IV-35.

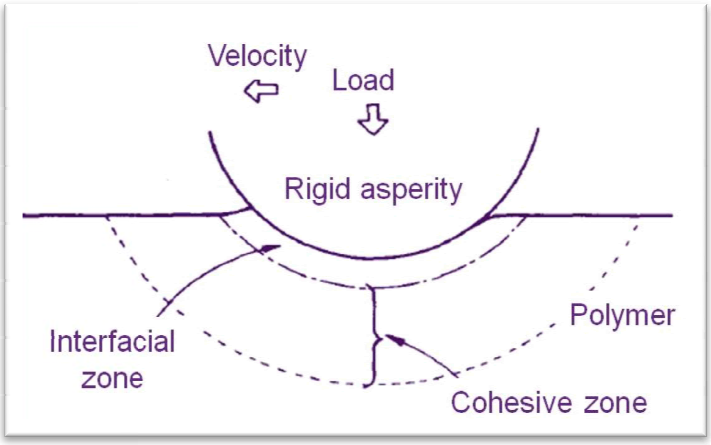

Figure IV-35: Fundamental aspects of wear of polymers [35]

Interfacial wear mechanisms take place at the counterbody/polymer interface and involve the dissipation of the frictional work within a very thin region and hence with a high energy density. These mechanisms involve the deformation in the sliding direction and the transfer of a thin polymer layer from the polymer to the counterbody. Concerning cohesive wear mechanisms, frictional work is dissipated in a thick region through the formation of subsurface cracks. These mechanisms are governed by a fatigue process that induces the propagation of the cracks to the surface, and hence, possibly a delamination of the material and then release of large wear debris. In our case, we did not observe delamination process, which may be due to the relatively low number of sliding cycles. Note that the observed cracks on Figures IV-25 and IV-26 may be due to the initiation of decohesion wear or to the deformation of surface defects due to the initial high roughness of the textured materials. The contact pressure is probably high at some asperities, which can lead to the formation of cracks as a dissipation process of stresses. As first approximation, we consider that the observed cracks on wear tracks do not significantly influence the wear volume of the materials. Therefore, it is supposed that the wear of non-textured and textured UHMWPE is mainly generated by interfacial wear mechanisms.

It has been shown that interfacial wear mechanisms depend on:

- **the adhesive forces** between the polymer and the counterface. The interfacial wear increases if the adhesive forces increases, and hence, if the contact area increases, initial roughness decreases, lubrication decreases and surfaces forces increase (Van der Waals, hydrogen). The contact area was calculated by Hertz's theory using the Young modulus given by DMA analysis. The contact area for non-deformed and deformed UHMWPE is similar and around 250 µm, so this parameter is not a key parameter in controlling wear. WLI measurements show that the initial roughness increases with the texturing process (Figure IV-12), demonstrating that interfacial wear may be less marked for textured than for non-textured UHMWPE. However, increasing roughness may induce the formation of surface cracks. FTIR showed no chemical modification of the structure when comparing non-textured and textured UHMWPE (Figure IV-24), so this is not a key parameter in our study. Based on the definition of sliding dissipated energy, we can suppose that the sliding dissipated energy is proportional to the coefficient of friction. Therefore, texturing from the strain 0.9 causes a decrease of COF when comparing with the reference material.

  SEM observations indicate wavy morphologies inside the wear tracks of the materials (Figure IV-26). The thickness of these waves is around 2 µm for the non-textured UHMWPE whereas it is 1 µm for textured UHMWPE. It can be supposed that texture may increase the load bearing capacity through the reduced waves, which decreases the coefficient of friction. In Figure IV-36 a schematic observation to understand this phenomenon is proposed. The two materials can be seen as brushes with two sizes of bristles, the thinner the bristle are, the higher the load bearing capacity.

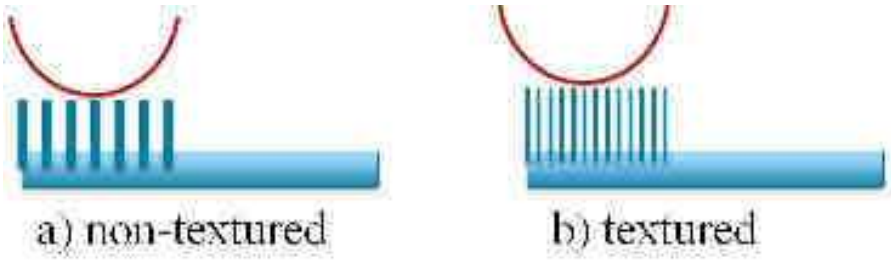

Figure IV-36: Schematic observation of the load bearing capacity of a) non-textured and b) textured UHMWPE that can be seen as brushes

- **the morphological dimension of the polymer**. Indeed, the thickness of the transferred polymer layer increases with increasing the morphological dimension. In the case of mild sliding conditions, the thinnest layer (10 nm) approaches the morphological dimensions of the polymer in term of lamella thickness, as shown in Figure IV-37.

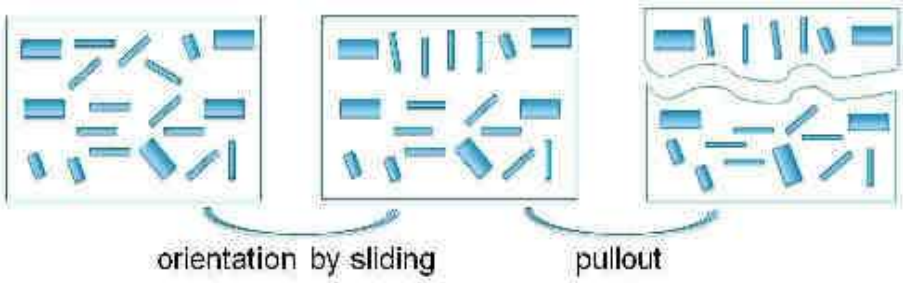

Figure IV-37: Transferred layer thickness

Based on our results, it appears that texturing causes a decrease of lamellae thickness from the imposed strain 0.9 (Figure IV-6). For the imposed strain 1.3, we obtained an average lamella thickness of 10 nm, which corresponds to a decrease of 50 % compared to the reference material. Note that this 50 % decrease of the lamella thickness corresponds to the same level of decrease in the wave thickness observed on wear tracks (Figure IV-26). These two phenomena seem to be linked. It is concluded that from the strain level 0.9, the thickness of the transferred layer decreases with increasing the imposed strain level.

Accordingly, the wear volume of textured UHMWPE is lower than that of non-textured UHMWPE considering the same number of transferred layers,

- **the strength of the polymer molecular network**, the higher the strength, the harder the transfer of the polymer layer and hence the lower the wear. A microfibrillar morphology has a high strength along texture direction, but a low strength perpendicular to the texture direction [5, 9, 36]. The high strength along the texture direction is explained by a high molecular resistance (solicitation of C-C covalent bonds, coupled with the solicitation of an important number of stretched tie molecule and entangled chains [9, 10]) that induces a hardening effect [37]. Thus, texture is suitable when sliding is performed along the chain direction, but is not suitable when sliding is performed in the perpendicular direction. DMA results indicate that for samples cut parallel to tensile direction, the α-relaxation is facilitated (Figure IV-13 and IV-14). We note the same result for samples cut perpendicular to tensile deformation (results not shown). This enhancement of the crystalline lamellae relaxation is probably linked to the decrease of lamellae thickness, and the possible increase of tie molecules density with the imposed strain. This isotropic relaxation behaviour of the stretched microstructure of UHMWPE demonstrates that we are not in presence of a real fully oriented micro-fibrillar microstructure. Indeed, lamellae are oriented parallel and perpendicular to tensile direction, and at 45°. Furthermore, lamellae forming chevrons are present. All these features make that in our case stretching induces the formation of a new specific microstructure of UHMWPE that may have quite isotropic molecular motions. The increased molecular motions with the imposed strain are not desirable because it enhance the orientation and the transfer of the polymer layer during interfacial wear mechanisms. Note that the disappearance of the β-relaxation may be due to the stretching of the tie molecules, since some authors attributed this relaxation to the motion of loose tie molecules [38, 39].

Overall, from the imposed strain 0.9, textured UHMWPE has a decreased sliding dissipated energy, coefficient of friction and wear volume compared to non-textured UHMWPE, whatever the sliding direction. This observation demonstrates that the mechanisms that increase the wear resistance (decrease of transferred polymer layer thickness, and increase of load bearing capacity of the

polymer) are enhanced compared to those decreasing it (increase of molecular motions that enhance the transfer of polymer layer). Most of the cited mechanisms in this section require a detailed study to prove their effective existence. For example, to demonstrate the increase of load bearing capacity of textured UHMWPE compared to the reference material finite element simulations are required to investigate this possible mechanism. Concerning the transferred polymer layer, further investigations are required to investigate its orientation state and thickness.

IV.5 Conclusions

As shown by SEM and WAXS, the elongation of UHMWPE up to about 300 % induces the formation of pseudo-microfibrillar morphology with chains oriented along the elongation direction and lamellae fragments forming chevrons. This new morphology has an increased roughness compared to non-textured UHMWPE, as revealed by WLI. DMA show that the α-relaxation process is more marked for oriented UHMWPE in comparison with the non-oriented material, demonstrating more molecular motions.

At macroscopic scale, the energy dissipated by friction on textured UHMWPE is comparatively much lower than on non-textured UHMWPE along and perpendicular to the texture direction, from the imposed strain 0.9. Up to 500,000 sliding cycles, we found a wear volume of non-textured samples at 0° and 90° of about 6×10^{-3} mm^3, whereas for the strained sample the wear volume is of about 1.86×10^{-3} mm^3 along tensile direction and of about 0.32×10^{-3} mm^3 perpendicular to tensile direction. As a result, textured UHMWPE has anti-wear properties. At microscopic scale, we found that sliding tracks are discontinuous on textured UHMWPE due to the high initial roughness, while they are continuous on non-textured UHMWPE.

We hypothesized that interfacial wear mechanisms were the main wear mechanisms in our materials. Texturing induces less marked interfacial wear mechanisms than the reference material. Indeed, it is thought that the transferred polymer layer may have a decreased thickness, and that the load bearing capacity may be increased in the case of the textured UHMWPE. Nevertheless, due to the increased molecular motions, the imposed strain may enhance the orientation of the polymer layer and its transfer from the polymer to the counterbody. This last mechanism may enhance interfacial wear, but is supposed to be less important than the mechanisms limiting interfacial wear.

IV.6 References

[1] F. Addiego, Caractérisation de la variation volumique du polyéthylène au cours de la déformation plastique en traction et en fluage, (2006).

[2] T.H. Tsuneo Seto, Kenzo Tanaka, Phase Transformation and Deformation Processes in Oriented Polyethylene, The Japan Society of Applied Physics, 7 (1968) pp. 31-42.

[3] M.F. Butler, A.M. Donald, W. Bras, G.R. Mant, G.E. Derbyshire, A.J. Ryan, A Real-Time Simultaneous Small- and Wide-Angle X-ray Scattering Study of In-Situ Deformation of Isotropic Polyethylene, Macromolecules, 28 (1995) 6383-6393.

[4] F. Addiego, A. Dahoun, C. G'Sell, J.-M. Hiver, Characterization of volume strain at large deformation under uniaxial tension in high-density polyethylene, Polymer, 47 (2006) 4387-4399.

[5] A. Galeski, Strength and toughness of crystalline polymer systems, Progress in Polymer Science, 28 (2003) 1643-1699.

[6] G.S.C. Haudin J.M., "Mécanismes microscopiques de déformation des polymères semi cristallins", In : Introduction à la mécanique des polymères, 1ère édition (1995) p.251-273.

[7] J. Petermann, J.M. Schultz, Lamellar separation during the deformation of high-density polyethylene, Journal of Materials Science, 13 (1978) 50-54.

[8] M. Aboulfaraj, C. G'Sell, B. Ulrich, A. Dahoun, In situ observation of the plastic deformation of polypropylene spherulites under uniaxial tension and simple shear in the scanning electron microscope, Polymer, 36 (1995) 731-742.

[9] F. Addiego, O. Buchheit, D. Ruch, S. Ahzi, A. Dahoun, Does Texturing of UHMWPE Increase Strength and Toughness?: A Pilot Study, Clinical Orthopaedics and Related Research®, 469 (2011) 2318-2326.

[10] Y. Boontongkong, R.E. Cohen, M. Spector, A. Bellare, Orientation of plane strain-compressed ultra-high-molecular-weight polyethylene, Polymer, 39 (1998) 6391-6400.

[11] R. Séguéla, On the natural draw ratio of semi-crystalline polymers: Review of the mechanical, physical and molecular aspects, Macromolecular Materials and Engineering, 292 (2007) 235-244.

[12] W.W. Adams, E.L. Thomas, Direct vizualization of microstructural deformation processes in polyethylene, in, 1985, pp. 8. 1-8. 4.

[13] K.-H. Nitta, M. Takayanagi, Role of tie molecules in the yielding deformation of isotactic polypropylene, Journal of Polymer Science Part B: Polymer Physics, 37 (1999) 357-368.

[14] J.M. Schultz, Review : Deformation mechanisms in crystalline polymers Polym. Mat. Sci., pages 2034–51, 197 (1974).

[15] J.A. Greenwood, J.B.P. Williamson, Contact of Nominally Flat Surfaces, Proceedings of the Royal Society of London. Series A. Mathematical and Physical Sciences, 295 (1966) 300-319.

[16] M. Minn, S. Sinha, Molecular Orientation, Crystallinity, and Topographical Changes in Sliding and their Frictional Effects for UHMWPE Film, Tribology Letters, 34 (2009) 133-140.

[17] J. Rault, Les polymères solides. Amorphes, élastomères, semi-cristallins, Cépaduès-Editions, Toulouse, (2002).

[18] R.H. Boyd, The energetics of kinks in polyethylene, Journal of Polymer Science: Polymer Physics Edition, 13 (1975) 2345-2355.

[19] M. Mansfield, R.H. Boyd, Molecular motions, the alpha relaxation, and chain transport in polyethylene crystals, J Polym Sci Polym Phys Ed, 16 (1978) 1227-1252.

[20] L. Richards, C. Brown, M.H. Stone, J. Fisher, E. Ingham, J.L. Tipper, Identification of nanometre-sized ultra-high molecular weight polyethylene wear particles in samples retrieved in vivo, Journal of Bone and Joint Surgery - Series B, 90 (2008) 1106-1113.

[21] S.P. Westphal, T.K. Ling, L. Woo, Polyethylene structural heterogeneity by thermal and rheological techniques, Thermochimica Acta, 272 (1996) 181-189.

[22] R.H. Boyd, Relaxation processes in crystalline polymers: experimental behaviour - a review, Polymer, 26 (1985) 323-347.

[23] R.A. Talja, Y.H. Roos, Phase and state transition effects on dielectric, mechanical, and thermal properties of polyols, Thermochimica Acta, 380 (2001) 109-121.

[24] I. Weuts, D. Kempen, K. Six, J. Peeters, G. Verreck, M. Brewster, G. Van Den Mooter, Evaluation of different calorimetric methods to determine the glass transition temperature and molecular mobility below Tg for amorphous drugs, International Journal of Pharmaceutics, 259 (2003) 17-25.

[25] R.G. Arridge, Polymers; Mechanical properties, Clarendon Press (Oxford Eng.), (1975) ix, 246 p.

[26] Q. Fu, Y. Men, G. Strobl, Understanding of the tensile deformation in HDPE/LDPE blends based on their crystal structure and phase morphology, Polymer, 44 (2003) 1927-1933.

[27] S. Edin, Dielectric studies of molecular β-relaxation in low density polyethylene: the influence of drawing and ionizing radiation, Polymer, 43 (2002) 5969-5978.

[28] H. Yoshida, A. Faust, J. Wilckens, M. Kitagawa, J. Fetto, E.Y.S. Chao, Three-dimensional dynamic hip contact area and pressure distribution during activities of daily living, Journal of Biomechanics, 39 (2006) 1996-2004.

[29] R. Büscher, A. Fischer, Metallurgical Aspects of Sliding Wear of fcc Materials for Medical Applications, Materialwissenschaft und Werkstofftechnik, 34 (2003) 966-975.

[30] A. Berradja, G. Willems, J.P. Celis, Tribological behaviour of orthodontic archwires under dry and wet sliding conditions in-vitro. II--Wear patterns, Australian orthodontic journal., 22 (2006) 21-29.

[31] H. Mohrbacher, B. Blanpain, J.P. Celis, J.R. Roos, L. Stals, M. Van Stappen, Oxidational wear of TiN coatings on tool steel and nitrided tool steel in unlubricated fretting, Wear, 188 (1995) 130-137.

[32] R. Colaço, M.P. Gispert, A.P. Serro, B. Saramago, An energy-based model for the wear of UHMWPE, Tribology Letters, 26 (2007) 119-124.

[33] K.S. Kanaga Karuppiah, A.L. Bruck, S. Sundararajan, J. Wang, Z. Lin, Z.-H. Xu, X. Li, Friction and wear behavior of ultra-high molecular weight polyethylene as a function of polymer crystallinity, Acta Biomaterialia, 4 (2008) 1401-1410.

[34] J. Song, P. Liu, M. Cremens, P. Bonutti, Effects of machining on tribological behavior of ultra high molecular weight polyethylene (UHMWPE) under dry reciprocating sliding, Wear, 225-229 (1999) 716-723.

[35] B. Briscoe, Wear of polymers: an essay on fundamental aspects, Tribology International, 14 (1981) 231-243.

[36] A. Wang, A. Essner, V.K. Polineni, C. Stark, J.H. Dumbleton, Lubrication and wear of ultra-high molecular weight polyethylene in total joint replacements, Tribology International, 31 (1998) 17-33.

[37] A. Peterlin, G. Meinel, Small-angle X-ray diffraction studies of plastically deformed polyethylene. III. Small draw ratios, Die Makromolekulare Chemie, 142 (1971) 227-240.

[38] K.h. Nitta, A. Tanaka, Dynamic mechanical properties of metallocene catalyzed linear polyethylenes, Polymer, 42 (2001) 1219-1226.

[39] J.A. Puértolas, M.J. Martínez-Morlanes, M.D. Mariscal, F.J. Medel, Thermal and dynamic mechanical properties of vitamin E infused and blended ultra-high molecular weight polyethylenes, Journal of Applied Polymer Science, 120 (2011) 2282-2291.

Chapter V

General conclusions and prospects

V.1 General conclusions

The main objective of this research was to study the impact of texture on the friction and wear behaviour of UHMWPE, and to assess whether texture is suitable or not for medical device applications.

Different textures of UHMWPE were achieved by solid-state deformation tests performed as uni-axial tensile procedures. By combining SAXS/WAXS analyses, SEM observations, WLI tests, and DMA investigations, we found that texturing causes a transformation of the initial lamellar structure into a pseudo-microfibrillar structure having lamellae blocks oriented perpendicular to the tensile direction, lamellae forming chevrons, and broken lamellae chevrons characterized by lamellae oriented parallel to the tensile direction. This new specific morphology has a lower crystallinity, a lower long spacing and thinner lamellae compared to the initial morphology. The α-relaxation of the textured UHMWPE has lower activation energy than the one of non-textured material. Besides that, textured UHMWPE has no β-relaxation mechanisms when comparing with non-textured UHMWPE. Note that overall, texturing leads to an increased roughness.

The sliding behaviour of the materials was studied in a tribometer configured as reciprocating ball-on-plate sliding mode. We noted that the sliding dissipated energy is quite similar for the non-textured state up to the textured state corresponding to an axial true strain of 0.6. On increasing the strain level from 0.6 up to 1.3, a marked decrease of the sliding dissipated energy was observed. In particular, the cumulative dissipated energy after 50,000 sliding cycles decreases from 18,250-17,600 J for non-textured UHMWPE to 11,700 and 6,700 J for the most textured UHMWPE achieved in this study at an axial strain of 1.3, parallel and perpendicular to the texture direction respectively. At a higher number of sliding cycles, namely 500,000, it was possible to assess a wear volume on the materials and we found a decrease of the volumetric loss by a factor of 3 and 6 when comparing non-textured UHMWPE with the most textured UHMWPE at 0° and 90° respectively. However, at 90° the textured UHMWPE exhibits some cracks which are not desirable and may cause the formation of debris at high number of sliding cycles.

The sliding behaviour of non-textured and textured UHMWPE was discussed on the basis of interfacial wear mechanisms characterized by the orientation and transfer of a thin polymer layer from the polymer to the counterbody. It was mentioned that texture causes i) a possible increase of the load bearing capacity, and ii) a possible decrease the thickness of the transferred polymer layer, compared to the reference material. These two phenomena reduce the interfacial wear. However, it was also mentioned that molecular motions of crystalline phase were enhanced with the texturing, which may induce more marked orientation and hence transfer of the polymer layer compared to non-textured UHMWPE. This last phenomenon was supposed less important than the two previous ones.

Textured UHMWPE exhibits a considerable decrease of the sliding dissipated energy and of the wear volume, parallel and perpendicular to the texture. These important results indicate that textured UHMWPE has anti-wear properties, and is thus suitable for medical device applications (total hip and knee arthroplasty), as well as for other applications like bulk material handling, mining and mineral processing equipment, sport equipment, machines construction, and protection equipment.

V.2 Prospects

Most of the wear mechanisms indicated in this manuscript needs to be confirmed by further experimental works and by simulation procedures. In particular, the released transferred polymer layers could be analysed to verify either texturing decrease their thickness and increase their orientation state. Furthermore, finite element simulation could be done to verify either texture could increase the load bearing capacity of UHMWPE.

Preliminary sliding tests in Ringer's solution have shown that the dissipated energy is lower when sliding is performed perpendicular to the tensile direction than non-textured and textured in 0° direction.

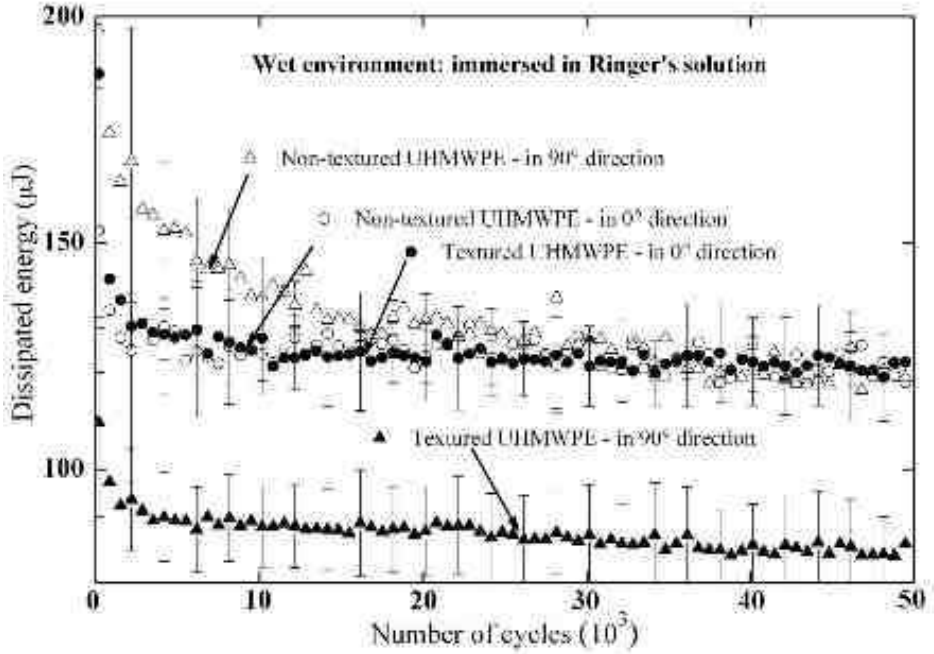

Figure V-1:Dissipated energy as function of reciprocating sliding cycles for non-textured and textured UHMWPE (strained up to 1.3) in 0° and 90° in Ringer's solution (with standard deviations).

It can be assumed that the Ringer's solution remains blocked when sliding is performed perpendicularly to the chains orientation, which could explain the lower dissipated energy, In future work, it would be of scientific interest to identify the wear mechanisms active in presence of such a water-based solution, and to compare them to those identified under dry sliding conditions in the present work.

In this works, the texturing was achieved by simple uni-axial tensile procedures with the maximum axial strain fixed with the VideoTraction. We investigated the behaviour of the dissipated energy on a textured material with a higher deformation level (up to a nominal strain of 4 corresponding to true strain higher to 1.3) using the Instron device. The dissipated energy as function of the number of cycles is given in the following pictures when sliding is performed at 0° (Figure V-2) and at 90° (Figure V-3).

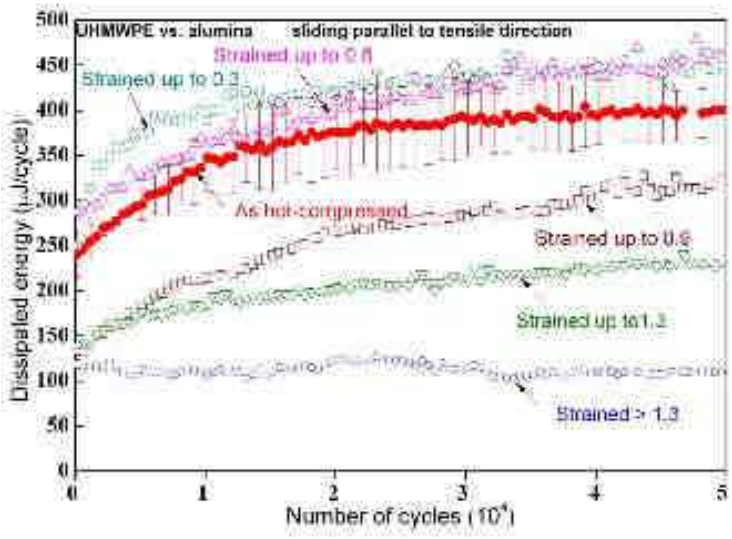

Figure V-2: Dissipated energy as function of the number of cycles for non-textured and textured UHMWPE (0.3, 0.6, 0.9, 1.3 and >1.3) when sliding is performed parallel to the tensile direction

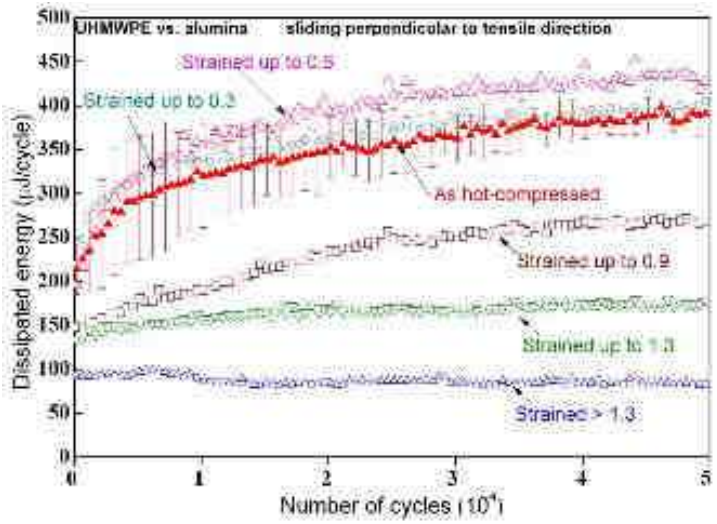

Figure V-3: Dissipated energy as function of the number of cycles for non-textured and textured UHMWPE (0.3, 0.6, 0.9, 1.3 and > 1.3) when sliding is performed perpendicular to the tensile direction

It will also be interesting to study the impact of other deformation paths like bi-axial tension, cold-rolling... on the sliding behaviour of UHMWPE. The goal would be to verify whether other

deformation paths can be used to obtain a higher decrease in dissipated sliding energy and wear volume than in the case of uni-axial tension.

Another possible theme for future research work could be to find a way to design a hip cup having a textured microstructure with deformation levels as those considered in the present manuscript. Then, a hip simulator testing conducted on such cups would allow to verify whether anti-wear properties related to texture are maintained or not under real end-users conditions.

In tribology, a standard procedure to express the wear rate as a function of the initial texture state is not available. Many studies have been developed to correlate wear volume with load, sliding distance, friction coefficient, hardness, etc, but none of them correlated wear volume with texture. Predicting the dissipated energy as a function of texture is a novel concept that should be developed in future research work.

Abstract - résumé

Abstract

Ultra-high molecular weight polyethylene (UHMWPE) is a material widely used as bearing material in joint prostheses whose durability depends on its chemical and mechanical properties. One of the main steps in the production of UHMWPE parts for prostheses is an irradiation-induced cross-linking that considerably improves wear resistance, but at the same time lowers drastically the chemical stability, tensile strength, and toughness of UHMWPE.
Texturing like e.g. the formation of a stretched molecular network, could be an alternative treatment to cross-linking, since it can increase strength and toughness of a polymer without altering its chemical properties. However, little information is yet available about the effect of chain orientation on the sliding and wear behaviour of textured UHMWPE. In this PhD thesis, the effect of the chain orientation state on the sliding and wear behaviour of UHMWPE is investigated as well as the underlying mechanisms.
Different texture states of UHMWPE were obtained by deformation under tensile stresses performed under an accurately control of the strain level. SAXS/WAXS analyses, SEM observations, WLI tests, and DMA investigations showed a transformation of the initial lamellar structure into a pseudo-microfibrillar structure containing lamellae forming chevrons and thinner lamellae, and characterized by a disappearance of the β-relaxation, and an increased roughness. To evaluate the tribological behaviour of such strained UHMWPE, test samples were subjected to reciprocating sliding with a ball-on-plate configuration, using corundum balls as counter-body. Such tests were performed parallel and perpendicular to the chain direction. From an axial strain level of 0.9, the sliding dissipated energy of textured UHMWPE decreases whatever the sliding direction compared to non-textured UHMWPE. In particular, the cumulative dissipated energy at 50,000 sliding cycles decreases from 18,250-17,600 J for untreated UHMWPE down to 11,700 and 6,700 J for the most textured UHMWPE (axial strain of 1.3), parallel and perpendicular to the texture direction respectively. At higher number of cycles (500,000 sliding cycles), a decrease of loss volume by a factor of 3 and 6 was noticed when comparing non-textured UHMWPE with the most textured UHMWPE at 0° and 90° respectively. The results were discussed on the basis of interfacial wear mechanisms that are characterized by the orientation and transfer of a thin polymer layer from the polymer to the counterbody. Texture may cause an increase of the load bearing capacity, and a decrease of the thickness of the transferred polymer layer compared to the non-textured material. These two phenomena may decrease the interfacial wear of UHMWPE. Nevertheless, texturing was proved to increase the molecular motions of the crystalline phase, which may increase the molecular orientation within the layer, and hence, facilitate the transfer of the polymer layer compared to the reference UHMWPE. This last phenomenon was supposed less important than the two previous ones. It was concluded that textured UHMWPE has anti-wear properties both in parallel and perpendicular directions to the texture direction. Therefore, this material appears suitable for medical device applications.

Keywords:
UHMWPE, microstructure, sliding, wear, texturing

Résumé

Le polyéthylène à ultra-haut poids moléculaire (PE-UHPM) est un matériau utilisé comme composant d'appui dans les prothèses articulaires, dont la durabilité dépend des propriétés chimiques et mécaniques de ce polymère. Une des principales étapes de la production de composants en PE-UHPM pour les prothèses est la réticulation par irradiation qui améliore considérablement la résistance à l'usure, mais dans le même temps, réduit drastiquement la stabilité chimique, la résistance à la traction et la résistance à la fracture du PE-UHPM.
La texturation, définit comme un procédé induisant la formation d'un réseau de molécules alignées, pourrait être un traitement alternatif à la réticulation, car elle peut augmenter la résistance à la traction et la résistance à la fracture d'un polymère sans altérer ses propriétés chimiques. Cependant, peu d'informations sont connues sur l'effet de l'orientation initiale des chaînes sur le glissement et le comportement à l'usure du PE-UHPM texturé. Dans cette thèse, l'effet de l'état d'orientation des chaînes sur le comportement au glissement et à l'usure du PE-UHPM est étudié, ainsi que les mécanismes sous-jacents.
Différents états de texture du PE-UHPM ont été obtenus par déformation en traction avec contrôle précis du niveau de déformation. Des analyses SAXS / WAXS, des observations MEB, des tests WLI, et des essais DMA ont montré une transformation de la structure lamellaire initiale en une structure pseudo-microfibrillaire i) contenant des lamelles arrangées en chevrons, ii) ayant une épaisseur de lamelle plus faible que l'état initial, iii) caractérisée par une disparition de la relaxation β, et iv) caractérisée par une augmentation de la rugosité. Pour évaluer le comportement tribologique de PE-UHPM texturés, les échantillons ont été soumis à un glissement alternatif (configuration bille-plan), en utilisant des billes de corindon comme contre-corps. Ces tests ont été effectués parallèlement et perpendiculairement à la direction des chaînes. A partir d'une déformation axiale de 0,9, l'énergie dissipée du PE-UHPM texturé diminue par rapport au PE-UHPM non-texturé et ce, quelle que soit la direction de glissement. En particulier, l'énergie dissipée cumulée à 50 000 cycles diminue de 18 250-17 600 J pour le PE-UHPM non-texturé à 11 700 et 6 700 J pour le PE-UHPM le plus texturé (déformation axiale de 1,3), respectivement dans la direction de la texture et perpendiculairement à la direction de la texture. Pour des plus grands nombres de cycles (500 000 cycles de glissement), une diminution du volume d'usure d'un facteur de 3 et 6 a été remarquée en comparant les échantillons non-texturés et les échantillons les plus texturés respectivement à 0° et 90°. Les résultats ont été discutés sur la base de mécanismes d'usure interfaciale caractérisés par un processus d'orientation et de transfert d'une fine couche de polymère de ce dernier vers le contre-corps. La texture pourrait induire une augmentation de la portance et une diminution de l'épaisseur de la couche transférée comparé au matériau non-texturé. Ces deux phénomènes pourraient ainsi diminuer l'usure interfaciale du PE-UHPM. Néanmoins, la texturation conduit à une augmentation des mouvements moléculaires de la phase cristalline, ce qui pourrait augmenter l'orientation moléculaire dans la couche et donc, faciliter son transfert par comparaison au matériau de référence. Ce dernier phénomène a été considéré comme étant moins important que les deux autres. Il est a été conclu que le PE-UHPM texturé possède des propriétés anti-usures selon les directions parallèle et perpendiculaire à la direction de la texture. Ce matériau apparaît donc souhaitable pour les prothèses médicales.

Mots-clés:
PE-UHPM, microstructure, glissement, usure, texturation